THE COLLEGE OF AERONAUTICS

CRANFIELD.

PRESSURE FLUCTUATIONS IN SHEAR FLOW TURBULENCE

PART 2

by

T. H. HODGSON

6. The Turbulent Wall Jet Experiments.

The major part of the experimental programme was devoted to boundary layer investigations because the turbulent boundary layer is the most common occurring type of wall turbulent shear flow in practical problems of aerodynamics. However we have seen, as described in section 4, the considerable experimental difficulties that were encountered in measuring the wall pressure fluctuations in turbulent boundary layers. In particular these difficulties were the small magnitude of the pressure signal relative to possible extraneous disturbances which interfered with spectra and correlation measurements, and also the lack of resolving power of the pressure transducers at the higher frequencies.

It was therefore desirable to make measurements in other types of turbulent wall shear flows, which might help to verify the deductions that have been inferred from the boundary layer tests. The possibility that the wall jet shear flow might fulfill this role was first suggested to the author by G.M. Lilley. Indeed, initial measurements showed that the ratio of the turbulent fluctuating pressure signal to extraneous signals was high and so a comprehensive programme of measurements was performed which has helped considerably in the understanding of the mechanism of the pressure fluctuations in turbulent shear flows.

The preliminary measurements in the radial turbulent wall jet

have been described by Hodgson and Lilley (1960). These measurements have been extended to include turbulent velocity and correlation measurements and were repeated for a two-dimensional wall jet. For brevity these two types of wall jet will be discussed simultaneously.

6.1 Theory of the mean flow

When a jet of air strikes a surface at right angles or air flows from a peripheral slot over a surface it forms what is known as a radial wall jet. Similarly if the jet or slot is planar the wall shear flow is termed a two-dimensional wall jet.

The mean flow in the wall jet has been studied theoretically by Glauert (1956), and experimentally by Bakke (1957) and Bradshaw et al. (1959) for the radial wall jet and by Bradshaw et al. (1960) for the two-dimensional wall jet. Although Glauert considered both laminar and turbulent wall jet flows, only the turbulent case will be required here.

To good approximation the wall jet flow may be regarded as a combination of an inner region with properties very similar to a boundary layer flow and an outer mixing region very similar to a jet flow. Glauert evaluated numerically a near-similarity solution for the turbulent case by assuming that the variation of shear stress with mean velocity in the inner region was the same as that in turbulent pipe flow, while in the outer region a constant eddy viscosity was assumed, with the value

being chosen to obtain a velocity profile in agreement with Bakke's experiments on the radial wall jet.

Bradshaw et al. (1959, 1960) have shown, using calibrated Stanton tubes, that in both the radial and two-dimensional cases the skin friction coefficient is of the order of 20 - 25% higher than would occur in pipe flow for the same Reynolds number.

For the radial wall jet case we will denote the radial mean velocity by U, with maximum value U_m, in the radial direction R with z the distance normal to the plate. For the two-dimensional case, x will be taken as the downstream direction with y normal to the plate.

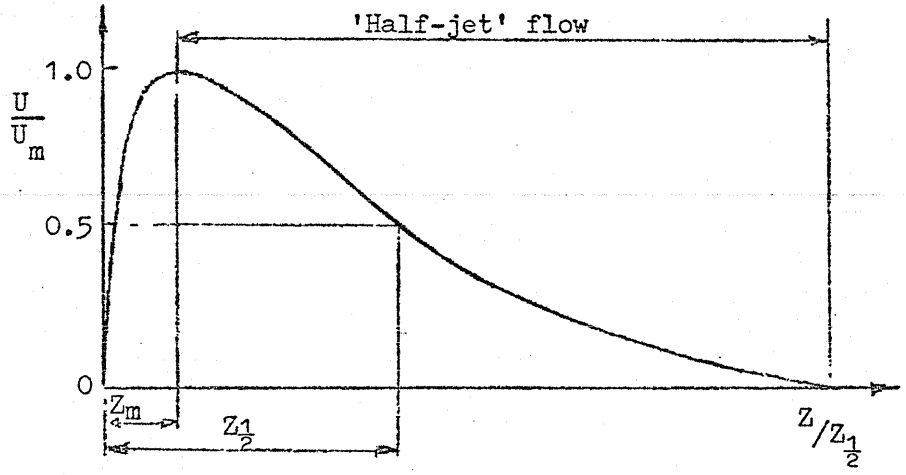

The thickness ratio $Z_m/Z_{\frac{1}{2}}$ in Glauert's solution varied slowly with the Reynolds number $\frac{U_m(Z_{\frac{1}{2}}-Z_m)}{\nu}$, where $Z_{\frac{1}{2}}$ is the ordinate to the

point in the outer mixing region for which $U/U_m = 0.5$ and Z_m is the ordinate of the maximum velocity point. Glauert found from Bakke's experiments that the velocity distribution parameter α was 1.2 at a Reynolds number of 4×10^4, which is close to that in the tests described below. With this value of α, $Z_m/Z_{\frac{1}{2}} \simeq 0.14$ and also at this Reynolds number Glauert predicted that

$$U_m \sim R^{-1.096} \text{ and } Z_{\frac{1}{2}} \sim R^{1.01} \qquad (6.1)$$

where the exponents are only slowly varying functions of Reynolds number.

For the two-dimensional case at this same value of the Reynolds number Glauert gave the peak mean velocity and thickness variation as

$$U_m \sim x^{-0.49} \text{ and } Y_{\frac{1}{2}} \sim x^{0.9} \qquad (6.2)$$

where $Y_{\frac{1}{2}}$ denotes the jet half-thickness. Bradshaw et al. (1960) have shown that Glauert's mean velocity profile for the radial wall jet closely agrees with the measured two-dimensional profile at the same Reynolds number over the outer region.

6.2 The test facilities

The radial wall jet

The test rig, shown in figures 41a and 41b, was geometrically

similar to that used by Bakke (1957). The jet diameter was 1.5 inches and air was supplied from pressurised reservoir tanks via a 6 inch diameter throttling valve and 200 feet of 6 inch diameter pipe, part of the laboratory ring-main supply, which passed horizontally 18 feet above the test site. The vertical downpipe was 3 inches diameter and 10 feet long, connected to the 6 inch main through a 3 inch isolating valve. This was followed by a smooth contraction containing a wire gauze and then 5 feet of 1.5 inch diameter smooth-bore pipe fitted with a 6 inch diameter flange to form the jet. The flange was 0.75 inch above the plate.

The plate was a smooth Tufnol sheet of 2 inches thickness and about 100 lb. weight. The plate was mounted horizontally on a steel framework which rested on the laboratory concrete floor. A massive plate was chosen as a precautionary measure against possible vibration of the plate from the jet impingement.

The test procedure was to open the 3 inch isolating valve fully and to control the air-flow by the main 6 inch valve at the reservoir tank. This was necessary to keep the noise from the isolating valve to a minimum.

The measuring region on the plate was 3 to 10 jet diameters from the jet axis, over which the jet half width $Z_{\frac{1}{2}}$ varied from 0.4 to 1.2 inches with a chosen maximum velocity range U_m of 140 to 40 ft/sec. The speed and thickness range corresponded to a Reynolds number $\frac{U_m (Z_{\frac{1}{2}} - Z_m)}{\nu} \simeq 3 \times 10^4$.

The two-dimensional wall jet

The two-dimensional wall jet facility is shown in figures 48a and 48b. Air was blown over a heavy smooth plywood plate, of 2 inches thickness, through a slot that was 0.1 inch wide and 12 inches long. The slot was part of a steel fabricated blowing box which was connected to the laboratory compressed air ring main through 3 inch diameter rubber hoses and an isolating valve. To ensure uniformity of the flow the blowing box contained a gauze and also flow straighteners at the slot corners and the box was supplied with air at both ends. The plate was fitted with sideplates to prevent strong three-dimensional effects. At the first measuring station x = 3 in. the flow mean velocity had attained quite acceptable spanwise uniformity.

Over the measuring region x = 3 to 5 inches the jet half-width varied from 0.28 to 1.03 inches with a chosen maximum velocity range of 170 to 80 ft/sec. corresponding to a Reynolds number, $\frac{U_m(Y_{\frac{1}{2}}-Y_m)}{\nu}$, in the range 3 to 4 x 10^4.

7.3 Discussion of results

7.3.1 The mean velocity profiles

The mean velocity profiles, measured using a pitot tube, for the radial and two-dimensional wall jets are shown in figures 42a and 49a respectively and were in good agreement with the outer layer profile calculated by Glauert corresponding to the test

Reynolds numbers. No corrections for turbulence or mean flow angle were made to the pitot tube readings, which explains the departure of the measured profiles from the theoretical profile at the outer edge of the layer. Here the relative turbulence level was not only high but the effect of entrainment meant that the mean flow angles were probably of the order of $40 - 50^{\circ}$.

The inner layer in the experiments was extremely thin and so for a more thorough investigation of the inner region profile it would have been preferable to use a hot-wire, especially near the wall. However, as will be seen below, it is the outer layer which is of greater interest here.

The positions of the velocity maxima were difficult to determine because of the roundness of the velocity profiles near the peak velocity region. In the radial case $Z_m/Z_{\frac{1}{2}} \simeq 0.18$, a value in fair agreement with Glauert's predicted thickness ratio of 0.14. The measured thickness ratio $Y_m/Y_{\frac{1}{2}}$ for the two-dimensional wall jet was also very close to this predicted value.

The maximum velocity U_m and the jet half-thickness $Z_{\frac{1}{2}}$ are plotted logarithmically against the radius R for the radial case in figure 45, and it is shown that

$$U_m \sim R^{-1.0} \text{ and } Z_{\frac{1}{2}} \sim R^{0.94} \qquad (6.3)$$

From the two-dimensional result, shown in figure 52,

$$U_m \sim x^{-0.46} \text{ and } Y_{\frac{1}{2}} \sim x^{0.9} \qquad (6.4)$$

These results (6.3) and (6.4) are, to the accuracy of measurement, in good agreement with Glauert's predicted variations of the maximum velocity and half-thickness given in equations (6.1) and (6.2).

At the time of commencement of the pressure measurements in the wall jet, no turbulent velocity data had been published by other workers. In order to perform an order of magnitude calculation for the mean square wall pressure. a comprehensive set of turbulent intensity and scale measurements were made for both cases of the wall jet using the hot-wire turbulence equipment described in section 3.6.

The measurements of the intensities of the longitudinal velocity component $u_2' = \sqrt{\overline{u_2^2}}$, and the lateral component $u_2' = \sqrt{\overline{u_2^2}}$ normal to the plate, and their one dimensional spectra, are plotted in figures 42b and 43a respectively for the radial case and figures 49b and 50a for the two-dimensional case. These measurements show, together with the spatial correlation measurements plotted in figures 47 and 54, that the turbulent flow in the outer region was very closely self-preserving in both cases.

One of the reasons why the wall jet was a sensible model for turbulent fluctuating pressure measurements was demonstrated by the large

turbulent intensity levels that were measured. For instance, over a considerable part of the wall jet profile, including the peak velocity region, the intensity of the longitudinal turbulent velocity component was over 40% of the maximum velocity U_m for the radial case and over 20% for the two-dimensional case, with the lateral turbulent intensity about half of these values.

It should be noted that no corrections to the turbulent velocity measurements were made to take account of the non-linear response of the hot-wire. This error would be expected to be largest near the outer edge of the layer where the local turbulent intensity was high. For turbulent intensities of order 25% the error could be of order 10%, and greater for larger intensities. For the present purposes 10 - 20% accuracy was sufficient and so resort to complicated linearising circuits was not necessary. Also no corrections were made to the readings to allow for the mean velocity angle which, for the reason given in the discussion of the mean velocity measurements, would be expected to be important only at the outer edge of the layer. It is noted that the measurements of turbulent intensity for the two-dimensional case were in good agreement with the preliminary results reported by Bradshaw et al. (1960).

Shortage of time only allowed the six spatial correlations coefficients $\bar{R}_{11}(x)$ and $\bar{R}_{22}(x)$ of the turbulent velocity in the half-jet region to be measured. Examination of the results

plotted in figures 47 and 54 shows that the longitudinal scale L_1 was about twice the lateral scale L_2 for both wall jet cases, with the lateral scale $L_2 \simeq 0.5\ (Z_{\frac{1}{2}} - Z_m)$ for the radial case and $L_2 \simeq 0.4\ (Y_{\frac{1}{2}} - Y_m)$ for the two-dimensional case. It would be expected that the anisotropy factor α, to be used in the root-mean-square calculations in the following section, would not be quite as small as the value for the boundary layer case where $L_1 \simeq 4L_2$ and where α was taken as $\frac{1}{3}$. The correlations in the r_3 direction (r_3 being the transverse separation parallel to the wall) for the radial case had a larger scale than in the two-dimensional case. This was probably due to the radial spreading of the former.

The spectra and scale measurements were taken at a point well into the outer region. This was chosen because the fluctuating wall pressure measurements, to be described in the next paragraph, showed clearly that the main contribution came from this region.

Fluctuating wall pressure measurements

The non-dimensional root-mean-square fluctuating wall pressure was found to be constant with downstream distance (see figure 55) with the values

$$\sqrt{\overline{p^2}}/\tfrac{1}{2}\rho U_m^2 = 0.134 \qquad (6.5)$$

for the radial case (which differs from the value 0.11 quoted by Hodgson and Lilley (1960) because of improved calibration of the pressure transducers) and

$$\sqrt{\overline{p^2}}/\tfrac{1}{2}\rho_0 U_m^2 = 0.045 \qquad (6.6)$$

for the two-dimensional case.

No variation of these results with transducer diameter, from measurements with both the M213 and BK4133 transducers, was detected so only the measurements taken with the M213 transducer have been presented. This is also shown by the spectra measurements plotted non-dimensionally against the Strouhal number in figures 43b and 50b, for over the main energy containing Strouhal number range there was a reasonable collapse of the measured results. The reason for the relatively high resolving power of the transducers, as compared with the boundary layer tests, was because the main energy containing frequencies were an order of magnitude lower than those in the boundary layer tests at the same Strouhal number, that is the wave-length or scale of the fluctuations was much larger.

The fact that the scale and magnitude of the measured pressure fluctuations were large, together with the constancy of the values of the non-dimensional root-mean-square wall pressure (6.5) and (6.6) with distance as was to be expected for a self-preserving flow, suggested that it was mainly the half-jet flow which contributed

most to the fluctuating wall pressure. This is shown clearly by comparing the measured turbulent velocity spectra in the outer region (see figures 43a and 50a) with the measured fluctuating wall pressure spectra, for the dominant energy containing range of the Strouhal number was of the same order in both cases.

Further confirmation of the above is obtained by considering the contribution from the inner region. The value of the skin friction coefficient in these tests can be inferred from Bradshaw's measurements to be of order $C_f = 0.006$. Hence with the boundary layer measurement previously given in section 4, where $\sqrt{\overline{p^2}}/\frac{1}{2}\rho_o U_1^2 = 2.2\ C_f$, the contribution from the inner layer to the non-dimensional wall pressure was of order 0.013, a value small compared with the measured values (6.5) and (6.6). Also the inner region, in the tests described, was very thin which meant that the transducer diameter to the inner layer thickness ratio was high (equivalent to a d/δ_1 ratio $\simeq 10$ to 30). Hence the M213 transducers, used in the tests, would measure only a small part of the inner region contribution because of the lack of resolving power at such a high d/δ_1 ratio.

It was to be expected from the large turbulent pressure signals that were measured, that the ratio of the turbulent pressure to any extraneous signals would have been high. In fact this ratio was nearly 40 decibels and was measured by placing a small streamlined section just ahead of the measuring station, preventing

flow across the transducer face. Thus extraneous signals from acoustic radiation from the jet exit, or acceleration pick-up in the transducer through vibration of the plate, were negligible relative to the turbulent pressure signal.

The most striking property of the wall pressure fluctuations from a comparison between the pressure and velocity spectra (see figures 43a,43b and 50a,50b) was the falling of the pressure spectra levels at low Strouhal numbers. The form of the variation of the measured pressure spectra with the Strouhal number agreed closely with the boundary layer pressure measurements on the glider (see figure 34). The falling spectrum level at low frequencies is regarded as confirmation of the assumption that was first made in section 2, namely that the main contribution to the fluctuating pressure in turbulent shear flows comes from the turbulence-mean shear interaction, for as was shown in the calculations of section 5 the pressure spectrum should have this form at low frequencies. It might be noted that had the turbulence-turbulence interaction been important the wall pressure frequency spectra would have been asymptotic to a non-zero value at low frequencies (see figure 40 and Appendix B).

Spatial correlations of the wall pressure

The transverse and longitudinal spatial correlation coefficients

of the wall pressure are plotted in figures 46 and 53. The transverse correlations decreased quite definitely to zero, indicating the freedom from interference to the measured turbulent signals by acoustic noise (which would have correlated significantly at large distances). The absence of a negative loop in the transverse measurements was further confirmation that the turbulence-turbulence contribution was very small. The transverse scale of the wall fluctuating pressure was of the order of the total jet thickness.

The curves of the longitudinal correlation coefficient for the upstream and downstream directions, although asymmetric because of the rapid growth of the layer, had relatively large negative values of order 0.2 to 0.3. The important discovery from these curves is that, to experimental accuracy, the integral under the longitudinal correlation curve is zero. This is believed to be the first experimental confirmation of the validity of the incompressible boundary condition governing the wall pressure covariance $P(\xi_1, o, \xi_3)$, that was first formulated by Phillips (1954) and given previously in section (2.3). That was

$$\int_{-\infty}^{\infty} \int_{-\infty}^{\infty} P(\xi_1, o, \xi_3) d\xi_1 d\xi_3 = 0 \qquad (6.7)$$

for a plane surface, where it should be noted that the vanishing of the integral in equation (6.7) was satisfied in the wall jet case

because

$$\int_{-\infty}^{\infty} P(\xi_1,o,o)d\xi_1 = 0 \qquad (6.8)$$

In fact, see section 5, this is just the way in which the turbulence-mean shear contribution to the wall fluctuating pressure would be expected to satisfy the Phillip's boundary condition.

Space-time correlations of the wall pressure

It is not possible to make use of the simple convected hypothesis of the pressure field to relate the autocorrelation to the longitudinal correlation because of the large variation of the mean velocity U with distance. However, the negative loop in the autocorrelation coefficient of the wall pressure (that is for $\xi_1 = o$) shown in figures 44 and 51 is consistent with the negative loops obtained in the longitudinal spatial pressure correlation measurements. It may be noted that to within experimental accuracy, the integral of the autocorrelation curves also vanished, which was consistent with the falling spectral measurements at low frequencies.

At the close transducer spacings the variation of the mean velocity over the separation distance is only small, and so we can obtain the local averaged convection speed U_c of the pressure pattern from the optimum time delay for these spacings. The results

show that

$U_c \simeq 0.93\ U_m$ for the radial case

and $U_c \simeq 0.88\ U_m$ for the two-dimensional case.

From the remarks made earlier that the half-jet flow must provide the main contribution to the wall fluctuating pressure, these convection speeds show that the dominant contribution comes from the region $Z/Z_{\frac{1}{2}}$ (or $Y/Y_{\frac{1}{2}}$) equal to 0.3 - 0.6.

6.3 Calculation of the wall root-mean-square pressure

In view of the rather complicated nature of the wall jet flow with the rapid growth of the layer and variation of the peak velocity, only an approximate calculation of the wall fluctuating pressure will be made. Nevertheless, the calculation does illustrate further many of the points made previously.

If we neglect the effects of inhomogeneity of the flow in the streamwise direction, and make the further assumption that the expression for the wall fluctuating pressure is the same in both the radial and two-dimensional cases and arises from the turbulence-mean shear contribution only, it was shown in section (5.1) that approximately

$$\overline{p^2} \simeq \frac{8\rho_0}{15}\,\alpha\,\bar{e}_{12}^{\,2}\ \overline{u_2^2}\ L_2^2 \qquad (6.9)$$

where $\bar{e}_{12}$, $\overline{u_2^2}$ and L_2 are representative values for the mean shear,

lateral turbulent intensity and lateral scale across the layer, and α is a factor less than unity to take account of anisotropy.

For the radial wall jet the values of $\bar{e}_{12}$ and $\overline{u_2^2}/U_m$ are nearly constant over most of the outer region and have values $\frac{0.6U_m}{Z_{\frac{1}{2}}-Z_m}$ and 0.22 respectively. If we take the lateral scale $L_2 = Z_{\frac{1}{2}}-Z_m$ as a representative value for the whole outer region based on the scale measurements at $Z/Z_{\frac{1}{2}} = 0.6$, then on substituting these values in equation (6.9) for the wall mean-square pressure, we obtain

$$\sqrt{\overline{p^2}}/\tfrac{1}{2}\rho_o U_m^2 \simeq 0.14 \qquad (6.10)$$

where the anisotropy factor $\alpha = \frac{1}{2}$, which is based on the longitudinal and lateral velocity scale measurements.

Similarly, if for the two-dimensional wall jet, we take $\bar{e}_{12} = \frac{0.6U_m}{Y_{\frac{1}{2}}-Y_m}$, $\frac{\overline{u_2^2}}{U_m^2} = 0.11$ and the scale $L_2 = 0.8\,(Y_{\frac{1}{2}}-Y_m)$, then with the same value for α we obtain

$$\sqrt{\overline{p^2}}/\tfrac{1}{2}\rho_o U_m^2 \simeq 0.055 \qquad (6.11)$$

These two calculations are in good agreement with the measured values (6.5) and (6.6). The ratio of the measured scales for the radial and two-dimensional cases, which was 5:4, and the ratio of 2:1 for the

turbulent intensities very nearly explains the 3:1 ratio of the measured values of the non-dimensional wall fluctuating pressure. The tendency towards greater anisotropy in the two-dimensional case could probably account for the calculated value being too high.

The interesting points to note in these calculations of the wall fluctuating pressure is the dominance of the turbulence-mean shear contribution of the outer region of the flow. Although the mean shear in the outer part of the layer is much smaller than that in the inner 'turbulent boundary layer type' flow, it was the large scale of the motion in the outer region which accounted for its greater contribution to the wall fluctuating pressure.

7. The noise radiated from a turbulent shear flow over a plane rigid surface

7.1 Lighthill's theory of aerodynamic noise from free turbulent flows

The theory of the generation of sound by turbulent flows has been given by Lighthill (1952, 1954) in great detail. He showed that the turbulent flow could be regarded as equivalent, acoustically, to a distribution of quadrupoles, whose strength per unit volume at any instant is

$$T_{ij} = \rho u_i u_j + p_{ij} - a_o^2 \rho \, \delta_{ij} \quad , \tag{7.1}$$

placed in an acoustic medium at rest, where p_{ij} is the compressive stress tensor and a_o is the velocity of sound in the medium.

The propagation of sound is governed by the equation

$$\frac{\partial^2 \rho}{\partial t^2} - a_o{}^2 \nabla^2 \rho = \frac{\partial^2 T_{ij}}{\partial x_i \partial x_j} \tag{7.2}$$

Lighthill solved equation (7.2) for the case of free turbulence in the absence of boundaries in the form

$$(\rho - \rho_o)(\underset{\sim}{x},t) = \frac{1}{4\pi a_o{}^2} \frac{\partial^2}{\partial x_i \partial x_j} \int T_{ij}(\underset{\sim}{y},t^*) \frac{d\underset{\sim}{y}}{|\underset{\sim}{x}-\underset{\sim}{y}|} \tag{7.3}$$

where $\underset{\sim}{x}$ is the field point and $\underset{\sim}{y}$ is the source point, and where the value of T_{ij} must be evaluated at the retarded time $t^* = t - \frac{|\underset{\sim}{x}-\underset{\sim}{y}|}{a_o}$

to allow for the different times of emission of sound waves from the source points $\underset{\sim}{y}$ that reach the field point $\underset{\sim}{x}$ simultaneously.

From equation (7.3) Lighthill showed that the intensity $i(\underset{\sim}{x})$ of the noise at a point $\underset{\sim}{x}$ many acoustic wavelengths from unit volume of turbulence placed at the origin of a turbulent flow region, itself small compared with $|\underset{\sim}{x}|$, is

$$i(\underset{\sim}{x}) = \frac{x_i x_j x_l x_m}{16\pi^2 \rho_o a_o^5 x^6} \int \overline{\frac{\partial^2 T_{ij}}{\partial t^2}(o,t^*) \frac{\partial^2 T_{lm}}{\partial t^2}(\underset{\sim}{z},t'^*)} d\underset{\sim}{z} \qquad (7.4)$$

where t^* and t'^* denote the retarded times between signals emitted separately at O and $\underset{\sim}{z}$ respectively and those received simultaneously at the distant point $\underset{\sim}{x}$ at time t, say. The integration is performed over the whole turbulent region. The covariance of $\frac{\partial^2 T_{ij}}{\partial t^2}$ will, however, be zero at all distances beyond a region comparable roughly with the average eddy size.

The covariance of $\frac{\partial^2 T_{ij}}{\partial t^2}$ in equation (7.4) is to be evaluated at retarded times but, as Lighthill has suggested, if the turbulence is at rest or moving at low Mach number the retarded time differences are negligible compared with times significant in the turbulence so that in some cases the covariance may be treated as a simultaneous covariance.

When the Mach number is not small the covariance of $\frac{\partial^2 T_{ij}}{\partial t^2}$ must be evaluated at retarded times. Lighthill showed, however, that the importance of the retarded times may be minimised in

equation (7.4) by viewing the turbulence in a moving frame of reference such that the time scale of $\frac{\partial^2 T_{ij}}{\partial t^2}$ is greatest, that is moving at a speed which Lighthill called the 'local eddy convection speed' or what we have called the average convection speed, U_c.

If $M_c = U_c/a_o$ is the eddy convection Mach number then the modification of equation (7.4) to moving axes is

$$i(\underset{\sim}{x}) = \frac{x_i x_j x_l x_m}{16\pi^2 \rho_o a_o^5 (\underset{\sim}{x}-\underset{\sim}{M}_c \cdot \underset{\sim}{x})^6} \int \overline{\frac{\partial^2 T_{ij}(o,t^*)}{\partial t^2} \frac{\partial^2 T_{lm}(\underset{\sim}{z},t'^*)}{\partial t^2}} d\underset{\sim}{z} \qquad (7.5)$$

where now T_{ij} is specified in the frame of reference moving at the speed U_c. Usually, with the same reasoning as above, the retarded time covariance can be replaced by the simpler simultaneous covariance.

In a region of intense mean shear, for instance in the mixing region of a jet, Lighthill then showed that the main contribution to $\frac{\partial^2 T_{ij}}{\partial t^2}$ is $\bar{e}_{ij} \frac{\partial p}{\partial t}$ where $\bar{e}_{ij} = \frac{\partial U_i}{\partial x_j} + \frac{\partial U_j}{\partial x_i}$ is the mean rate of strain. If the mean shear is $\bar{e}_{12}$ and is taken as constant, the sound power output P_V per unit volume of turbulence at the origin, found from equation (7.5) by integrating over a large sphere centred about $\underset{\sim}{x} = o$, is

$$P_V \simeq \frac{[1 + O(M_c^2)]}{15\pi\rho_o a_o^5} \bar{e}_{12}^2 \int \overline{\frac{\partial p(o,t^*)}{\partial t} \frac{\partial p(\underset{\sim}{z},t'^*)}{\partial t}} d\underset{\sim}{z} \qquad (7.6)$$

Thus the important quantity that is required is the $\frac{\partial p}{\partial t}$ retarded

time covariance. There is no obvious reason a priori why the simultaneous covariance of $\frac{\partial p}{\partial t}$ should vanish. Hence if we neglected retarded times and therefore use the simultaneous covariance in equation (7.6) then following Lighthill, we may write

$$P_V \simeq \frac{[1 + O(M_c^2)]}{15\pi\rho_o a_o^5} \cdot \bar{e}_{12}^2 \overline{\left(\frac{\partial p}{\partial t}\right)^2} V \qquad (7.7)$$

where $\overline{\left(\frac{\partial p}{\partial t}\right)^2}$ is to be evaluated in the moving frame, and in this frame V is defined to be

$$V = \int \frac{\overline{\frac{\partial p}{\partial t}(o,t)\,\frac{\partial p}{\partial t}(\underset{\sim}{z},t)}}{\overline{\left(\frac{\partial p}{\partial t}\right)^2}}\, d\underset{\sim}{z} \qquad (7.8)$$

which Lighthill has called the 'average eddy volume'. Lilley (1958) has calculated $\overline{\left(\frac{\partial p}{\partial t}\right)^2}$ and V from the Poisson equation (2.3) for a two-dimensional mixing region using kinematically possible forms of the velocity correlations. It may be noted that the radiated noise from low Mach number flows can always be evaluated from the appropriate covariance in the Lighthill theory by finally assuming to a good approximation that the turbulence flow is incompressible.

As mentioned previously, measurements of the fluctuating pressure within a turbulent flow are not practically feasible with present transducers and therefore measurements of the critical source terms

in Lighthill's theory of the noise from free turbulent flows are not yet available. However, in the case of turbulent shear flows over plane boundaries we can make use of the wall fluctuating pressure measurements described in sections 4 and 6 to investigate these critical source terms.

7.2 Theory of the noise radiated from a turbulent shear flow over a rigid plane boundary.

Curle (1955) has used the general solution of the inhomogeneous wave equation (7.2) for the case of turbulent flow in the presence of a rigid boundary S and obtained the fluctuating density of the radiated noise field as

$$\rho-\rho_o = \frac{1}{4\pi a_o^2} \frac{\partial^2}{\partial x_i \partial x_j} \int_v T_{ij}(\underset{\sim}{y},t^*) \frac{d\underset{\sim}{y}}{|\underset{\sim}{x}-\underset{\sim}{y}|}$$

$$- \frac{1}{4\pi a_o^2} \frac{\partial}{\partial x_i} \int_s P_i(\underset{\sim}{y},t^*) \frac{dS(\underset{\sim}{y})}{|\underset{\sim}{x}-\underset{\sim}{y}|} \qquad (7.9)$$

If this result is compared with the corresponding result obtained by Lighthill for free turbulent flows equation (7.3), it may be seen that the latter is modified by an additional term which is a surface integral involving a distribution of dipoles with strength P_i per unit area, where P_i is exactly the force per unit area exerted by

the solid boundaries on the fluid in the x_i direction.

By using the particular image Green's function for a plane surface Doak (1960) has obtained the solution of the inhomogeneous wave equation (7.2) in a form more easily interpreted in terms of the wall fluctuating pressure measurements. He found that the corresponding result to equation (7.4) the far-field radiated noise intensity $i(\underset{\sim}{x})$ from unit area of the plane surface $x_2 = o$ centred about the origin is

$$i(\underset{\sim}{x}) = \frac{x_2^2}{4\pi^2 \rho_o a_o^3 x^4} \int \overline{\frac{\partial p(o,t^*)}{\partial t} \frac{\partial p(\underset{\sim}{z},t'^*)}{\partial t}} dS(\underset{\sim}{z}) \qquad (7.10)$$

where Doak argued that the corresponding volume integral was negligible compared with the surface integral.

If the flow Mach number is small the approximation might be made, as has been used in the free turbulence problem, that the retarded time $\frac{\partial p}{\partial t}$ covariance in equation (7.10) can be replaced by the simpler simultaneous covariance. Hence it would seem plausible to evaluate the $\frac{\partial p}{\partial t}$ simultaneous covariance from measured wall fluctuating pressures or alternatively, following the work of Lilley (1958), this covariance could be calculated on the assumption of incompressible turbulent flow.

It is necessary to emphasize at this stage, as will be shown later, that the correlation area equivalent to the surface integral in equation (7.10) is, at the most, $O(\delta^2)$ where δ is the thickness of the shear layer, and is therefore very nearly vanishingly small. It is for

this reason that great care must be taken in the covariance evaluation.

The wall pressure correlation measurements, for both the turbulent boundary layer and wall jet flows over a plane surface, have shown that significant areas of negative correlation exist (see, for instance, figures 56a and 56b). The wall jet measurements, the glider boundary layer measurements and, to a lesser extent, the $2\frac{1}{2}$in. x $2\frac{1}{2}$in. tunnel measurements have all shown that in low Mach number flows the area integral of the simultaneous wall pressure covariance, to experimental accuracy, vanishes. Also the incompressible calculations of the wave-number spectrum $\Pi(\underset{\sim}{k})$ for the turbulence-mean shear and the turbulence-turbulence contributions have shown that $\Pi(\underset{\sim}{k})$ vanishes at $\underset{\sim}{k} = o$. This is, of course, the incompressible boundary condition first given by Phillips (1954) and later by Kraichnan (1956b) that

$$\int_{-\infty}^{\infty}\int_{-\infty}^{\infty} \overline{p(\underset{\sim}{x},t)p(\underset{\sim}{x}',t)}\, dx_1 dx_3 = o \qquad (7.11)$$

for plane boundaries, where $\underset{\sim}{x}$ and $\underset{\sim}{x}'$ are points on the surface. That is, the total instantaneous force on the plane boundary is zero. In particular the condition given in equation (2.45) is relevant here, namely that at the surface

$$\int_{-\infty}^{\infty}\int_{-\infty}^{\infty} \overline{\frac{\partial p(\underset{\sim}{x},t)}{\partial t}\frac{\partial p(\underset{\sim}{x}',t)}{\partial t}}\, dx_1 dx_3 = o \qquad (7.12)$$

Hence we see that the estimation of the noise radiated by turbulent flows over plane surfaces from calculations or measurements of the simultaneous $\frac{\partial p}{\partial t}$ covariance is a particular case in that this simultaneous covariance must exactly vanish. Therefore in calculating the radiated noise using equation (7.10) the retarded times must be retained, even if the covariance is referred to axes moving with the average convection speed.*

If, following Lilley (1958), we write $dW(\underset{\sim}{k},\omega)$ as the Fourier Stieltjes transform of the wall fluctuating pressure, that is

$$\frac{\partial p}{\partial t}(\underset{\sim}{y},t) = i\iint \omega e^{i\omega t} e^{i\underset{\sim}{k}\cdot\underset{\sim}{y}} dW(\underset{\sim}{k},\omega) \qquad (7.13)$$

where $\underset{\sim}{y} = (y_1, o, y_3)$ and $\underset{\sim}{k} = (k_1, k_3)$ the two-dimensional wave-number vector in the plane, then at the retarded time t^*

$$\frac{\partial p}{\partial t}(\underset{\sim}{y},t^*) = i\iint \omega e^{i\omega(t-\frac{x}{a_o})} e^{i\omega\frac{\underset{\sim}{x}\cdot\underset{\sim}{y}}{a_o x}} e^{i\underset{\sim}{k}\cdot\underset{\sim}{y}} dW(\underset{\sim}{k},\omega) \qquad (7.14)$$

since $t^* = t - \frac{|\underset{\sim}{x}-\underset{\sim}{y}|}{a_o} \simeq t - \frac{x}{a_o} + \frac{\underset{\sim}{x}\cdot\underset{\sim}{y}}{a_o x}$

The $\frac{\partial p}{\partial t}$ covariance, evaluated at retarded times, is then

$$\overline{\frac{\partial p}{\partial t}(\underset{\sim}{y},t^*)\frac{\partial p}{\partial t}(\underset{\sim}{z},t'^*)} = \iint \omega^2 e^{i\underset{\sim}{k}\cdot\underset{\sim}{\xi}} e^{-i\omega\frac{\underset{\sim}{x}\cdot\underset{\sim}{\xi}}{a_o x}} \overline{\Pi}(\underset{\sim}{k},\omega) d\underset{\sim}{k}\, d\omega \qquad (7.15)$$

---

* The argument given by Phillips (1954, 1956), that the dipole radiation from a turbulent flow over an infinite flat plate is zero, cannot be justified since it is based on the condition of the vanishing of the simultaneous covariance.

where the separation distance $\underset{\sim}{\xi} = (\xi_1, o, \xi_3) = \underset{\sim}{z} - \underset{\sim}{y}$, and so the area integral A of the retarded time $\frac{\partial p}{\partial t}$ covariance is

$$A(\underset{\sim}{x}) = \int \overline{\frac{\partial p(\underset{\sim}{y}, t^*)}{\partial t} \frac{\partial p(\underset{\sim}{z}, t'^*)}{\partial t}} dS(\underset{\sim}{\xi})$$

$$= \int \omega^2 \Pi \left(- \frac{\omega \underset{\sim}{\xi}}{a_o x}, \omega \right) d\omega \qquad (7.16)$$

where A depends on the position of the field point relative to the origin.

Lilley (1958), Lighthill (1961) and J. Williams (1960) have all observed that in most cases $\Pi(- \frac{\omega \underset{\sim}{\xi}}{a_o x}, \omega)$ is practically equal to $\Pi(o, \omega)$. Of course in the present case $\Pi(o, \omega)$ for an incompressible flow is zero. Thus the effect of the retarded times must be taken into account. The calculation of equation (7.16) will not be performed here but it could be evaluated, following the methods as were used by Lilley for the free shear flow case, using incompressible calculations from the Poisson equation (2.3) for the wall fluctuating pressure.

To conclude this discussion of the theory of dipole noise radiated from turbulent shear flows over rigid boundaries, it is worth calculating the order of magnitude of the effective correlation area A of the dipole sources for the boundary layer case, using the measurements of the noise radiated from the turbulent flow on a cowled circular cylinder by Wilson (1959) and the boundary layer wall pressure measurements described in Section 4. Since we are

concerned with an order of magnitude calculation we will use Doak's result in equation (7.10) for the plane surface problem to obtain the noise power output per unit length of the cylinder as

$$P_c \approx \frac{[1+O(M_c)^2]R}{3\rho_o a_o^3} \cdot \overline{\left(\frac{\partial p}{\partial t}\right)^2} \quad \bar{A} \qquad (7.17)$$

where R is the cylinder radius and is the corresponding equation to equation (7.7) for the free turbulence case where $\overline{\left(\frac{\partial p}{\partial t}\right)^2}$ will now be evaluated in the moving frame and $\bar{A}$ is the average over angles of the correlation area $A(\chi)$ of the dipole sources, in the moving frame.

If ${}^{m}\Pi(\omega)$ is the frequency spectrum of the 'true' time fluctuations of the wall pressure that would be measured in the frame of reference moving at the speed U_c, then

$$\overline{\left(\frac{\partial p}{\partial t}\right)^2} = \int_{-\infty}^{\infty} \omega^2 {}^{m}\Pi(\omega) d\omega \qquad (7.18)$$

From the space-time correlation coefficient measurements of the boundary layer fluctuating wall measurement shown in figure 22 we can obtain the autocorrelation coefficient ${}^{m}\bar{P}(\tau)$ of the 'true' time fluctuations since it is the envelope of the optimum time delay correlation maxima.

If we take ${}^{m}\bar{P}(\tau)$ to have the form $e^{-\omega_o^2 \tau^2}$, where ω_o is the reciprocal of the integral time scale T of the 'true' time fluctuations as measured in the moving frame, then the pressure

spectrum is

$$ {}^{m}\Pi(\omega) = \overline{p^2} \cdot \frac{1}{\omega_o \pi} \cdot e^{-\omega^2 / 4\omega_o^2} \qquad (7.19) $$

which gives, from equation (7.18), the value of $\overline{\left(\frac{\partial p}{\partial t}\right)^2}$ as $\overline{p^2}\omega_o^2$. From figure 22 the autocorrelation coefficient $\bar{P}_m(\tau)$ has the value 0.5 when $\tau = 0.2 \times 10^{-3}$ seconds or $\omega_o \simeq 4 \times 10^3$ radians/sec. and $\frac{\omega_o \delta_1}{U_1} = 0.05$. Hence

$$ \overline{\left(\frac{\partial p}{\partial t}\right)^2} = (0.05)^2 \, \overline{p^2} \left(\frac{U_1}{\delta_1}\right)^2 \qquad (7.20) $$

the same value as was calculated by Lighthill (1961) from Willmarth's measurements.

It should be noted that equation (7.20) is probably a lower estimate since the form $e^{-\omega_o^2 \tau^2}$ is not an accurate description of the measured moving frame autocorrelation for the boundary layer, as can be seen from figure 22 or from the results of Willis described by Richards (1961). This was also the case for the wall jet, see the space-time correlation measurements shown in figures 44 and 51. But if we used the form $e^{-\omega_o \tau}$, which fits the experimental curves for values of the time delay τ not too small, the value of $\overline{\left(\frac{\partial p}{\partial t}\right)^2}$ would then be infinite!*

* Of course, it is because the value of $\overline{\left(\frac{\partial p}{\partial t}\right)^2}$ depends on the higher frequency part of the spectrum ${}^{m}\Pi(\omega)$, that is on the smaller time delays in the moving frame autocorrelation ${}^{m}P(\tau)$ which are difficult to obtain with present instrumentation, which prevents an exact evaluation.

It may be noted from Lighthill's theory that, neglecting Doppler effects, a fair estimate of $\overline{\left(\frac{\partial p}{\partial t}\right)^2}$ in the moving frame is $\omega_d^2 \overline{p^2}$ where ω_d is a dominant frequency of the radiated sound. From Wilson's measurements $\omega_d \simeq 0.2$ to $0.4\ U_1/\delta_1$.

Wilson also confirmed that the radiated noise intensity was proportional to U_1^6, that is dipole radiation, and measured the acoustic efficiency η, from a knowledge of the input power to drive the cylinder and the integral around the cylinder of the noise output power, to be $0.3 \times 10^{-6} M^3$ where the test reference Mach number was 0.228.

Hence from equation (7.17) and the value of ω_d above we have

$$\eta = \frac{\omega_d^2 \overline{p^2}\ \bar{A}\ R}{3\rho_o a_o^3 (\frac{1}{2}\rho_o U_1^2 C_f) U_1\ 2\pi R} = 0.3 \times 10^{-6} M^3 \qquad (7.21)$$

If we take $\sqrt{\overline{p^2}}/\frac{1}{2}\rho_o U_1^2 = 2.2\ C_f$ from the experimental results of section 4 and put the skin friction coefficient $C_f = 0.0025$, say, then

$$\bar{A} \simeq 0.02 \text{ to } 0.1 \delta_1^2 \qquad (7.22)$$

which is an exceedingly small quantity. It is therefore clear that with the accuracy of present instrumentation it is almost impossible to measure $\bar{A}$ to the required accuracy.

This value of $\bar{A}$ may be compared firstly with the value deduced from the results of Harrison (1958) by Doak (1960) who squared the transverse scale or longitudinal scale of the wall pressure and obtained $\bar{A} = 170\delta_1^2$.

which gave an acoustic efficiency $\eta = 0.6 \times 10^{-2} M^3$, that is three orders of magnitude greater than Wilson's measurement, and secondly with the estimate made by Lighthill (1961) who took the integrated value of Willmarth's fixed-frame autocorrelation curve as the effective radius of the correlation area and obtained $\bar{A} = (1.2\delta_1)^2$ with a corresponding acoustic efficiency of $10^{-6} M^3$. It is clear from the assumptions made that even the latter calculation is still an upper estimate.

Finally we can compare the radiated dipole power to the radiated quadrupole power, on the assumption that the strength of the quadrupole sources in the boundary layer are similar to those in the jet, using Wilson's acoustic efficiency measurement and the result given by Lilley (1958) that the total quadrupole acoustic power ouput from unit volume of turbulence at the origin is given approximately by

$$P_v \simeq \frac{0.3}{a_0^5}\left[1+O(M_c^2)\right] \rho_0^2 \bar{e}_{12} \overline{u_2^2} \; L^5 \alpha \qquad (7.23)$$

where $\overline{u_2^2}$ is the mean square intensity of the lateral turbulent velocity component, L is the turbulent scale and α is an anisotropy factor ($\simeq \frac{1}{3}$).

If we take the mean shear $\bar{e}_{12} = U_1/\delta$, $L = 1.5\delta_1$ and $\overline{u_2^2}/U_1^2 = U_T^2$ from the measurements of Klebanoff (see figures 2 and 3) then for low Mach number turbulent boundary layer flow the ratio

$$\frac{\text{dipole power output}}{\text{quadrupole power output}} = O(M_1^{-2}) \qquad (7.24)$$

which agrees with the estimate by Doak (1960). This confirms the earlier remarks of Lighthill (1952), that at low Mach numbers dipole radiation is more efficient than quadrupole and that in the boundary layer type problems although dipole radiation is small, the quadrupole radiation is even smaller.

Conclusions

The following conclusions were obtained from an experimental and theoretical investigation of the fluctuating pressure in turbulent shear flows at low Mach numbers.

1. The main contribution to the fluctuating pressure in turbulent shear flows was found to arise from the amplifying effect of the mean shear. The root-mean-square value of the non-dimensional wall fluctuating pressure was found to be

$$\frac{\sqrt{\overline{p^2}}}{\frac{1}{2}\rho_0 U_1^2} = 2.2\, C_f$$

for the turbulent boundary layer and

$$\frac{\sqrt{\overline{p^2}}}{\frac{1}{2}\rho_0 U_m^2} = 0.134 \text{ and } 0.045$$

for the radial and two-dimensional wall jets respectively (where U_m is the local peak velocity).

2. The power spectral density of the wall fluctuating pressure, although falling, like the turbulent velocity spectra, with increasing frequency at high frequencies, decreased with decreasing frequency at low frequencies as the square of the frequency.

3. The average convection speed of the fluctuating pressure field as observed at the wall was $\simeq 0.8$ times the external mean velocity for

the turbulent boundary layer case and ≃ 0,9 times the local peak velocity for the wall jets.

4. The surface integral of the measured wall pressure covariance, to within experimental accuracy, was found to vanish for the wall jets and for the turbulent boundary layer when interference effects were absent, as for instance in measurements on a glider wing.

5. An investigation of the source terms responsible for the radiated noise from turbulent shear flow at low Mach numbers over a plane boundary showed that they could only be evaluated from the wall fluctuating pressures if retarded times were included.

Although the experimental programme was restricted to wall fluctuating pressure measurements in wall turbulent shear flows because of current limitations in pressure transducer design, nevertheless the same techniques could be used for measurements within turbulent flows when an acceptable transducer becomes available in the future. The theoretical calculations of the wall fluctuating pressure may easily be extended to evaluate the fluctuating pressure within the turbulent flow.

Appendix A.

The Evaluation of an Integral.

It has been shown in section 2 (see equation 2.21) that the wall pressure covariance is given by the integral

$$I = \frac{\rho_0^2}{\pi^2}\int_{-\infty}^{\infty} dy_1 \int_{0}^{\infty} dy_2 \int_{-\infty}^{\infty} dy_3 \int_{-\infty}^{\infty} dr_1 \int_{-y_2}^{\infty} dr_2 \int_{-\infty}^{\infty} dr_3 R_{22}(y_2;\underset{\sim}{r}) g(y_2) g(y_2+r_2)$$

$$\cdot \frac{\partial}{\partial y_1} \frac{1}{|\underset{\sim}{x}-\underset{\sim}{y}|} \cdot \frac{\partial}{\partial r_1} \frac{1}{|\underset{\sim}{x}-\underset{\sim}{y}-\underset{\sim}{r}|} \qquad (A.1)$$

where $g(y_2) = \sqrt{\overline{u_2^2}}(y_2).\overline{e}_{12}(y_2)$ has been written for convenience.

Kraichnan (1956a) has evaluated a similar integral for the free shear flow case following a method given by Feynman (1949) for integrals which occur in quantum mechanics. Here we will use a similar method to evaluate the integrations over y_1 and y_3 in equation (A.1).

Consider $$I_1 = \int_{-\infty}^{\infty}\int_{-\infty}^{\infty} \frac{\partial}{\partial y_1} \frac{1}{|\underset{\sim}{x}-\underset{\sim}{y}|} \cdot \frac{\partial}{\partial r_1} \frac{1}{|\underset{\sim}{x}-\underset{\sim}{y}-\underset{\sim}{r}|} dy_1 dy_3 \qquad (A.2)$$

This integral is convergent at infinity and will be unaltered by change of origin. We note that $\underset{\sim}{x}$ and $\underset{\sim}{r}$ are constants in the integration.

We define new variables

$$\underset{\sim}{\zeta} = \underset{\sim}{y} - \underset{\sim}{x} \qquad \underset{\sim}{z} = \underset{\sim}{\xi} - \underset{\sim}{r} \qquad (A.3)$$

with the separations $\underset{\sim}{\xi}$ and $\underset{\sim}{r}$ of the field points and source points respectively as before

$$\underset{\sim}{\xi} = \underset{\sim}{x}' - \underset{\sim}{x}, \quad \underset{\sim}{r} = \underset{\sim}{y}' - \underset{\sim}{y}$$

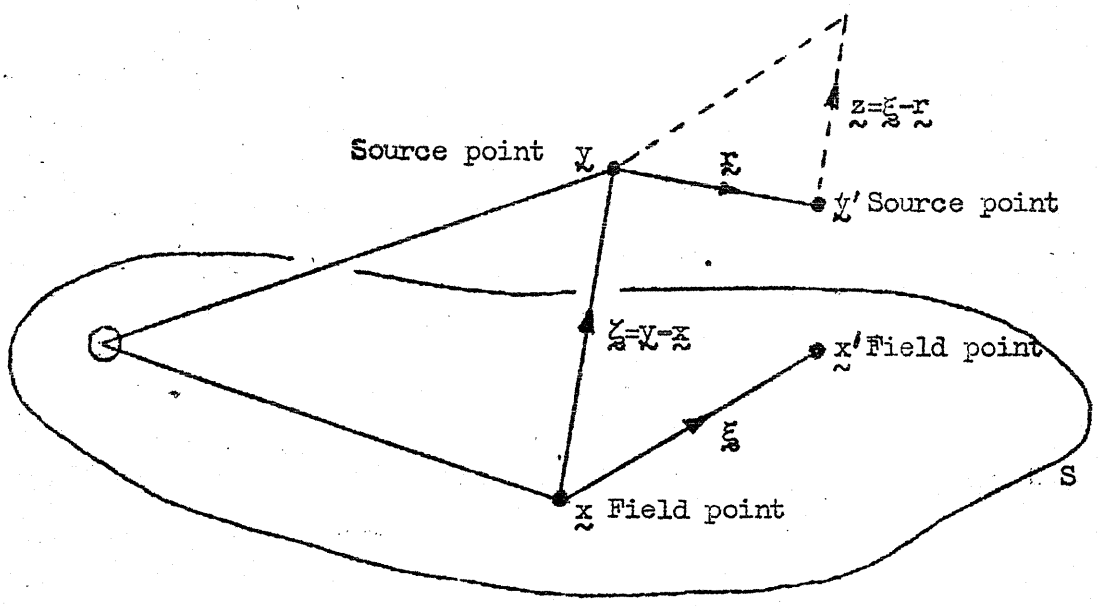

Now using the definitions (A.3)

$$\frac{\partial}{\partial y_i}\ \frac{1}{|\underset{\sim}{x}-\underset{\sim}{y}|} = -\frac{\partial}{\partial x_i}\ \frac{1}{|\underset{\sim}{x}-\underset{\sim}{y}|} = \frac{\partial}{\partial \xi_i}\ \frac{1}{|\underset{\sim}{x}-\underset{\sim}{y}-\underset{\sim}{\xi}|} = -\frac{\partial}{\partial \xi_i}\left(\frac{1}{\zeta}\right) \qquad (A.4)$$

where $\zeta = |\underset{\sim}{\zeta}| = \sqrt{\zeta_1^2+\zeta_2^2+\zeta_3^2}$, and

$$\frac{\partial}{\partial r_i}\ \frac{1}{|\underset{\sim}{x}'-\underset{\sim}{y}-\underset{\sim}{r}|} = -\frac{\partial}{\partial z_i}\ \frac{1}{|\underset{\sim}{x}'-\underset{\sim}{y}+\underset{\sim}{z}-\underset{\sim}{\xi}|} = \frac{\partial}{\partial z_i}\ \frac{1}{|\underset{\sim}{\zeta}-\underset{\sim}{z}|} \qquad (A.5)$$

and so using (A.4) and (A.5) in equation (A.2) we have

$$I_1 = -\int_{-\infty}^{\infty}\int_{-\infty}^{\infty} \frac{\partial}{\partial \xi_1}\left(\frac{1}{\zeta}\right)\frac{\partial}{\partial z_1}\,\frac{1}{|\underset{\sim}{\zeta}-\underset{\sim}{z}|}\,d\zeta_1\,d\zeta_3$$

$$= -\lim_{L\to\pm\infty}\frac{\partial^2}{\partial\xi_1\partial z_1}\int_{-L}^{L}\int_{-L}^{L}\frac{1}{\zeta|\underset{\sim}{\zeta}-\underset{\sim}{z}|}\,d\zeta_1\,d\zeta_3 \qquad (A.6)$$

We now introduce the integral identity

$$\frac{1}{|\underset{\sim}{a}|\cdot|\underset{\sim}{b}|} = \frac{2}{\pi}\int_0^{\infty}\frac{1}{(a^2+b^2\lambda^2)}\,d\lambda \qquad (A.7)$$

where in our case $a^2 = |\underset{\sim}{\zeta}-\underset{\sim}{z}|^2$, $b^2 = \zeta^2$

Changing the variable of integration once more to

$$\underset{\sim}{\zeta}' = \underset{\sim}{\zeta} - \frac{\underset{\sim}{z}}{(1+\lambda^2)} \qquad (A.8)$$

and using (A.7) and (A.8), equation (A.6) becomes

$$I_1 = -\lim_{L\to\pm\infty}\frac{\partial^2}{\partial\xi_1\partial z_1}\left\{\frac{2}{\pi}\int_0^{\infty}\frac{d\lambda}{(1+\lambda^2)}\int_{-L}^{L}d\zeta_1'\int_{-L}^{L}d\zeta_3'\left[\zeta'^2+\frac{z^2\lambda^2}{(1+\lambda^2)^2}\right]^{-1}\right\}$$

The differentiation with respect to z_1 may be performed since $\underset{\sim}{z}$ is independent of ζ

$$I_1 = \frac{\partial}{\partial\xi_1}\,\frac{4z_1}{\pi}\int_0^{\infty}\frac{\lambda^2\lambda}{(1+\lambda^2)^3}\int_{-\infty}^{\infty}d\zeta_1'\int_{-\infty}^{\infty}d\zeta_3'\left[\zeta'^2+\frac{z^2\lambda^2}{(1+\lambda^2)^2}\right]^{-2} \qquad (A.9)$$

The integrations over ζ_1' and ζ_3' can now be performed using polars to give

$$I_1 = \frac{\partial}{\partial\xi_1}\,4z_1\int_0^{\infty}\frac{\lambda^2 d\lambda}{(1+\lambda^2)^2\left[\zeta_2^2(1+\lambda^2)^2+\lambda^2z^2\right]} \qquad (A.10)$$

But since $x_2 = x_2' = \xi_2 = 0$ on the plane, $\zeta_2 = y_2$ and $z_2 = -r_2$

and so $\zeta_2' = y_2 + \dfrac{r_2}{(1+\lambda^2)}$ from (A.8), and therefore

$$I_1 = \frac{\partial}{\partial \xi_1} 4z_1 \int_0^{\infty} \frac{\lambda^2 d\lambda}{(1+\lambda^2)\left[\left\{y_2(1+\lambda^2)+r_2\right\}^2 + z^2\lambda^2\right]} \qquad (A.11)$$

If we now write

$$I_2 = \int_0^{\infty} \frac{\lambda^2 d\lambda}{(1+\lambda^2)\left[\left\{y_2(1+\lambda^2)+r_2\right\}^2 + z^2\lambda^2\right]}$$

$$= \int_0^{\infty} \frac{\lambda^2 d\lambda}{\lambda^6+p\lambda^4+q\lambda^2+r} \qquad \text{say,} \qquad (A.12)$$

then $I_2 = \dfrac{\pi\sqrt{r}}{\alpha(\alpha^2-p)\sqrt{r}-2r}$

where α is the biggest root of

$$(x^2-p)^2-8x\sqrt{r}-4q = 0 \qquad \text{(see De Haan 1939 p. 47, Table 20)}$$

Now $\alpha = 1+\sqrt{\left(\dfrac{z}{y_2}\right)^2+4\left(\dfrac{r_2}{y_2}\right)+4}$

and so

$$I_2 = \frac{\pi}{2\sqrt{4y_2^2+4r_2y_2+z^2}\left[2y_2+r_2+\sqrt{4y_2^2+4r_2y_2+z^2}\right]} \qquad (A.13)$$

Substituting the expression for I_2 in I_1 and then in equation (A.1) we obtain

$$I = \frac{2\rho_o^2}{\pi} \frac{\partial}{\partial \xi_1} \int_0^{\infty} dy_2 \int_{-y_2}^{\infty} dr_2 \int_{-\infty}^{\infty} dr_1 \int_{-\infty}^{\infty} dr_3 \; g(y_2)g(y_2+r_2)\bar{R}_{22}(y_2;\underset{\sim}{r})$$

$$\frac{(\xi_1 - r_1)}{\sqrt{(2y_2+r_2)^2+(\xi_1-r_1)^2+(\xi_3-r_3)^2}\left[2y_2+r_2+\sqrt{(2y_2+r_2)^2+(\xi_1-r_1)^2+(\xi_3-r_3)^2}\right]}$$

(A.14)

Hodgson and Lilley (1960) as a first approximation to equation (A.14) took an average value of g^2 across the layer, g_o^2 say, and also R_{22} independent of y_2, in which case the y_2 integration can be performed so that

$$I \simeq \frac{2}{\pi}\rho_o^2 g_o^2 \int_{-\infty}^{\infty} dr_1 \int_0^{\infty} dr_2 \int_{-\infty}^{\infty} dr_3 \; \bar{R}_{22}(\underset{\sim}{r}) \frac{\partial}{\partial \xi_1} \frac{(\xi_1 - r_1)}{(|\underset{\sim}{\xi}-\underset{\sim}{r}|+r_2)}$$

The denominator of the integral was further approximated so that

$$I \simeq \frac{\rho_o^2}{\pi} g_o^2 \int_{-\infty}^{\infty} dr_1 \int_0^{\infty} dr_2 \int_{-\infty}^{\infty} dr_3 \; \bar{R}_{22}(\underset{\sim}{r}) \frac{\partial}{\partial \xi_1} \frac{(\xi_1 - r_1)}{|\underset{\sim}{\xi}-\underset{\sim}{r}|} \qquad (A.15)$$

which is twice the value obtained by Lilley (1958) for the free shear flow case with constant mean shear and intensity, except that equation (A.15) is an integral over the half-space $r_2 > o$.

Appendix B

The contribution to the wall fluctuating pressure of the turbulence-turbulence terms.

In the analysis of sections 2 and 5 it has been assumed that the turbulence-turbulence contribution to the fluctuating pressure can be neglected compared with the turbulence-mean shear interaction. In this appendix the turbulence-turbulence interaction will be investigated. Since an order of magnitude analysis only is required it will be assumed that the turbulence-turbulence contribution to the fluctuating pressure is independent of the turbulence-mean shear interaction. Hence in this appendix, from equation (2.4), we can write

$$\nabla^2 p = -\rho_o \frac{\partial^2}{\partial x_i \partial x_j} (u_i u_j - \overline{u_i u_j}) \qquad (B.1)$$

where $p(\underset{\sim}{x},t)$ is the fluctuating pressure due to the turbulence-turbulence interaction and $u_i(\underset{\sim}{x},t)$ denotes the fluctuating turbulent velocity components.

As in section 2 the turbulence is assumed to be homogeneous in planes parallel to the wall, that is in the directions x_1 and x_3. By the use of the continuity condition (2.1), equation (B.1) may be rewritten as

$$\nabla^2 p = -\rho_o \left[\frac{\partial u_i}{\partial x_j} \frac{\partial u_j}{\partial x_i} + \left(\frac{\partial u_2}{\partial x_2}\right)^2 + 2 \frac{\partial u_i}{\partial x_2} \frac{\partial u_2}{\partial x_i} \right.$$

$$\left. - \overline{\frac{\partial u_i}{\partial x_j} \frac{\partial u_j}{\partial x_i}} - \overline{\left(\frac{\partial u_2}{\partial x_2}\right)^2} - 2 \overline{\frac{\partial u_i}{\partial x_2} \frac{\partial u_2}{\partial x_i}} \right] \qquad (B.2)$$

where, unless stated otherwise, i,j now take the values 1 or 3.

With the same Fourier-Stieltjes transforms of the pressure and velocity defined in equations (5.20) and (5.21), the two-dimensional transform of equation (B.2) is

$$\left(\frac{d^2}{dx_2^2} - k^2\right) dW(x_2;\underset{\sim}{k}) = \rho_o \int_{\underset{\sim}{k}'} \left[(k_i - k_i')k_j' dZ_i(x_2;\underset{\sim}{k}') dZ_j(x_2;\underset{\sim}{k}-\underset{\sim}{k}') \right.$$

$$- \left\{\frac{d}{dx_2} dZ_2(x_2;\underset{\sim}{k}')\right\} \left\{\frac{d}{dx_2} dZ_2(x_2;\underset{\sim}{k}-\underset{\sim}{k}')\right\}$$

$$-2i\rho_o (k_i - k_i') \left\{\frac{d}{dx_2} dZ_i(x_2;\underset{\sim}{k}')\right\} dZ_2(x_2;\underset{\sim}{k}-\underset{\sim}{k}')$$

$$\left. - \text{mean terms etc.} \right] \qquad (B.3)$$

where $\underset{\sim}{k} = (k_1, k_3)$ is the two-dimensional wave-number vector and $k^2 = k_1^2 + k_3^2$. For convenience the mean terms in equations (B.5) to (B.7) will be omitted.

The transform of the equation of continuity (2.1) is

$$\frac{d}{dx_2} dZ_2(x_2;\underset{\sim}{k}) + ik_i dZ_i(x_2;\underset{\sim}{k}) = 0 \qquad (B.4)$$

and using this form in equation (B.3) gives

$$\left(\frac{d^2}{dx_2^2} - k^2\right) dW(x_2;\underset{\sim}{k}) = \rho_o \int_{\underset{\sim}{k}'} \Big[(2k_i k_j - k_i' k_j - k_j' k_i) dZ_i(x_2;\underset{\sim}{k}') dZ_j(x_2;\underset{\sim}{k}-\underset{\sim}{k}')$$

$$-2i(k_i - k_i') \left\{ \frac{d}{dx_2} dZ_i(x_2;\underset{\sim}{k}') \right\} dZ_2(x_2;\underset{\sim}{k}-\underset{\sim}{k}') \Big] \qquad (B.5)$$

which is a second order linear differential equation in x_2. This equation for the transform of the fluctuating pressure is easily solved by the Laplace transform method. With the boundary conditions $p = o$ at $x_2 = \infty$, $\frac{\partial p}{\partial x_2} = o$ at $x_2 = o$ and $u_2 = o$ at $x_2 = o$, the transform of the fluctuating pressure at the wall is given by

$$dW(o;\underset{\sim}{k}) = -\rho_o \int_0^\infty e^{-kx_2'} dx_2'$$

$$\cdot \int_{\underset{\sim}{k}'} \Big[\frac{1}{k} (2k_i k_j - k_i' k_j - k_j' k_i) dZ_i(x_2';\underset{\sim}{k}') dZ_j(x_2';\underset{\sim}{k}-\underset{\sim}{k}')$$

$$- 2i(k_i - k_i') dZ_i(x_2';\underset{\sim}{k}') dZ_2(x_2';\underset{\sim}{k}-\underset{\sim}{k}') \Big] \qquad (B.6)$$

Squaring equ. (B.6) and taking the ensemble average leads to

$$\overline{(o;\underset{\sim}{k})dW(o;\underset{\sim}{k}'')} = \rho_o^2 \int_0^\infty \int_0^\infty e^{-(kx_2' + k''x_2'')} dx_2' dx_2''$$

$$\cdot \int_{\underset{\sim}{k}'} \int_{\underset{\sim}{k}'''} \left[\frac{1}{kk''} (2k_i k_j - k_i' k_j - k_j k_i')(2k_l'' k_m'' - k_l''' k_m'' - k_m''' k_l'') \right.$$
$$\cdot \overline{dZ_i^*(x_2';\underset{\sim}{k}')\, dZ_j^*(x_2';\underset{\sim}{k}-\underset{\sim}{k}')\, dZ_l(x_2'';\underset{\sim}{k}''')\, dZ_m(x_2''';\underset{\sim}{k}''-\underset{\sim}{k}''')}$$

$$+4(k_i - k_i')(k_l'' - k_l''')\overline{dZ_i^*(x_2';\underset{\sim}{k}')\, dZ_2^*(x_2';\underset{\sim}{k}-\underset{\sim}{k}')\, dZ_l(x_2'';\underset{\sim}{k}''')\, dZ_2(x_2'';\underset{\sim}{k}''-\underset{\sim}{k}''')}$$

$$+\frac{2i}{k''}(k_i - k_i')(2k_l'' k_m'' - k_l''' k_m'' - k_m''' k_l'')$$
$$\cdot \overline{dZ_i^*(x_2';\underset{\sim}{k}')\, dZ_2^*(x_2';\underset{\sim}{k}-\underset{\sim}{k}')\, dZ_l(x_2'';\underset{\sim}{k}''')\, dZ_m(x_2'';\underset{\sim}{k}''-\underset{\sim}{k}''')}$$

$$-\frac{2i}{k}(k_l'' - k_l''')(2k_i k_j - k_i' k_j - k_j k_i')$$
$$\left. \cdot \overline{dZ_i^*(x_2';\underset{\sim}{k}')\, dZ_j^*(x_2';\underset{\sim}{k}-\underset{\sim}{k}')\, dZ_l(x_2'';\underset{\sim}{k}''')\, dZ_2(x_2'';\underset{\sim}{k}''-\underset{\sim}{k}''')} \right]$$

$$i,j,l,m = 1 \text{ or } 3 \qquad \text{(B.7)}$$

where the asterisk denotes the complex conjugate.

At this stage it is not possible to proceed further unless some hypothesis is made regarding the statistical properties of the turbulent velocity field. The same hypothesis that was assumed by Batchelor (1951) for the corresponding isotropic turbulence calculation will be made, namely that the joint probability distribution of the velocities at two points is normal, in which case the fourth order velocity covariances in equation (B.7) reduce to second order covariances only. That is the first term on the right hand side of equation (B.7) may

be written

$$\overline{dZ_i^*(x_2';\underset{\sim}{k}')dZ_j^*(x_2';\underset{\sim}{k}-\underset{\sim}{k}')dZ_l(x_2'';\underset{\sim}{k}''')dZ_m(x_2'';\underset{\sim}{k}''-\underset{\sim}{k}''')}$$

$$= \overline{dZ_i^*(x_2';\underset{\sim}{k}')dZ_l(x_2'';\underset{\sim}{k}''')} \cdot \overline{dZ_j^*(x_2';\underset{\sim}{k}-\underset{\sim}{k}')dZ_m(x_2'';\underset{\sim}{k}''-\underset{\sim}{k}''')}$$

$$+ \overline{dZ_i^*(x_2';\underset{\sim}{k}')dZ_m(x_2'';\underset{\sim}{k}''-\underset{\sim}{k}''')} \cdot \overline{dZ_j^*(x_2';\underset{\sim}{k}-\underset{\sim}{k}')dZ_l(x_2'';\underset{\sim}{k}''')}$$

$$+ \overline{dZ_i^*(x_2';\underset{\sim}{k}')dZ_j(x_2';\underset{\sim}{k}-\underset{\sim}{k}')} \cdot \overline{dZ_l^*(x_2'';\underset{\sim}{k}''')dZ_m(x_2'';\underset{\sim}{k}''-\underset{\sim}{k}''')} \qquad (B.8)$$

and similarly for the other three terms.

As mentioned previously in the introduction Batchelor reasoned that the use of this normality hypothesis in the isotropic problem was consistent with the experimental result for grid turbulence that the velocity distribution at one point was closely normal. However, the hypothesis could not be exactly true since the hypothesis implied that the triple velocity correlations vanished.*

These triple correlations represent the effects of the non-linear inertia terms in the equations of motion. The correlation measurements by Stewart (1951) and Uberoi (1953) in grid turbulence

---

* The 'turbulence-mean shear turbulence-turbulence' cross terms $U(x_2') \overline{u_j(x_2')u_l(x_2'')u_m(x_2'')}$ etc. which would result from squaring equation (2.3) to obtain the total mean-square fluctuating pressure would also vanish since they contain triple turbulent velocity correlations. Hence the step leading to equation (B.1), in which the turbulence-turbulence contribution was considered independently as compared with the turbulence-mean shear contribution, is justified for the present calculation where the normality hypothesis is used.

showed that the hypothesis was justified at large separation, that is for the larger energy-containing eddies, but was less accurate at small separations, that is for the higher wave-numbers or smaller eddies which owe their existence entirely to the influence of the non-linear forces.

The only justification for using the hypothesis in the case of the present boundary layer turbulence problem (besides enabling the analysis to be continued) was that Klebanoff (1954) has shown that the probability distribution of the velocity at one point was closely normal for the region $0 < y_2/\delta < 0.8$, that is very nearly over the whole of the boundary layer region. At the moment information about the joint probability distribution of the velocities at two points in the boundary layer is not yet available. However, since we are here primarily interested in the lower wave numbers where the hypothesis is likely to be most accurate the results to be obtained should not differ too much from the correct values.

As in section (5.2) because of homogeneity in the x_1 and x_3 directions the second order covariances can be shown to vanish

everywhere unless the wave-number increments $d\underset{\sim}{k}$, etc. overlap (see Batchelor (1953) and Moyal (1952)) that is,

$$\overline{dW^*(o;\underset{\sim}{k})dW(o;\underset{\sim}{k}'')} = \Pi(o;\underset{\sim}{k})\delta(\underset{\sim}{k}-\underset{\sim}{k}'')d\underset{\sim}{k}\,d\underset{\sim}{k}'' \qquad (B.9)$$

and

$$\overline{dZ_i^*(x_2';\underset{\sim}{k}')dZ_1(x_2'';\underset{\sim}{k}''')} = \Phi_{i1}(x_2',x_2'';\underset{\sim}{k}')\delta(\underset{\sim}{k}'-\underset{\sim}{k}''')d\underset{\sim}{k}'d\underset{\sim}{k}''' \qquad (B.10)$$

where $\Pi(o;\underset{\sim}{k})$ is the two-dimensional power spectral density of the wall fluctuating pressure and $\Phi_{ij}(x_2',x_2'';\underset{\sim}{k})$ is the two-dimensional spectrum function of the turbulent velocity field and $\delta(\underset{\sim}{k})$ is the Dirac delta function.

If equation (B.8) is now used in (B.7), where it should be noted that the mean value terms omitted for convenience in (B.7) now cancel,* then after use of equations (B.9) and (B.10) the integrations over $\underset{\sim}{k}''$ and $\underset{\sim}{k}'''$ can be performed to give

$$\Pi(o;\underset{\sim}{k}) = \rho_o^2 \int_0^\infty\int_0^\infty e^{-k(x_2'+x_2'')} dx_2'dx_2''$$

$$\cdot \int_{\underset{\sim}{k}'} \left[\frac{2k_1k_m}{k^2}(2k_ik_j - k_i'k_j - k_j'k_i)\Phi_{il}(x_2',x_2'';\underset{\sim}{k}')\Phi_{jm}(x_2',x_2'';\underset{\sim}{k}-\underset{\sim}{k}')\right.$$

---

* As in Batchelor's case it was necessary to retain these mean terms from equation (B.1) to ensure that the Fourier integral defining the power spectral density of the pressure was convergent at infinity.

$$+4(k_i-k_i)\left\{(k_1-k_1')\Phi_{il}(x_2',x_2'';\underset{\sim}{k}')\Phi_{22}(x_2',x_2'';\underset{\sim}{k}-\underset{\sim}{k}'')\right.$$

$$\left.+k_1'\Phi_{i2}(x_2',x_2'';\underset{\sim}{k}')\Phi_{21}(x_2',x_2'';\underset{\sim}{k}-\underset{\sim}{k}')\right\}$$

$$+\frac{4i}{k}\left\{(k_i-k_i')k_1k_m\Phi_{il}(x_2',x_2'';\underset{\sim}{k}')\Phi_{2m}(x_2',x_2''.k-k')\right.$$

$$\left.-(k_1-k_1')k_ik_j\Phi_{il}(x_2',x_2'';\underset{\sim}{k}')\Phi_{j2}(x_2',x_2'';\underset{\sim}{k}-\underset{\sim}{k}')\right\}$$

(B.11)

which is a general expression for the wall fluctuating pressure spectrum in the two-dimensional wave-number space $\underset{\sim}{k}$ with the hypothesis of normality of the two-point probability distribution of the turbulent velocity field.

It is now necessary to complete the description of the turbulent velocity field by specifying the two-dimensional spectrum functions $\Phi_{ij}(x_2',x_2'';\underset{\sim}{k})$ etc. in equation (B.11). As discussed previously for the turbulence-mean shear calculations in sections 2 and 5, these spectrum functions are functions of position in the boundary layer (the turbulence intensity, scale and form of the spectrum functions varying with distance x_2 from the wall) because of the marked inhomogeneity and anisotropy of boundary layer turbulence.

A possible form for the spectrum function that could be used follows from the mirrow-flow model suggested by Kraichnan (1956b) which was employed in section 5.2 and was defined by equations (5.30a, b, c). With this form $\Phi_{ij}(x_2',x_2'';\underset{\sim}{k})$ could be expressed

in terms of $\bar{\bar{\Phi}}_{ij}(x_2'-x_2'';\underset{\sim}{k})$ and $\bar{\bar{\Phi}}_{ij}(x_2'+x_2'';\underset{\sim}{k})$ where, with the notation of section 5, the spectrum functions $\bar{\bar{\Phi}}_{ij}$ refer to a homogeneous field. Even so, the analysis using the mirrow flow model would still be difficult to do and would probably require a difficult numerical calculation.

Instead, the following forms for the spectrum functions are adopted:

$$\bar{\Phi}_{ij}(x_2',x_2'';k) = \frac{\overline{u^2(x_2)}}{16\pi} L^4 e^{-k^2L^2/4} (k^2\delta_{ij}-k_ik_j) e^{-\frac{|x_2''-x_2'|}{L}} \qquad i,j = 1,3 \tag{B.12}$$

and

$$\bar{\Phi}_{22}(x_2',x_2'';k) = \frac{\overline{u^2(x_2')}}{16\pi} L^4 k^2 e^{-k^2L^2/4} e^{-\frac{|x_2''-x_2'|}{L}} \tag{B.13}$$

Equations (B.12) and (B.13) have been obtained by writing equivalent two-dimensional forms of the usual three-dimensional isotropic spectrum function $\bar{\bar{\Phi}}_{ij}(\underset{\sim}{k})$ that was given previously in equation (5.35). The expressions may be regarded as the description of a model of turbulence which is 'isotropic' in the plane $\underset{\sim}{k}$ (that is in the x_1 and x_3 directions) where the $e^{-|x_2''-x_2'|/L}$ factor represents the correlation between planes parallel to the wall. It is admitted that this model is highly artificial. However, the spatial velocity correlation coefficients $\bar{R}_{11}$, $\bar{R}_{22}$ and $\bar{R}_{33}$ corresponding to (B.12) and (B.13), which are given by

$$\bar{R}_{11}(\underset{\sim}{r}) = \left(1 - \frac{2r_3^2}{L^2}\right) e^{-r_1^2/L^2} e^{-|r_2|/L} e^{-r_3^2/L^2} \qquad \text{(B.14a)}$$

$$\bar{R}_{22}(\underset{\sim}{r}) = \left(1 - \frac{(r_1^2+r_3^2)}{L^2}\right) e^{-r_1^2/L^2} e^{-|r_2|/L} e^{-r_3^2/L^2} \qquad \text{(B.14b)}$$

$$\bar{R}_{33}(\underset{\sim}{r}) = \left(1 - \frac{2r_1^2}{L^2}\right) e^{-r_1^2/L^2} e^{-|r_2|/L} e^{-r_3^2/L^2} \qquad \text{(B.14c)}$$

are, at least, a fair description of the measurements of Grant (1958), say,

If the mirror-flow model, based on an isotropic field, were used then it is easily demonstrated from the defining equations (5.30a, b, c) that the spectrum function $\Phi_{i_2}(x_2', x_2''; \underset{\sim}{k})$ with i,j = 1 or 3 vanishes, so the contribution of this term in equation (B.11) to the wall pressure spectrum will be assumed small enough to neglect.

If equations (B.12) and (B.13) are now substituted in (B.11), the expression for the wall pressure spectrum becomes

$$\Pi(o;\underset{\sim}{k}) = \frac{\rho_o^2 L^8}{256\pi^2} \int_0^\infty e^{-2kx_2'} \overline{u^2(x_2)}\, dx_2' \int_{-x_2'}^{\infty} e^{-ky_2} \overline{u^2(x_2'+y_2)}\, e^{-2|y_2|/L} dy_2$$

$$\cdot \int_{-\infty}^{\infty} e^{-k'^2 L^2/4}\, e^{-|\underset{\sim}{k}-\underset{\sim}{k}'|^2 L^2/4}$$

$$\cdot \left[\frac{2}{k^2} k_l k_m (2k_i k_j - k_i' k_j - k_i k_j')(k'^2 \delta_{il} - k_i' k_l')\left\{|\underset{\sim}{k}-\underset{\sim}{k}'|^2 \delta_{jm} + (k_j - k_j')(k_m - k_m')\right\}\right.$$

$$\left. + 4(k_i - k_i')(k_l - k_l')(k'^2 \delta_{il} - k_i' k_l')\left|\underset{\sim}{k}-\underset{\sim}{k}'\right|^2\right] d\underset{\sim}{k}' \qquad \text{(B.15)}$$

where x_2'' is written as $x_2'+y_2$.

For further simplification the turbulent intensity $\overline{u^2}$ and the scale L will be taken as independent of distance from the wall. The integrals over x_2' and y_2 in equation (B.15) may then be performed, followed by the integration over $\underset{\sim}{k}'$. The analysis is tedious and has been omitted for convenience. The final result for the wall pressure spectrum is

$$\Pi(o;\underset{\sim}{k}) = \frac{\rho^2 \overline{u^2} L^3}{128\pi} \frac{k}{(kL+2)} (k^2L^2+22) e^{-k^2L^2/8} \qquad (B.16)$$

which is the important result of this appendix.

The mean-square fluctuating pressure at the wall is obtained by integrating (B.16), that is

$$\overline{p^2}_{x_2=o} = \int \Pi(o;\underset{\sim}{k}) d\underset{\sim}{k}$$

$$= \rho_o^2 \left(\overline{u^2}\right)^2 \qquad (B.17)$$

which is exactly the value found by Kraichnan (1956a) for the free field case of isotropic turbulence with isotropic correlation scalar $f = e^{-r^2/L^2}$. But as mentioned in the introduction Batchelor calculated, from a more accurate form of the velocity correlation, that for isotropic turbulence

$$\overline{p^2} = 0.34 \rho_o^2 \left(\overline{u^2}\right)^2 \qquad (B.18)$$

which indicates that the mean-square pressure calculations are very dependent on the assumed form of the velocity correlation.

Hence it would be expected that the value of the mean-square pressure found in equation (B.17), where the form e^{-r^2/L^2} was used for the R_{11} and R_{33} correlations, would be greatly reduced to a value close to the result (B.18) that was obtained by Batchelor for free-field isotropic turbulence, had a better fit to the experimental measurements been used. Also the result (B.18) would probably be further reduced in the boundary layer case after accounting for the effects of anisotropy. As in section (5.2) these effects can be partially allowed for by taking $\overline{u^2} = \frac{1}{3}(\overline{u_1^2} + \overline{u_2^2} + \overline{u_3^2})$, which from Klebanoff's measurements of figure 2 had a maximum value of order $2U_\tau^2$. Hence from equation (B.18) a conservative estimate for the non-dimensional wall fluctuating pressure is

$$\sqrt{\overline{p^2}}/_{\frac{1}{2}\rho_0 U_1^2} \simeq 0.5\, C_f \qquad (B.19)$$

Comparing this value (B.19) with the experimentally measured value of $2.2\, C_f$ and the calculated turbulence-mean shear contribution of $2.56 C_f$ it is seen that the contribution of the turbulence-turbulence terms to the wall root-mean-square pressure is only likely to be of order 20% of the total, that is on a mean-square basis only of order 4%. This is the same order of magnitude that was deduced by Kraichnan (1956b).

It may be seen from the equation (B.16) that the calculated form of the pressure spectrum function $\Pi(o;\underset{\sim}{k})$ at the wall does satisfy the required boundary condition (2.44), namely that

$$\Pi(o;\underset{\sim}{k})_{k=o} = 0 \qquad \text{(B.20)}$$

The form of equation (B.16) is also symmetric in k_1 and k_3 which was to be expected since the turbulence was assumed 'isotropic' in the x_1 and x_3 directions.

Taking a representative value of the scale L as $3\delta_1$, from Klebanoff's measurements (see figure 3), the integration over k_3 of (B.16) may be performed numerically to obtain the one-dimensional longitudinal spectrum function

$$\Pi(o;k_1) = \int_{-\infty}^{\infty} \Pi(o;\underset{\sim}{k})dk_3 \qquad \text{(B.21)}$$

By use of the convected hypothesis of the pressure field discussed in section (5.1) the frequency spectrum $\Pi(\omega)$ of the wall fluctuating pressure may be obtained from (B.21) by putting $k_1 = \omega/U_c$, where the value of the averaged convection velocity U_c is taken as $0.8U_1$ from the measurements described in section 4. The non-dimensional spectrum function that was obtained has been plotted against the Strouhal number $\omega\delta_1/U_1$ in figure 40 for comparison with the measured spectrum. The spectrum level of the calculated turbulence -

turbulence contribution was fixed by taking the root-mean-square pressure to be given by equation (B.19).

The spectrum of the turbulence-turbulence contribution has a finite value at zero frequency, that is the integral under the longitudinal spatial correlation does not vanish. The longitudinal spatial correlation of the wall pressure obtained by Fourier transforming the turbulence-turbulence spectrum in figure 40 would have a small negative loop, and because of the symmetry in the x_1 and x_3 directions the transverse correlation would be identical. However, as we have shown above, the integral of the spatial correlation over the plane is zero.

Appendix C

Specialised Electronic Apparatus.

C1. The time correlator.

The time correlator is an electronic device used to form the function $\overline{p_1(t)p_2(t+\tau)}$ from two time fluctuating quantities $p_1(t)$ and $p_2(t)$, say, which may be measurements at the same position (auto-correlation) or at two different positions (space-time correlation). The correlator therefore consisted of a time delay unit to delay $p_2(t)$ a time τ relative to $p_1(t)$, a multiplier to form the product, and an averaging device to obtain the time mean of the product.

C1.1 Choice of system

There are two methods by which a time varying signal can be delayed in time. In a sampling system the signal is converted into pulse form, travels along a delay line and is recovered at some time later. In the analogue system the signal is usually recorded on a magnetic drum or tape via a recording head. It is then recovered as the tape passes a playback head at some time later.

A sampling system for use in aerodynamic problems has been described by Skinner (1956). However this 'analogue to digital' system can be rather complicated, usually has limited bandwidth and the total sampling time has to be much greater than that for

the analogue system. Also it may be convenient to store data for processing later and so a storage facility would still be required.

A continuous system using a rotating magnetic drum has been described by Goff (1955). A drum was not feasible for the present application because of the prohibitive cost and complicated head-traversing gear required. Also, the heads must be out of contact with the drum and then only limited bandwidth is obtained. Data storage is difficult without employing some form of spiral traversing gear for the heads and a further disadvantage is that the drum cannot be used again until the data processing has been completed.

On the other hand a magnetic tape-recorder as a time delay unit would seem to be a good proposition. The overall cost is relatively low, it offers excellent storage facilities, the tape is expendable and wide bandwidth can be achieved with acceptable tape speeds.

However, the use of a magnetic tape-recorder as a time delay unit has one major drawback. The drive mechanism of a tape-recorder capstan is never uniform. This causes small random variations in the tape speed, some at very low frequencies of a few cycles per second (wow) and some at higher frequencies (flutter). Part of the flutter is caused by the tape being not quite dimensionally stable. The tape tends to stretch randomly

and also vibrates like a violin string between heads and tape-guides, at the same time skewing across the heads.

This random departure from uniformity of the tape speed introduces spurious random time discrepancies between the played-back signal and the un-recorded signal, that is phase differences between the two signals. Also, with a carrier recording system, large wow and flutter can modulate the high-frequency carrier causing spurious random signals to appear over the operating bandwidth, therefore reducing the system 'signal to noise' ratio.

An excellent way of demonstrating the effects of wow and flutter is to connect the un-recorded and played-back signals to the two inputs of a double-beam oscilloscope. If one trace is 'locked' with the oscilloscope time-base the other trace can appear as a complete blurr due to the random phase changes.

The system employed partly overcame this difficulty by recording both signals on two separate tracks of the tape. This technique was also employed by Holmes and Dukes (1954) who used a tape recorder with two recording heads and two playback heads. It was then argued that the speed deviations would occur with the same amplitude and phase on both tracks and so the relative phase shift between the two signals would be zero. Unfortunately tape speed fluctuations are not only random but, because of the skewing, bowing, rubbing and stretching of the

tape, are correlated randomly along the tape. All of these causes will be accentuated by using a multi-head system because of the large head spacing and increased number of tape guides and rubbing surfaces. Toutan (1954) has found that the bandwidth of a four-head system is severely limited. The random phase shifts due to these causes was reduced to a minimum by using the system shown diagrammatically in figure 57b.

Instead of a continuous recording and playback system using four heads, only two heads, one for each track, for both recording and playback were used. This avoided large spacing between heads and also meant that the number of rubbing surfaces and tape guides were kept to a minimum. The two signals were recorded, using one head for each channel, on two separate tracks of an endless loop of tape for the duration of one loop length. The system was then switched to playback and one head was then moved manually relative to the other to obtain time delay. The improvement in performance obtained with this system is demonstrated in figure 58 which shows the autocorrelation of a 2 kc/s square-wave (the autocorrelation of which is a triangular wave) and a 100 kc/s sine-wave. The resolution of the correlator was about 0.6 microseconds. To be unable to process data continuously was really no disadvantage of the system since one of the main reasons for using tape was to allow data storage. Had the twin-track system described not been adopted, the bandwidth of the

correlator would have been restricted to less than 10 kc/s because of the reasons mentioned.

C1.2 The tape deck

The tape deck is shown in figure 57a, and was manufactured to specification (Data Recording Company). Magnetic tape of 0.5 in. width was used for good dimensional stability. The two heads, used for both recording and playback, possessed four tracks each. The track width was 0.060 in., the magnetic gaps were 0.0001 in. wide and the inductance of the head windings was 60mH.

The capstan was chromium plated, precision ground and ran in high-quality selected roller-bearings. The capstan was directly driven from a two-speed pole-changing Croydon synchronous motor and the tape speed was 40 in./sec. or 80 in./sec. The higher speed was always employed because of the better high-frequency response obtainable. The capstan spindle carried a heavy flywheel to reduce speed variations and there was also a second identical idling capstan. The tape was prevented from slipping on the capstans by rubber rollers held by electric actuators. A large-inductance head for erasing the tape was also mounted on the deck.

The two record/playback heads were mounted as close as possible to each other in the zero time-delay position. The

fixed head was partly enclosed in a mumetal screen to prevent 50 c/s pick-up from the motor and cross-talk between heads. The moving head was mounted on a sliding carriage located by two parallel slots and three roller bearings. The time delay was set using a 2 in. diameter barrel micrometer movement marked in 0.0001 in. increments with the range 0 - 2 in. A coil spring retained the sliding carriage in contact with the micrometer stem. The leads to each head were enclosed in copper tubes for electrostatic screening.

Measurements of the tape speed fluctuations taken on a GB Kalee meter showed that the rms wow (below 20 c/s) was 0.01% and the rms flutter (20 c/s - 200 c/s) was 0.04%. It should be emphasized again that these low values of wow and flutter (which were exceptionally small) were due to the use of only two heads with close spacing, the minimum number of tape guides and very high precision engineering of the tape deck.

The tape-loop length was 160 in. which was equivalent to a recording time of two seconds. In order to analyse a representative sample of the data, the sample length should generally be 10 - 100 times the lowest period to be analysed. The lowest frequency in the fluctuating signals measured was 40 c/s, that is a wavelength of 0.025 seconds. The sample time of 2 seconds was found in all cases to be quite adequate. The tape was joined using an edge to edge butt-joint formed in a specially constructed

splicing jig.

In order to record an exact loop-length sample of the fluctuating signal the timing circuit of figure 60 was employed. A small slit was formed on the tape by scraping away the magnetic coating. Referring to figure 57b, as the slit passed a small light source directed towards an OCP71 photo-electric cell a pulse was produced which via the timing circuit then switched the channels to record. When the slit passed a second time, recording was switched off. The circuits were then switched manually to playback. The cycle could not repeat until the timing circuit was primed.

C1.3 Recording circuits

The frequency modulation system of recording was used throughout the work. The circuit was a modified commercial design and is reproduced in figures 59 and 61. This system had the great advantage of very high amplitude accuracy. The frequency response of DC-20 kc/s, shown in figure 59, was found to be quite sufficient for all the presented measurements. An amplitude modulated system was also built with bandwidth 300c/s - 100kc/s and was connected to the two spare tracks on the four-track recording/playback heads. This then enabled data to be recorded with bandwidth DC-100 kc/s. As mentioned previously the amplitude modulated system was not necessary for the present work.

The frequency modulation system employed a 75 kc/s carrier with a maximum derivation of $\pm 40\%$. The output signal was 4 volt for the same input, and the signal to noise ratio was 40db. In order to ensure that the random signals were not extensively 'clipped' a level of 0.5 volts rms was usually recorded.

C.2 The multiplier

A variety of electronic methods of multiplying two fluctuating voltages together are known. One common application of multipliers is in analogue computing where usually great accuracy is required with very limited bandwidth. However, for the present purpose in turbulence measurements, the bandwidth that was required was at least 10 kc/s, but the accuracy needed to be only a few per cent.

The necessary wide bandwidth was obtained using the analogue method of multiplication working on the 'quarter-squaring' principle. The circuit was a development of that described by Miller et al. (1955) and is shown in figure 63. The circuit was designed around two Raytheon QK329 squaring valves. With these valves, squaring to 1% accuracy was possible up to a frequency of 60 Mc/s, so the multiplier bandwidth was only limited by the other circuitry. For optimum operation the QK329 values required an input signal of 50 volts, when the output current was then approximately 0.25mA.

Push-pull sum and difference signals (x+y) and (x-y) respectively of the two input signals x and y, obtained from two inverting amplifiers and an accurate bridge, were squared by the two QK329 squaring valves. The difference of the squared signals $(x+y)^2$ and $(x-y)^2$ was then obtained in a subtracting amplifier to form the product 4xy (times a constant).

Inversion and subtraction were obtained by wide-bandwidth DC amplifiers operating with feedback. The circuit described by Miller et al. was severely limited in bandwidth because the DC amplifiers were of the computing type. Computing DC amplifiers are usually designed for extremely small phase angles at low frequencies and were not really suitable for the present application because their bandwidth is limited. The DC amplifier circuit that was used is shown in figure 63 and possessed a bandwidth of over 500 kc/s. Even so,the multiplier could not be used at frequencies so high that phase lags in the DC amplifiers produced bridge unbalance and subtractor inaccuracy. The upper limit of frequency response was a little over 100 kc/s for the present circuit, compared with 10 kc/s for the original design.

The multiplier was preceded by amplifiers of 24db gain,with an upper frequency limit 480 kc/s,to produce the required drive voltage. For convenience these amplifiers were AC coupled. Although no drift correcting circuits were employed it was found that if the multiplier was switched-on two or three hours

beforehand no trouble from drift was experienced. The drift was approximately 1% full-scale output per hour.

The mean value of the fluctuating DC output voltage was obtained by a Pye mirror-galvonometer with a time constant variable from 2 - 10 seconds. This galvonometer was sufficiently accurate for the present purposes and could be read quickly. As the tape-loop butt-joint passed over the playback heads a slight transient in the multiplier output was produced which did not interfere with the recording of the required averaged output on the galvonometer.

The overall bandwidth of the multipliers was 5 c/s - 100 kc/s, the signal to noise ratio was 40db and the accuracy was approximately 1% full-scale output. With one input at maximum and the other at zero the output was never greater than 1%. The setting-up procedure was described in detail by Miller et al. A convenient day to day method was to check the autocorrelation of a sine-wave, which is a cosine wave (see figure 58), and so the output had to oscillate between equal positive and negative values as the time delay was varied for correct operation.

No calibration of the tape recorder and multiplier was required when measuring correlation coefficients. The procedure was to read the mean product $K\overline{xy}$, say, of the two signals x and y recorded on the tape; then one signal x, say, was connected to both multiplier inputs to give the square $K\overline{x^2}$ and similarly for y. The correlation

coefficient $\bar{R}$ was then given by

$$\bar{R} = \frac{K\overline{xy}}{\sqrt{K\,\overline{x^2}}\sqrt{K\,\overline{y^2}}} = \frac{\overline{xy}}{\sqrt{\overline{x^2}}\sqrt{\overline{y^2}}}$$

which was independent of the tape-recorder and multiplier calibrations.

C.3 The Integrator

The circuit used to integrate the fluctuating DC output voltage of the Dawe true mean-square meter for the fluctuating pressure measurements is shown diagrammatically in figure 62. It consisted essentially of a Solartron DC computer amplifier with capacitive feedback and a gating circuit to measure the integrating time. The feedback capacitor was a low-leakage polystyrene type, a necessity for accurate integration. The integrating time-constant could be switched to either 0.5, 1.0 or 2.0 seconds.

The integrating time was measured accurately by first rectifying the 50 c/s AC mains voltage (which is accurate in frequency to $\pm$1% or better) and then passing the rectified signal through a 100 c/s tuned amplifier to produce sinusoidal drive to a row of decatron counting tubes. When the 'start' button was pressed the timing gate was opened permitting pulses at 10 pps to enter the counting chain. Simultaneous with this

operation, relay A switched the DC amplifier into the integrating configuration and relay B, which was in series with the input line, closed to connect the input signal. The counting chain then counted off 100 or 1000 pulses during which time the input signal was integrated for the chosen integrating time of 10 or 100 seconds. Then relay B automatically opened, disconnecting the input signal and leaving the integrating capacitor in a charged state, when the integrated voltage was then read at leisure on an accurate voltmeter. The low source impedance of the DC amplifier was now utilised to discharge the integrating capacitor to exactly zero charge by pressing the reset button which closed relay A. The circuit was then ready to be primed again for the next reading.

References

Bakke, P. (1957) An Experimental Investigation of a Wall Jet. Jn. Fluid Mech. 2. Part 5, p. 467.

Barratt, M.J. (1960) On the Convection Velocity of Turbulence in a Jet Stream. University of Southampton Report No. 110.

Batchelor, G.K. (1953) The Theory of Homogeneous Turbulence. Cambridge University Press.

Batchelor, G.K. (1951) Pressure Fluctuations in Isotropic Turbulence. Proc. Cam. Phil. Soc., 47, p. 359.

Bradshaw, P., and Love, E.M. (1959) The Normal Impingement of a Circular Air Jet on a Flat Surface. A.R.C. 21,268.

Bradshaw, P., and Gee, M.T. (1960) Turbulent Wall Jets with and without an External Stream. A.R.C. 22,008.

Bradshaw, P., and Gregory, M. (1961) Calibration of Preston Tubes on a Flat Plate using Measurements of Local Skin Friction. ARC R. and M. 3185.

Bradshaw, P. (1962) Turbulence Measurements in an Axial Jet (To be Published)

Bull, M.K. (1960) Instrumentation for and preliminary measurements of space-time correlations and convection velocities of the pressure field of a turbulent boundary-layer. University of Southampton AASU Report No. 149.

Coles, D. (1954) The Problem of the Turbulent Boundary Layer. Z.A.M.P. 5, p. 181.

Corcos, G.M. and Liepmann, H.W. (1956) On the Contribution of Turbulent Boundary Layers to the Noise Inside a Fuselage. NACA TM 1420.

Curle, N.	(1955)	The Influence of Solid Boundaries upon Aerodynamic Sound. Proc. Roy. Soc. A231, p. 505.
Doak, P.E.	(1960)	Acoustic Radiation from a Turbulent Fluid containing Foreign Bodies. Proc. Roy. Soc. A254, p. 129.
Favre, A.	(1958)	Quelques Resultats d'Experiences sur la Turbulence Correlations Spatio - Temporelles Spectres. Publ. Sci. Tech. Minist. de l'Air No. 73.
Favre, A.J., Gaviglio, J.J., and Dumas, R.	(1957)	Space-Time Double Correlations in a Turbulent Boundary Layer. J. Fluid Mech. 2, Part 4, p. 313.
Favre, A.J., Gaviglio, J.J., and Dumas, R.	(1958)	Further Space-Time Correlations of Velocity in a Turbulent Boundary Layer. J. Fluid Mech. 3, Part 4, p. 344.
Feynman, R.P.	(1949)	Phys. Rev. 76, p. 769.
Glauert, M.B.	(1956)	The Wall Jet. Jn. Fluid Mech. 1, Part 6, p. 625.
Goff, K.W.	(1955)	An Analog Electronic Correlator for Acoustic Measurements. J. Acoust. Soc. Am. 27, p. 223.
Grant, H.L.	(1958)	The Large Eddies of Turbulent Motion. Jn. Fluid Mech. 4, Part 2, p. 149.
Haan, D.B.de	(1939)	Nouvelles Tables d'Integrales definies. Corrected edition of 1867. New York, Stechert.
Harrison, M.	(1958)	Pressure Fluctuations on the Wall Adjacent to a Turbulent Boundary Layer. Hydromechanics Laboratory Report 1260, David Taylor Model Basin.
Heisenberg, W.	(1948)	Zur Statistischen Theorie der Turbulenz Z. Phys. 124, p. 628. Also NACA TM 1431.
Hodgson, T.H., and Lilley, G.M.	(1960)	On Surface Pressure Fluctuations in Turbulent Boundary Layers. Agard Report 276.
Holmes, J.N., and Dukes, J.M.C.	(1954)	A Speech-waveform Correlator. Proc. I.E.E. 101, Pt. III, No.72, p. 225.

Klebanoff, P.S.	(1954)	Characteristics of Turbulence in a Boundary Layer with Zero Pressure Gradient NACA TN 3178.
Kraichnan, R.H.	(1956a)	Pressure Field within Homogeneous Anisotropic Turbulence. J. Acoust. Soc. Am. 28, p. 64.
Kraichnan, R.H.	(1956b)	Pressure Fluctuations in Turbulent Flow over a Flat Plate. J. Acoust. Soc. Am. 28, p. 378.
Kraichnan, R.H.	(1957)	Noise Transmission from Boundary Layer Pressure Fluctuations. J. Acoust. Soc. Am. 29, p. 65.
Kobashi, Y.	(1957)	Measurements of Pressure Fluctuations in the wake of a cylinder. Jour. Phys. Soc. Japan 12, p. 533.
Lane-Smith, M.R.	(1959)	Pressure Fluctuations in a Turbulent Boundary Layer. M. Sc. Thesis. Manchester University.
Laufer, J.	(1955)	The Structure of Turbulence in Fully Developed Pipe Flow. NACA Report 1174.
Laufer, J.	(1961)	Sound Radiation from a Turbulent Boundary Layer. California Institute of Technology JPL Tech. Report 32-119.
Laurence, J.C., and Landes, L.G.	(1953)	Auxiliary Equipment and Techniques for Adapting the Constant Temperature Hot-wire Anemometer to Specific Airflow Phenomena. NACA TN 2843.
Lilley, G.M.	(1945)	Some Theoretical Aspects of Nozzle Design. M.Sc. Thesis. London University.
Lilley, G.M.	(1958)	On the Noise from Air Jets ARC 20,376.
Lilley, G.M.	(1960)	Pressure Fluctuations in an Incompressible Boundary Layer. College of Aeronautics, Cranfield. Report 133.

Lighthill, M.J.	(1952)	On Sound Generated Aerodynamically Part I. Proc. Roy. Soc. A211, p. 564.
	(1954)	Part II. Proc. Roy. Soc. A222, p. 1.
Lighthill, M.J.	(1961)	Sound Generated Aerodynamically. The Bakerian Lecture, 1961. R.A.E. Tech. Memo. DIR.8.
McLeod, N.H., and Jordan, G.H.	(1958)	Preliminary Flight Survey of Fuselage and Boundary Layer Sound-Pressure Levels. NACA RM H58B11.
Miller, J.A., Soltes, A.S., and Scott, R.E.	(1955)	Wide-Band Analog Function Multiplier. Electronics. Feb. p. 160.
Moyal, J.E.	(1952)	The Spectra of Turbulence in a Compressible Fluid; Eddy Turbulence and Random Noise, Proc. Camb. Phil. Soc. 48, p. 329.
Mull, H.R., and Algranti, J.S.	(1956)	Preliminary Flight Survey of Aerodynamic Noise on an Aeroplane Wing. NACA RM E55K07.
Mull, H.R., and Algranti, J.S.	(1960)	Flight Measurement of Wall-pressure Fluctuations and Boundary Layer Turbulence. NASA TN D-280.
Obukhov, A.M.	(1949)	Pressure Pulsations in a Turbulent Flow. C.R. Acad. Sci. U.R.S.S. 66, p. 17. Also Ministry of Supply, England. Translation P 21452T.
Phillips, O.M.	(1954)	Surface Noise from a Plane Turbulent Boundary Layer ARC 16,963.
Phillips, O.M.	(1956)	On the Aerodynamic Surface Sound from a Plane Turbulent Boundary Layer. Proc. Roy. Soc. A234, p. 327.
Ribner, H.S.	(1956)	Boundary Layer Induced Noise in the Interior of Aircraft. Inst. Aerophysics, University Toronto Report 37.
Richards, E.J.	(1961)	Aerodynamic Noise Sources, Paper B3 presented at 'Control of Noise' Conference, National Physical Laboratory, Teddington.

Riegels, F.W.	(1961)	Aerofoil Sections. Butterworth and Co. Ltd., London.
Sandborn, V.A., and Slogar, R.J.	(1955)	Study of the Momentum Distribution of Turbulent Boundary Layers in Adverse Pressure Gradients. NACA TN 3264.
Skinner, G.T.	(1956)	Time-correlator for Problems in Aerodynamics. NACA Tech. Note 3682.
Skudrzyk, E.F., and Haddle, C.P.	(1960)	Noise Production in a Turbulent Boundary Layer by Smooth and Rough Surfaces. J. Acoust. Am. Soc. 32, p.
Stewart, R.W.	(1951)	Proc. Cambridge Royal Soc. 47, p. 146.
Strasberg, M., and Cooper, R.D.	(1956)	Measurements of the Fluctuating Pressure and Velocity in the Wake behind a Cylinder. Paper I.101, Ninth International Congress of Applied Mechanics, Brussels.
Strehlow, R.A.	(1949)	A Method for Electroplating Fine Wires. University of Wisconsin Report CM-551.
Tack, D.H., Smith, M.W., and Lambert, R.F.	(1961)	Wall Pressure Correlations in Turbulent Airflow. J. Acoust. Soc. Am. 33, p. 410.
Taylor, G.I.	(1938)	The Spectrum of Turbulence. Proc. Royal Soc. A164, p. 476.
Toutan, M.	(1954)	A Variable Magnetic-tape Delay Line. L'Onde Electrique, March.
Townsend, A.A.	(1956)	The Structure of Turbulent Shear Flow. Cambridge University Press.
Townsend, A.A.	(1957)	The Turbulent Boundary Layer. Paper presented at Boundary Layer Research Symposium, Freiburg.

Uberoi, M.S.	(1953)	Quadruple Velocity Correlations and Pressure Fluctuations in Isotropic Turbulence. J.Aero.Sci. 20, p. 197.
Williams, D.J.M.	(1960)	Measurements of the Surface Pressure Fluctuations in a Turbulent Boundary Layer in Air at Supersonic Speeds. University of Southampton, A.A.S.U. Report 162.
Williams, J.E.F.	(1960)	On Noise from Convected Turbulence. University of Southampton, Ph.D. Thesis.
Willmarth, W.W.	(1956)	Wall Pressure Fluctuations in a Turbulent Boundary Layer. J. Acoust. Soc. Am. 28, p. 1048 (also N.A.C.A. TN 4139)
Willmarth, W.W.	(1958)	Small Barium Titanate Transducer for Aerodynamic or Acoustic Pressure Measurements. Rev. Sci. Instr. 29, No.3, March.
Willmarth, W.W.	(1959a)	Space-time Correlations and Spectra of Wall Pressure in a Turbulent Boundary Layer. NASA Memo 3-17-59W.
Willmarth, W.W.	(1959b)	Statistical Properties of the Pressure Field in a Turbulent Boundary Layer. Paper presented at WADC - Minnesota Conference on Acoustical Fatigue, September.
Wilson, L.N.	(1959)	An Experimental Investigation of the Noise Flow around a Rotating Cylinder. Inst. Aerophysics, University of Toronto, Report No. 57.

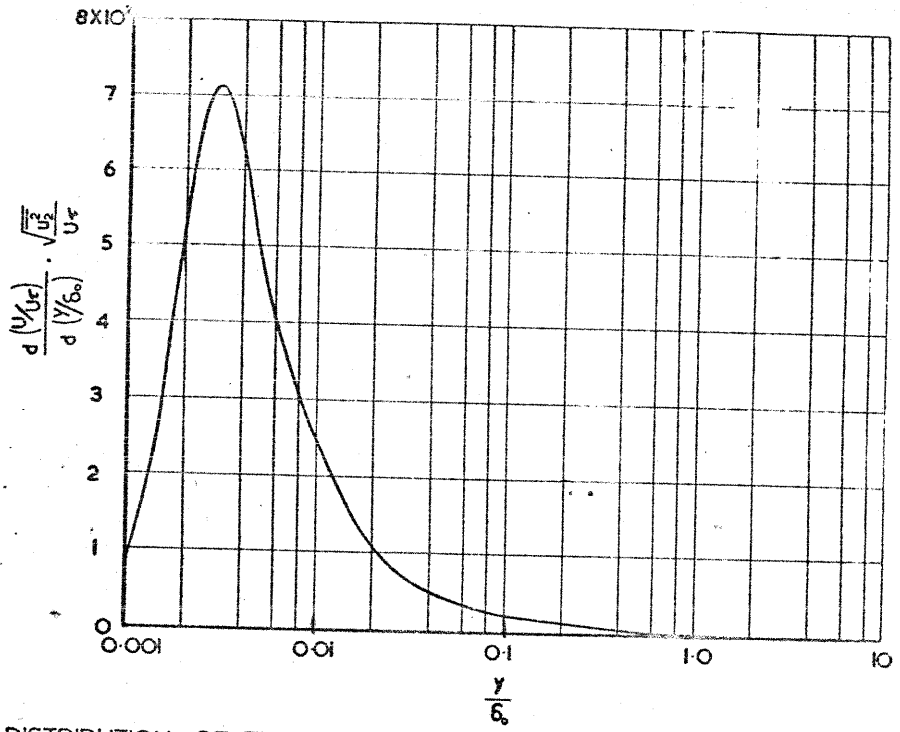

FIG.1. DISTRIBUTION OF THE PRODUCT OF MEAN SHEAR AND INTENSITY OF THE LATERAL VELOCITY COMPONENT IN A TURBULENT BOUNDARY LAYER

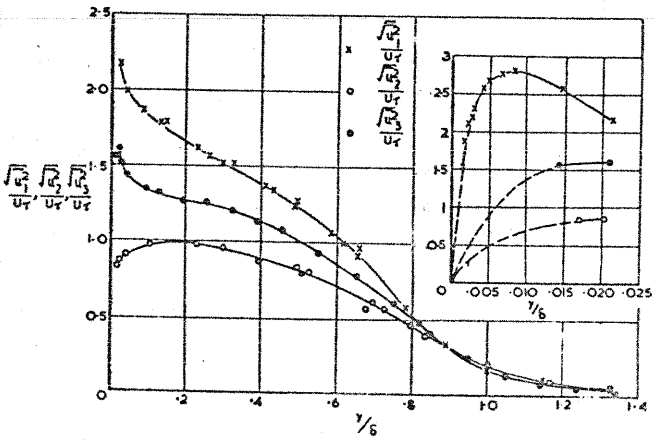

2. DISTRIBUTION OF TURBULENCE INTENSITIES IN A TURBULENT BOUNDARY LAYER. (KLEBANOFF 1954.)

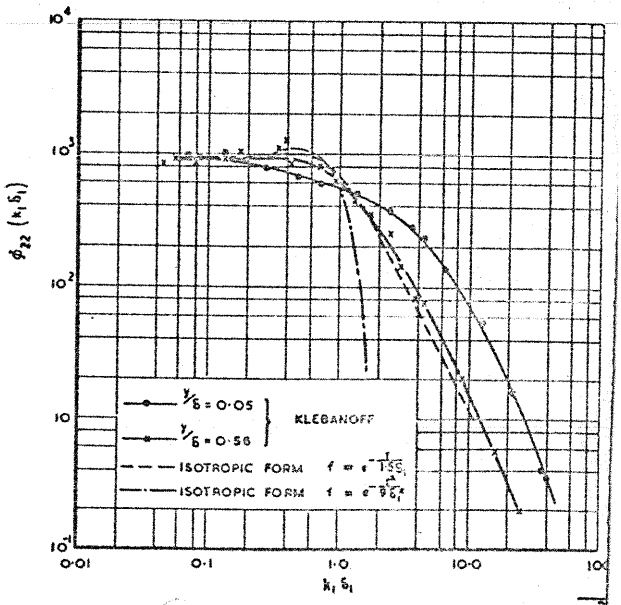

FIG.3. SPECTRA OF LATERAL VELOCITY COMPONENT $\overline{u_2^2}$ IN A TURBULENT BOUNDARY LAYER (KLEBANOFF 19

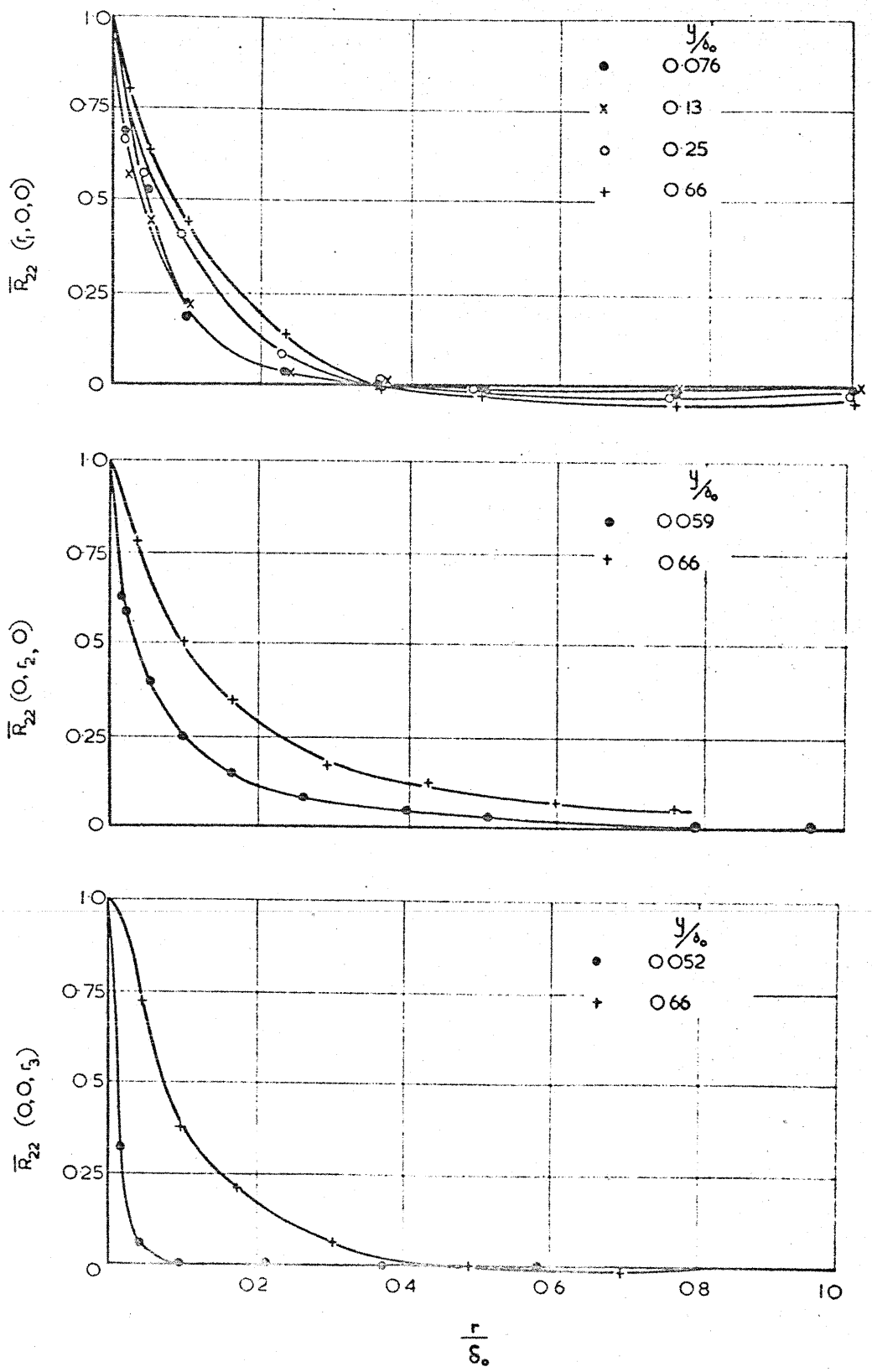

FIG 4. LATERAL VELOCITY CORRELATIONS IN A TURBULENT BOUNDARY LAYER. (GRANT 1958)

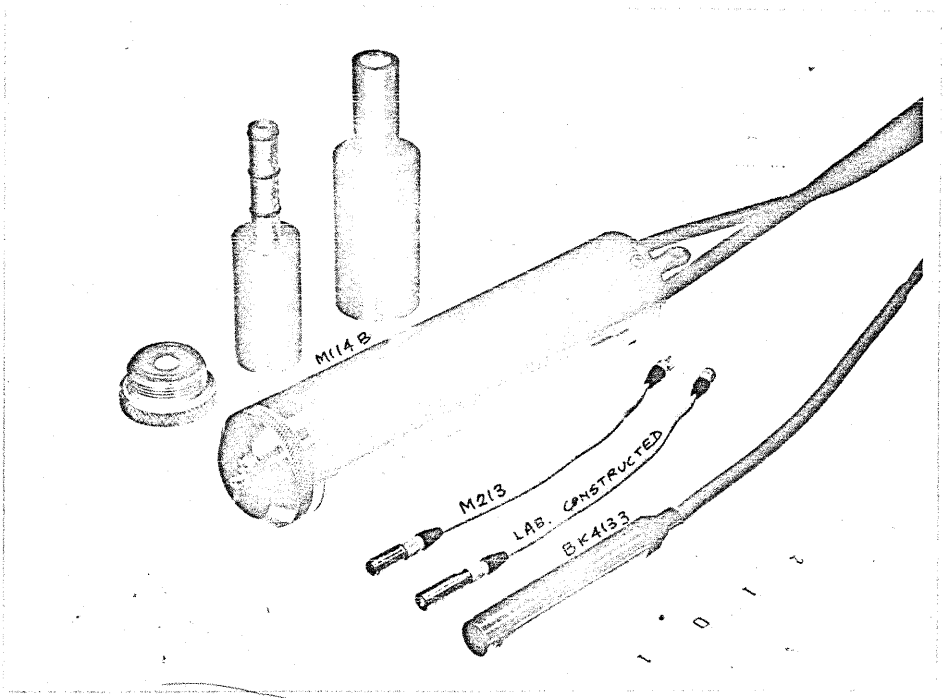

FIG. 5. THE M213, LABORATORY CONSTRUCTED AND BK4133 TRANSDUCERS, AND THEIR CATHODE FOLLOWERS.

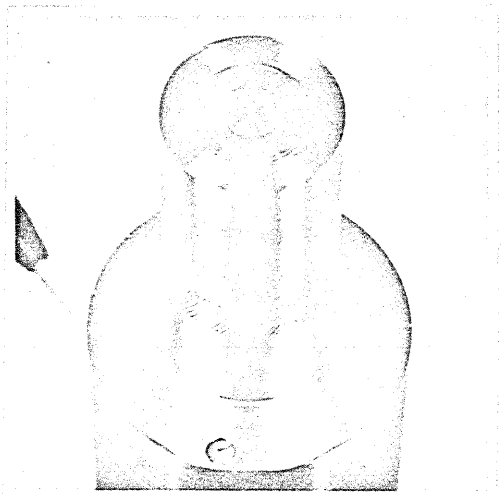

FIG. 6. CLOSE-UP OF M213 TRANSDUCER FLUSH MOUNTING.

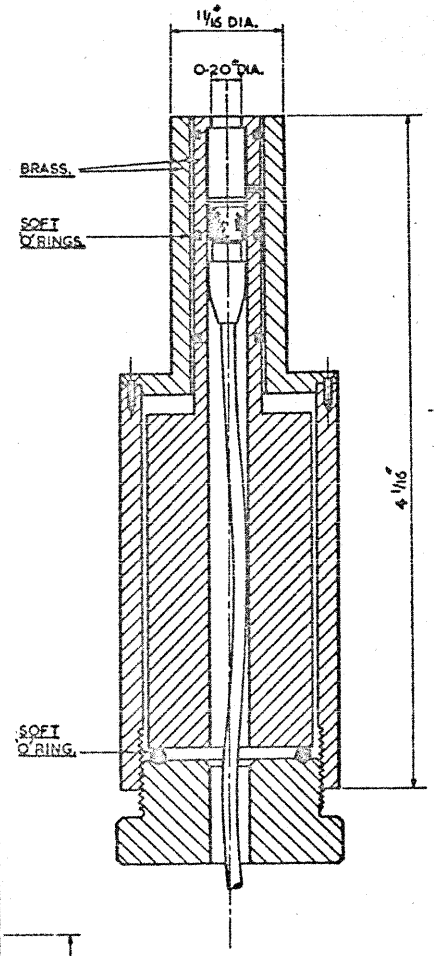

FIG. 7.

FLUSH MOUNTING OF M-213 CRYSTAL TRANSDUCER.

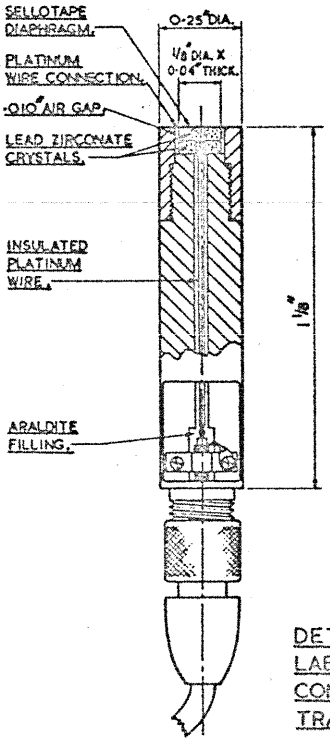

FIG. 8.

DETAILS OF LABORATORY CONSTRUCTED TRANSDUCER.

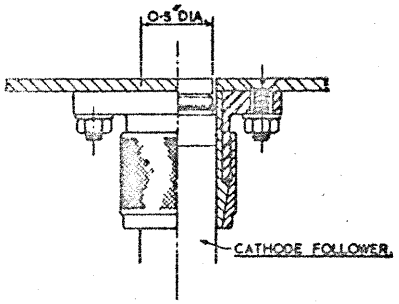

FIG. 9.

FLUSH MOUNTING OF BK CONDENSER TRANSDUCER.

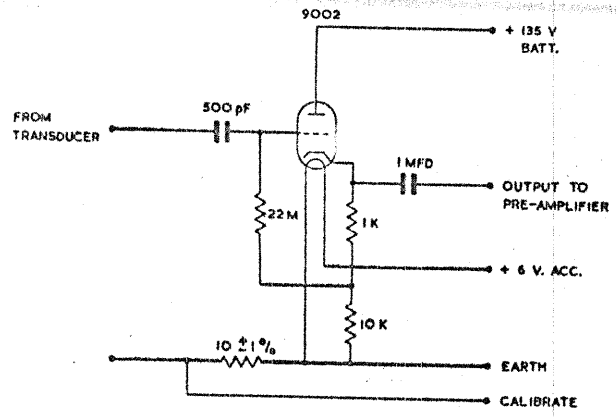

CATHODE FOLLOWER FOR MASSA M213 TRANSDUCER.

FIG. 10a.

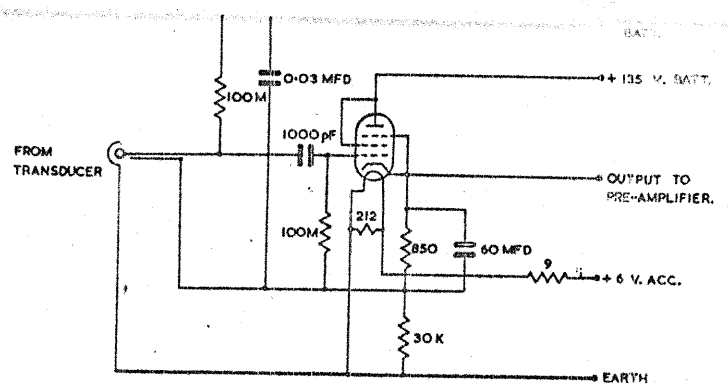

CATHODE FOLLOWER FOR BK4133 TRANSDUCER.

FIG. 10b.

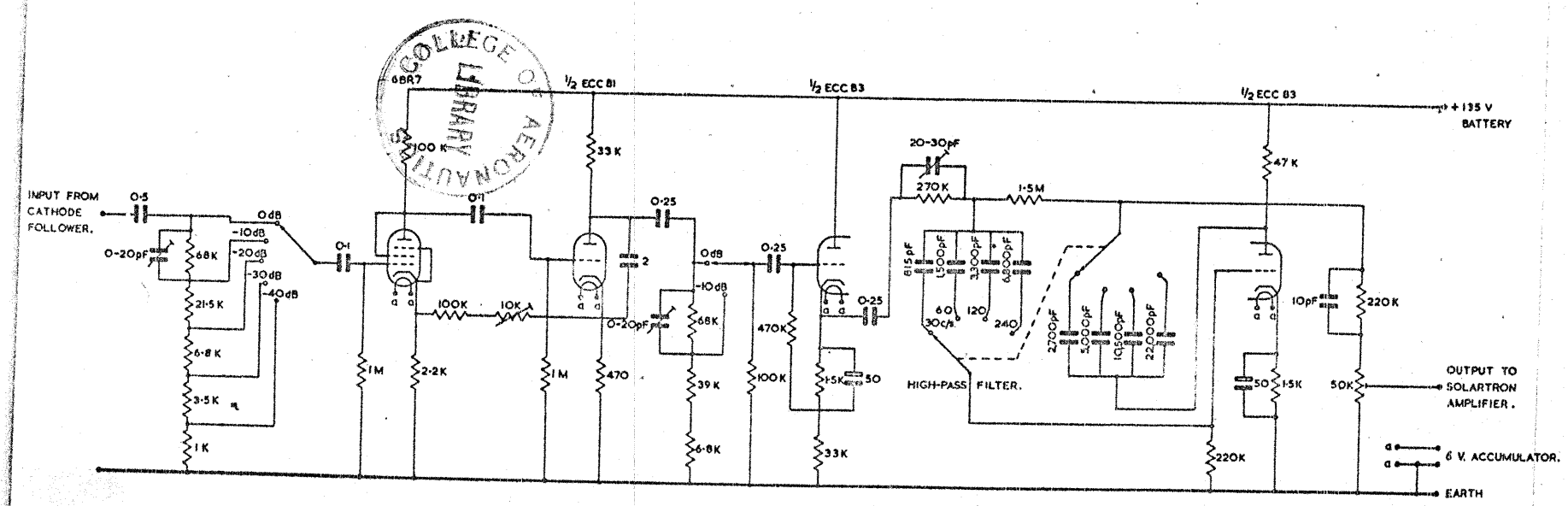

LOW NOISE BATTERY OPERATED PRE-AMPLIFIER.

FIG. 10c.

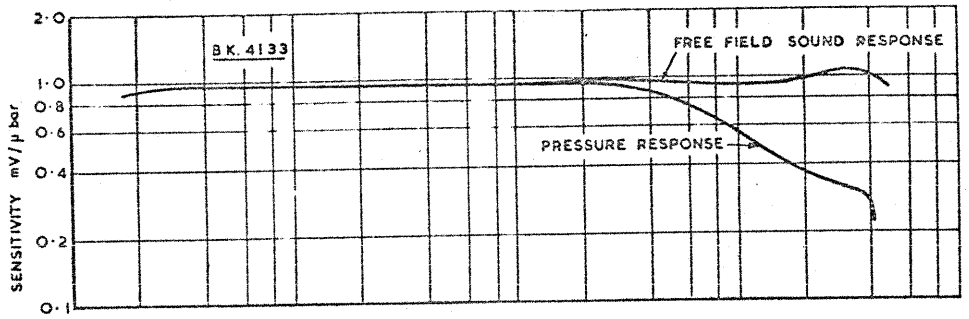

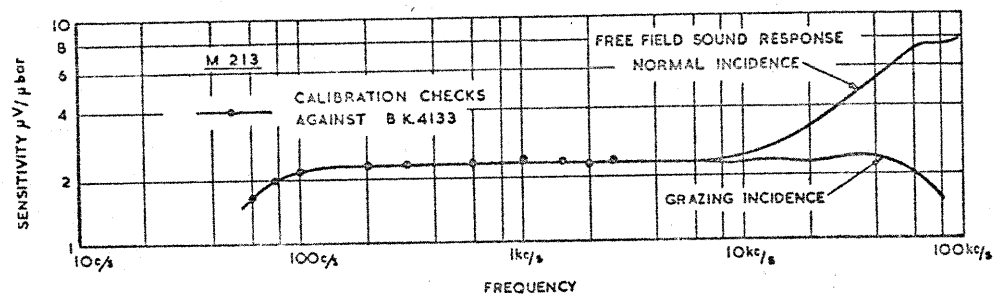

FIG.11. CALIBRATION CURVES FOR MASSA M 213 AND BRUEL and KJAER 4133 TRANDUCERS

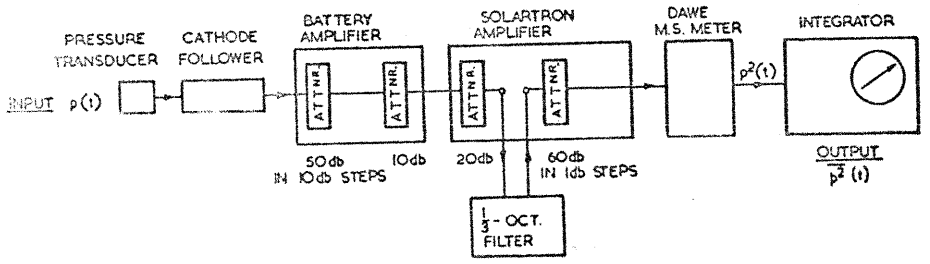

FIG.12. DIAGRAM OF EQUIPMENT FOR FLUCTUATING PRESSURE MEASUREMENT

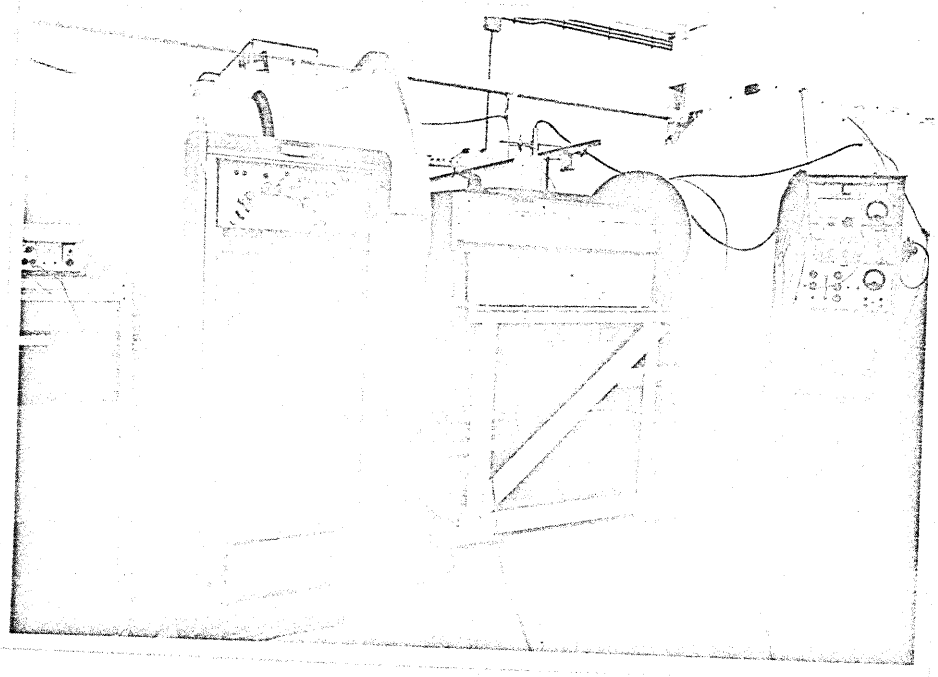

FIG. 13a. VIEW OF FLAT PLATE FACILITY.

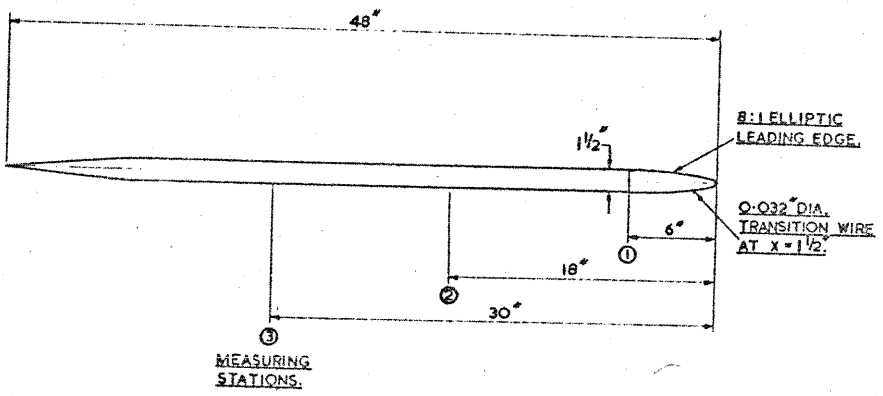

FIG. 13b. MEASURING STATIONS FOR FLAT PLATE AT ZERO INCIDENCE.

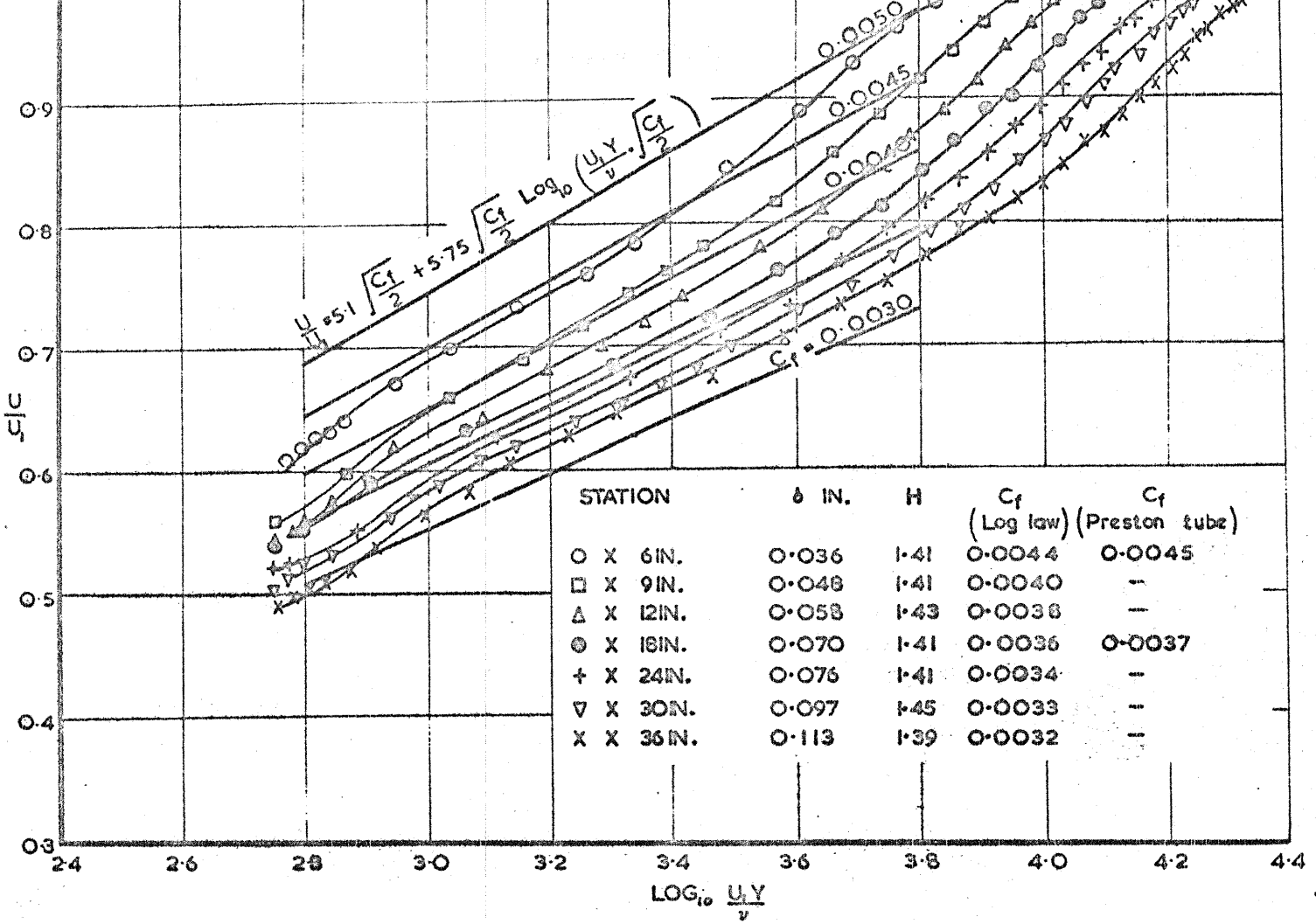

FIG. 14. FLAT PLATE AT ZERO INCIDENCE. TURBULENT BOUNDARY LAYER VELOCITY PROFILES. $U_1 = 67$ ft/sec.

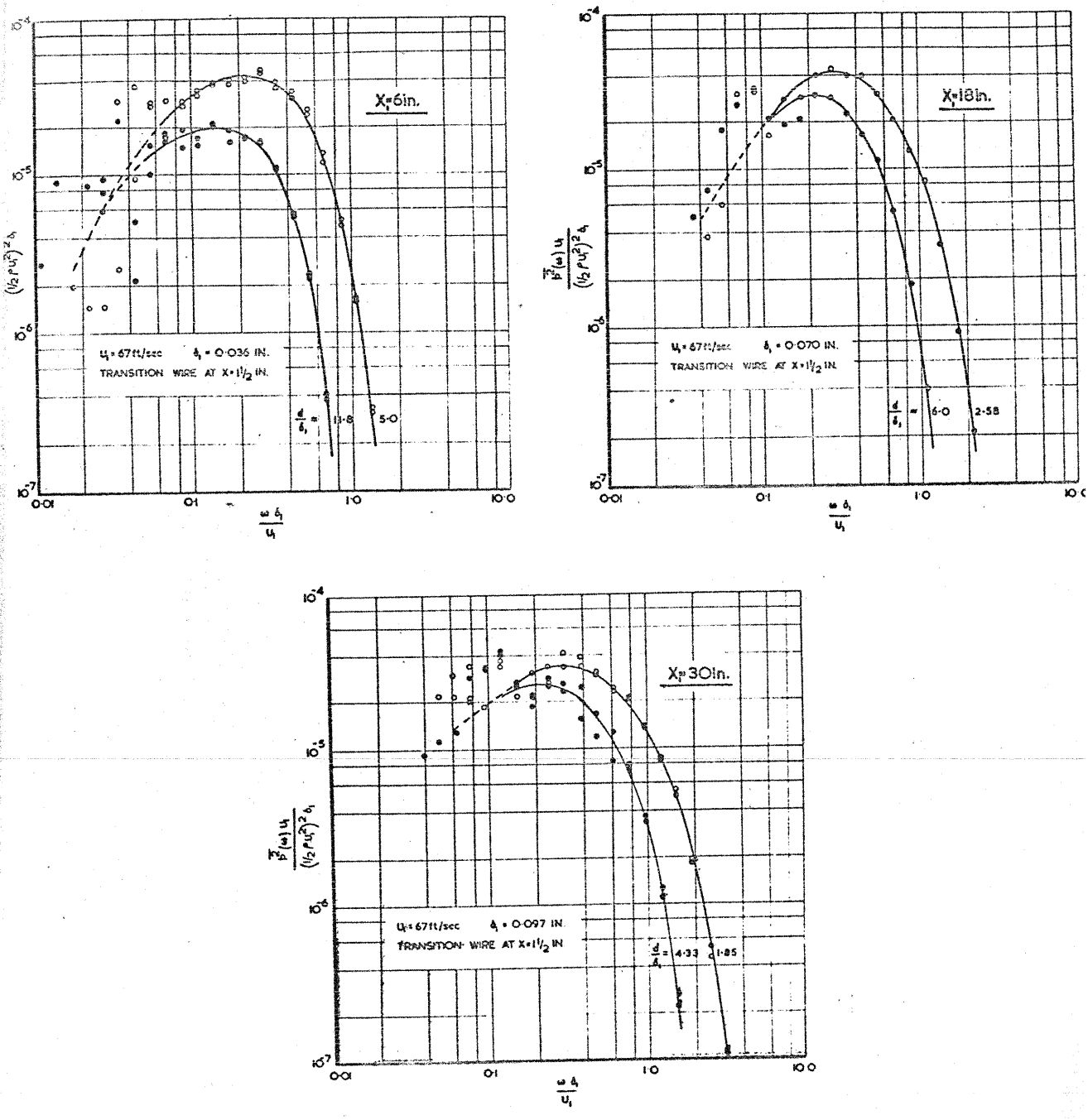

FIG.15. FLAT PLATE AT ZERO INCIDENCE. POWER SPECTRAL DENSITY OF SURFACE PRESSURE FLUCTUATIONS IN A TURBULENT BOUNDARY LAYER.

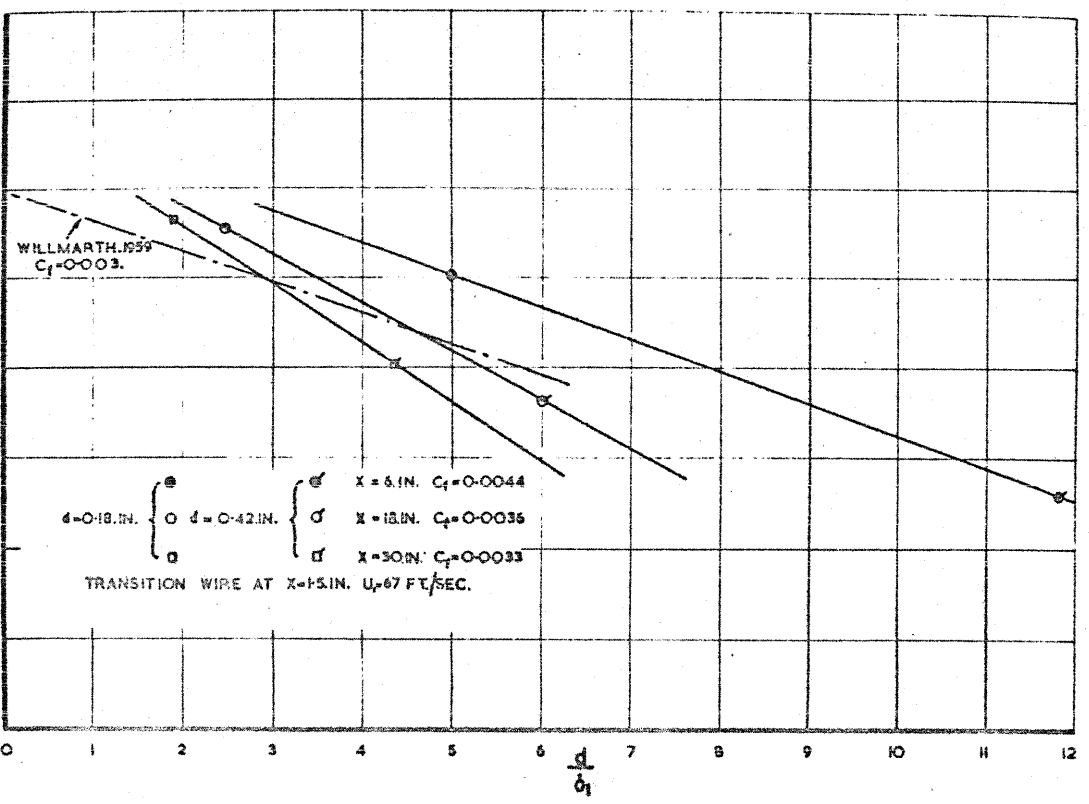

FLAT PLATE AT ZERO INCIDENCE. VARIATION OF NON-DIMENSIONAL RMS WALL PRESSURE FLUCTUATIONS IN A TURBULENT BOUNDARY LAYER WITH MICROPHONE DIAMETER.

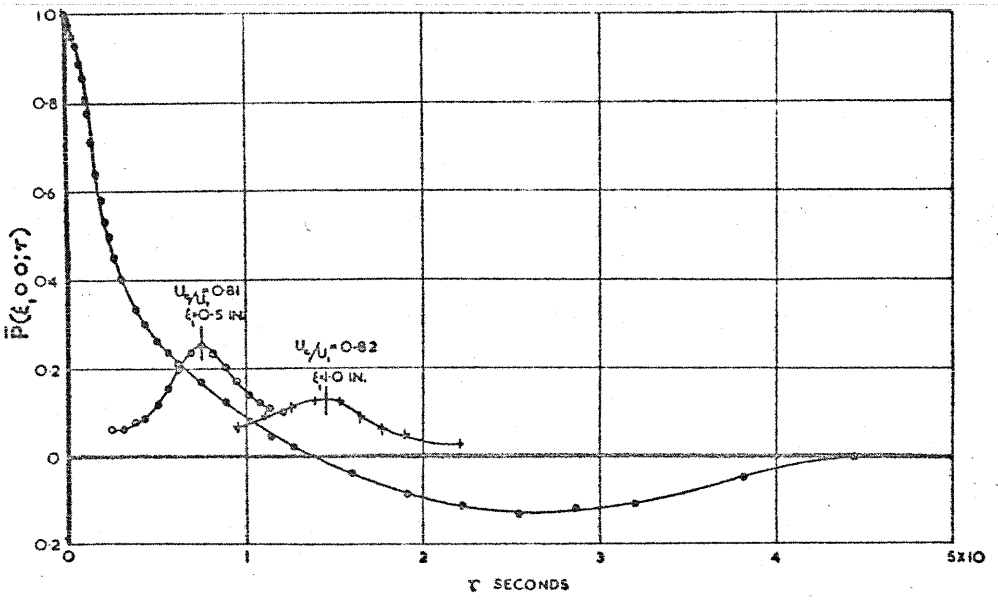

FIG.17. FLAT PLATE AT ZERO INCIDENCE. SPACE-TIME CORRELATIONS OF SURFACE PRESSURE FLUCTUATIONS (AFTER 250c/s HIGH PASS FILTER)

13 A.

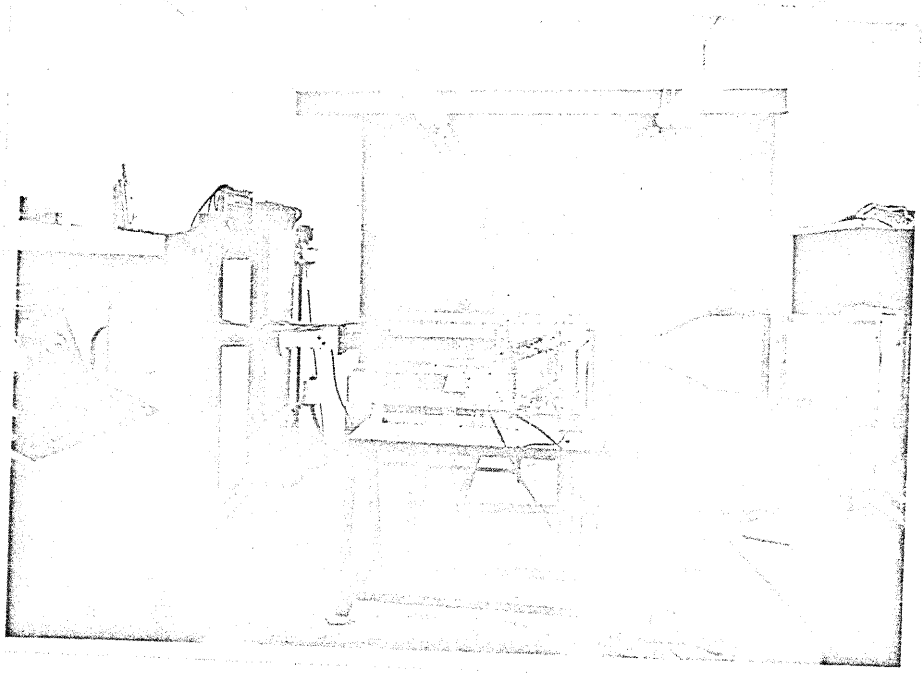

18 A.

FIG.18a. VIEW OF $2\frac{1}{2}$ IN. X $2\frac{1}{2}$ IN. WIND TUNNEL.

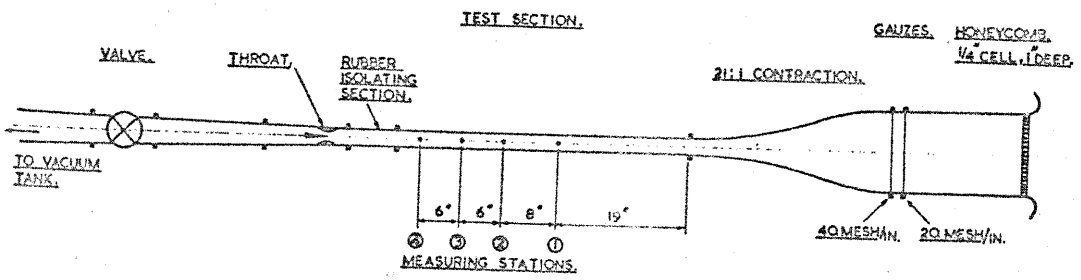

FIG.18b. DIAGRAM OF 2 1/2 IN. X 2 1/2 IN. WIND TUNNEL.

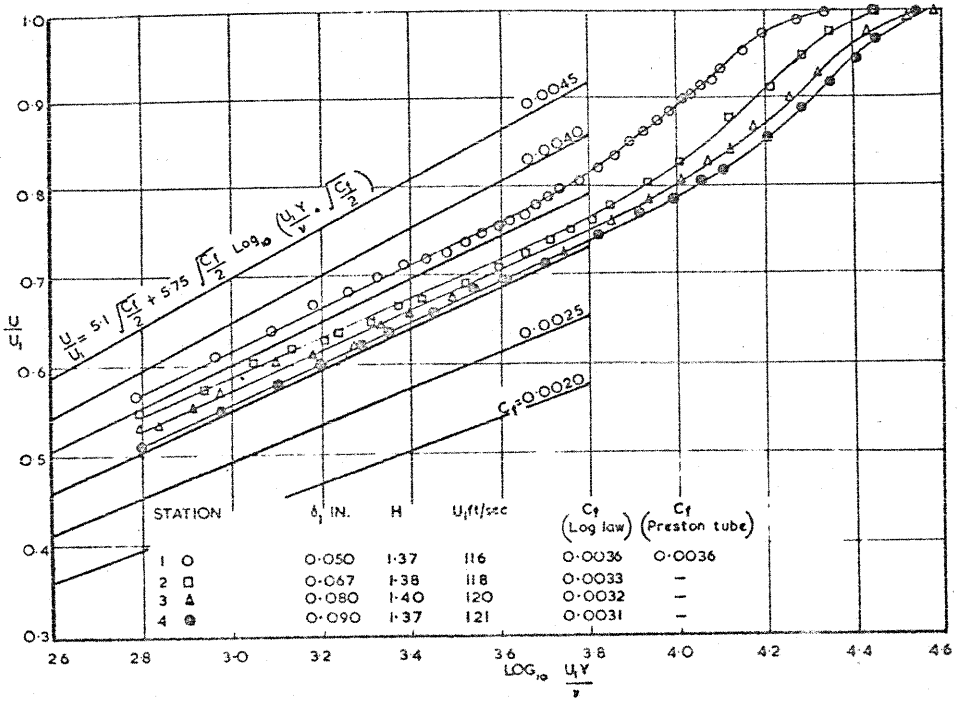

Fig.19a. 2½ IN X 2½ IN. TUNNEL. TURBULENT BOUNDARY LAYER VELOCITY PROFILES ON WORKING-SECTION WALL.

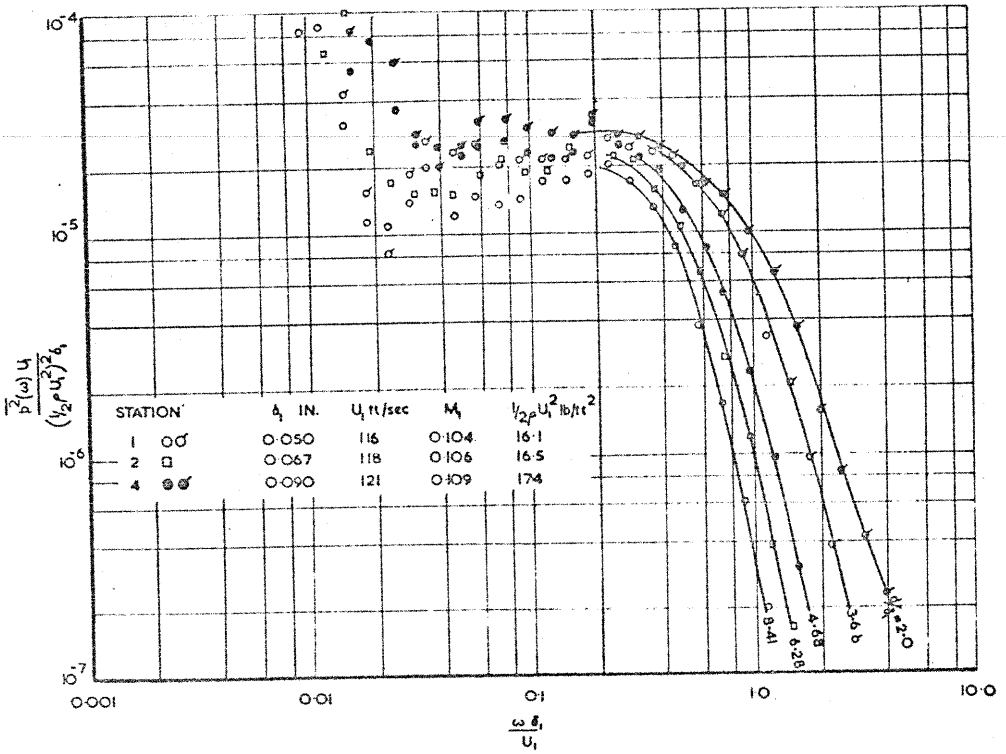

Fig.19b. 2½ IN. X 2½ IN. TUNNEL. POWER SPECTRAL DENSITY OF SURFACE PRESSURE FLUCTUATIONS IN A TURBULENT BOUNDARY LAYER.

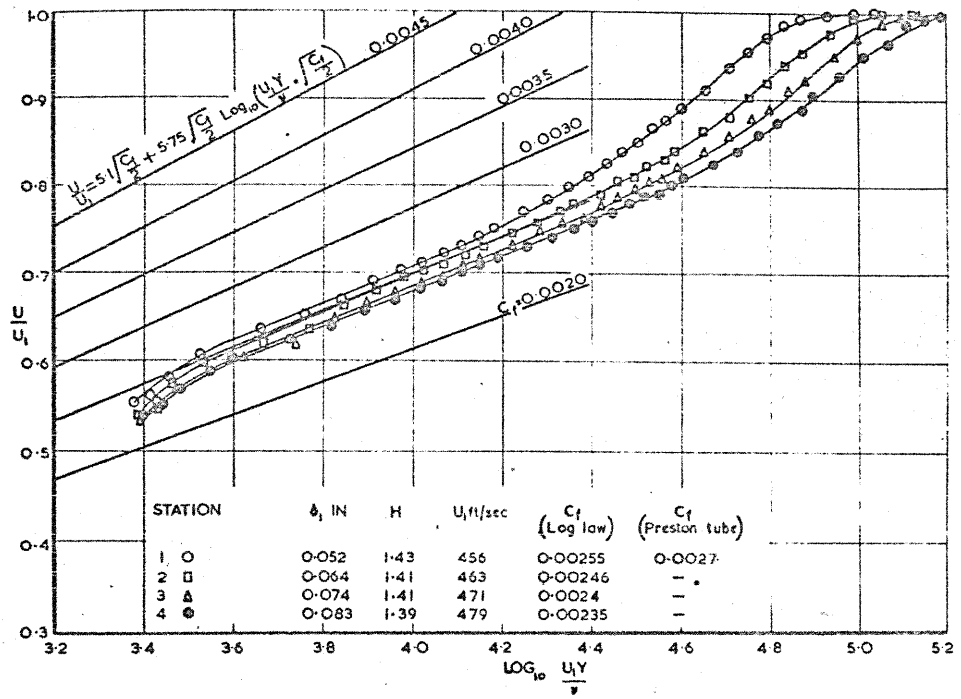

FIG. 20a. $2\frac{1}{2}$ IN X $2\frac{1}{2}$ IN. TUNNEL. TURBULENT BOUNDARY LAYER VELOCITY PROFILES ON WORKING-SECTION WALL.

$\frac{\cdot 052}{12} \times \frac{456}{1\cdot 59\times 10^{-4}}$

$\simeq 1\cdot 2 \times 10^{4}$

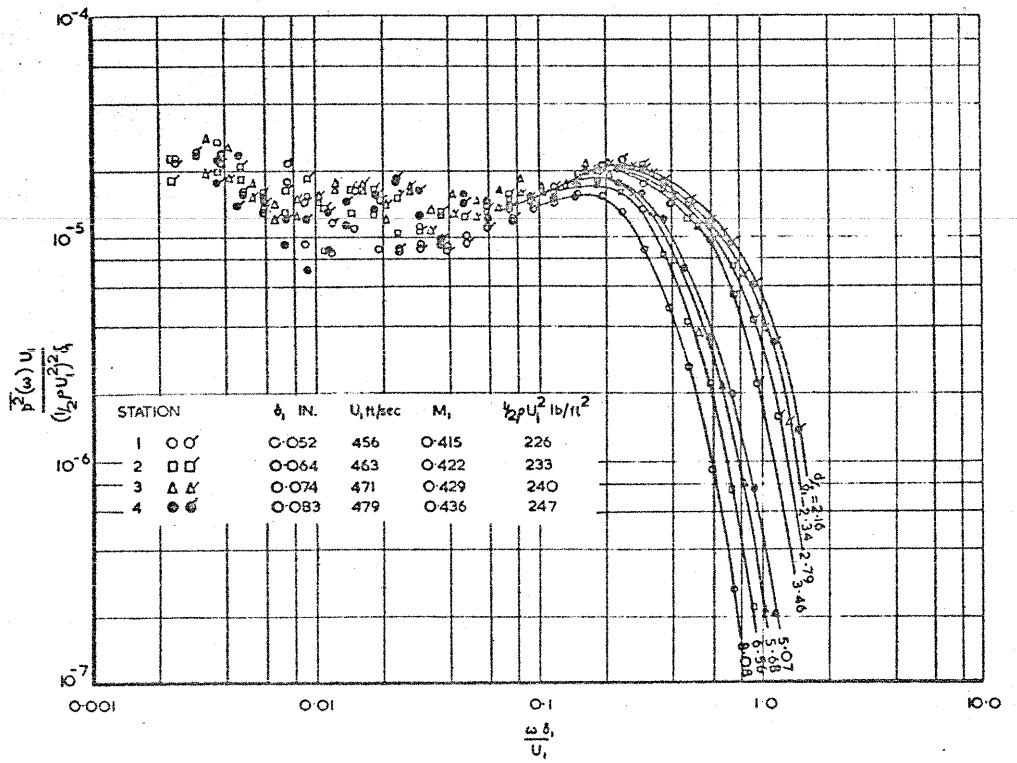

FIG. 20b. $2\frac{1}{2}$ IN. X $2\frac{1}{2}$ IN. TUNNEL. POWER SPECTRAL DENSITY OF SURFACE PRESSURE FLUCTUATIONS IN A TURBULENT BOUNDARY LAYER.

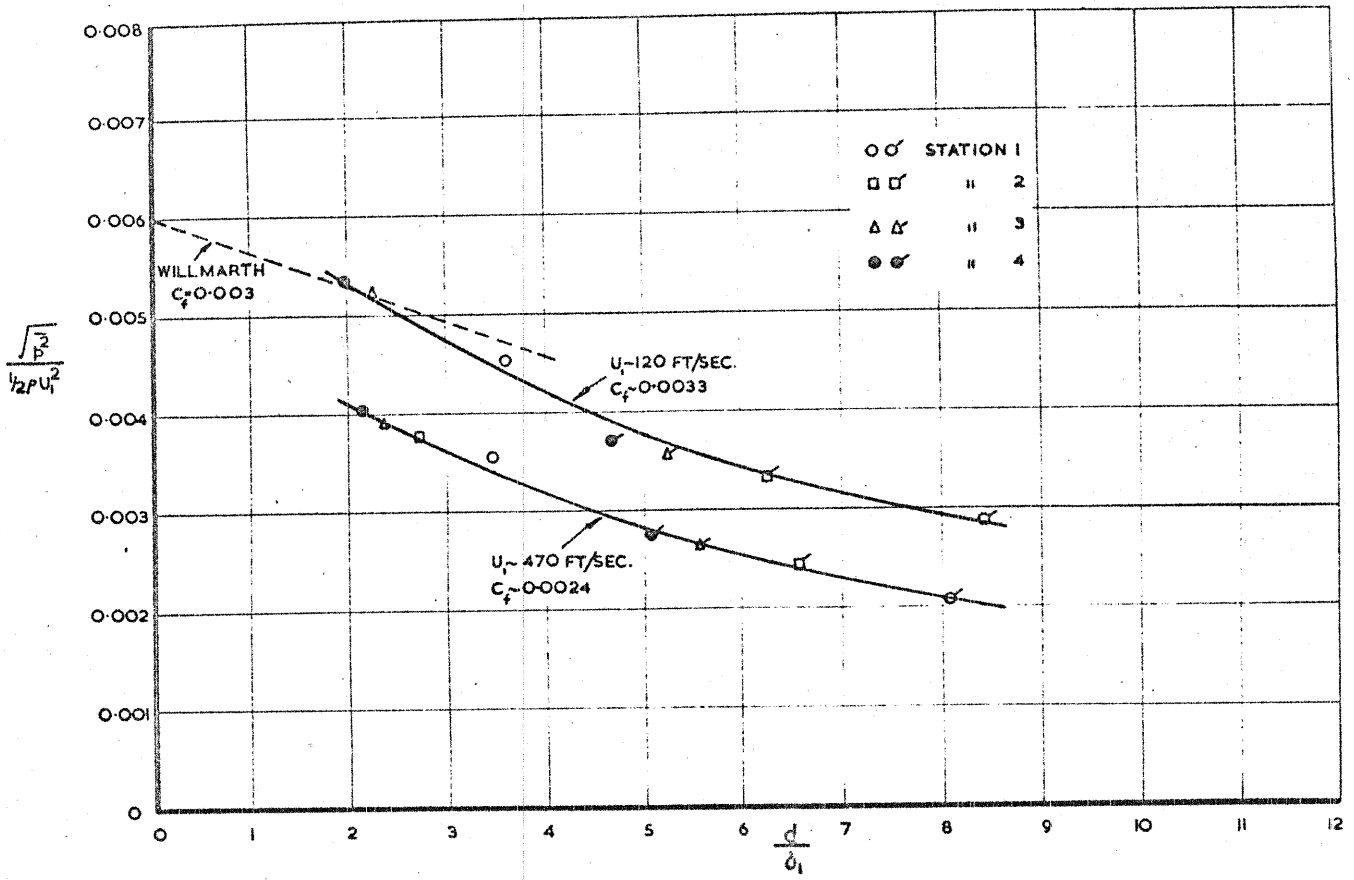

FIG. 21. 2½ IN X 2½ IN. TUNNEL. VARIATION OF NON-DIMENSIONAL RMS WALL PRESSURE FLUCTUATIONS IN A TURBULENT BOUNDARY LAYER WITH MICROPHONE DIAMETER.

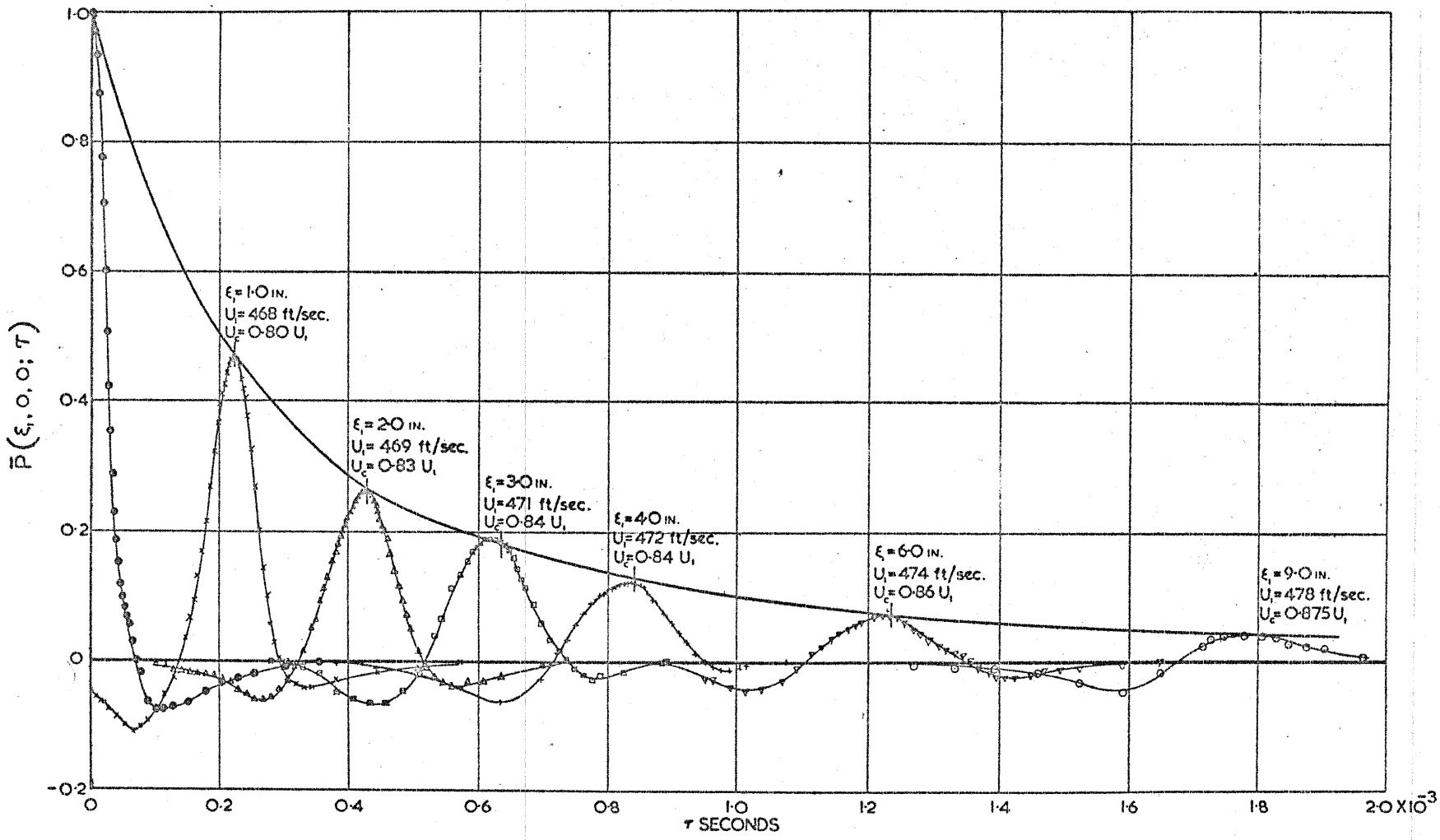

G. 22. 2½ IN. X 2½ IN. TUNNEL. LONGITUDINAL SPACE-TIME CORRELATION OF WALL PRESSURE FLUCTUATIO IN A TURBULENT BOUNDARY LAYER. M_1 = 0·426, U_1 = 467 ft/sec., δ_1 = 0·069 IN. AT FIXED STATION.

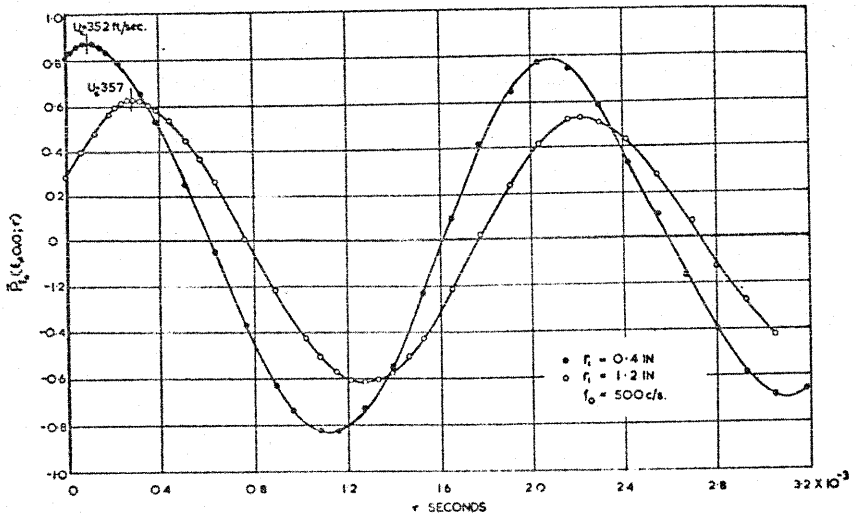

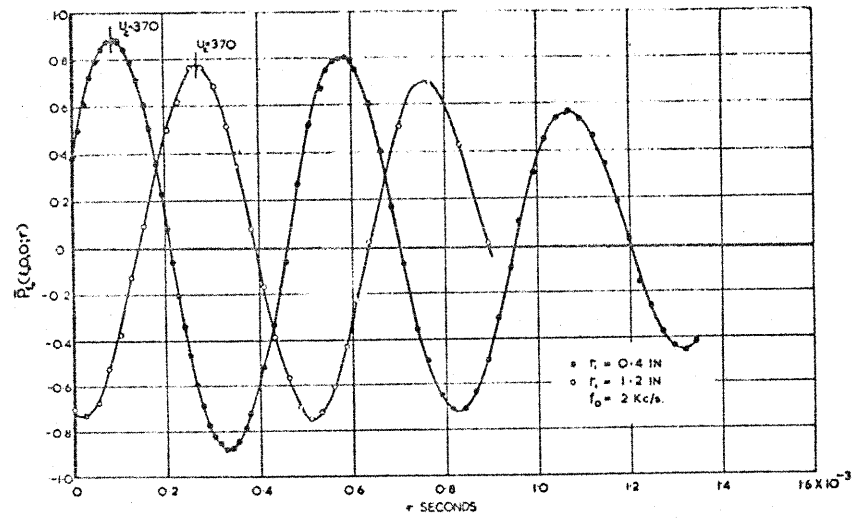

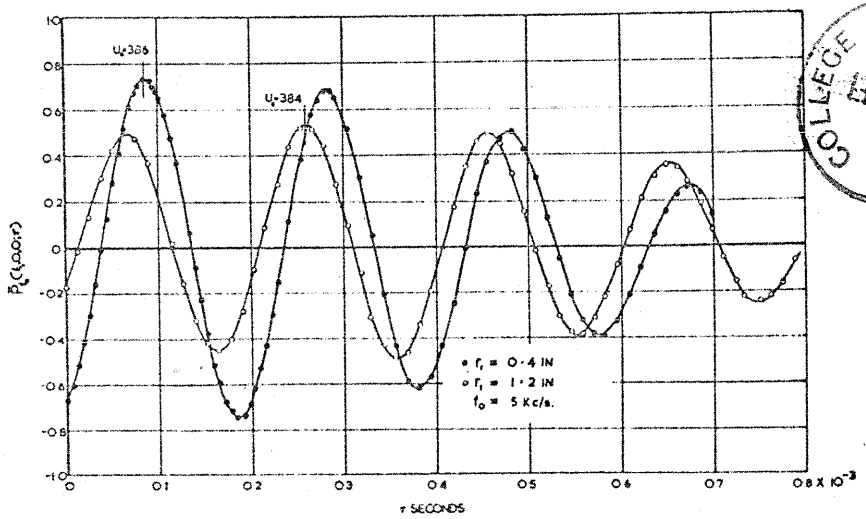

FIG. 23. $2\frac{1}{2}$ IN X $2\frac{1}{2}$ IN. TUNNEL. SPACE-TIME CORRELATIONS OF PRESSURE FLUCTUATIONS IN A TURBULENT BOUNDARY LAYER AFTER $\frac{1}{3}$-OCTAVE FILTERING. U_1 = 464 ft/sec. δ_1 = 0·066 IN. AT FIXED STATION.

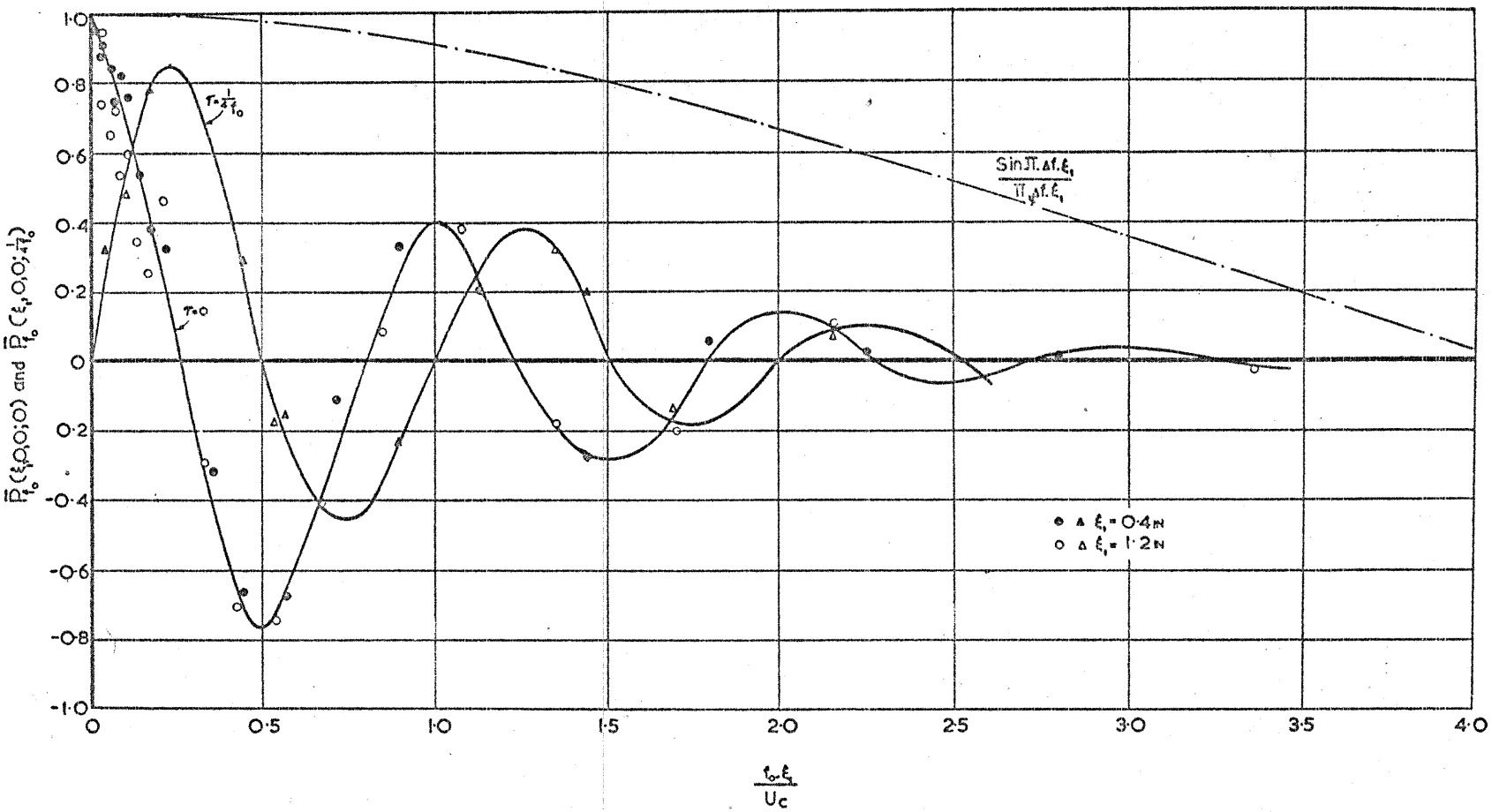

G. 24. 2½ IN. X 2½ IN. TUNNEL. SPATIAL CORRELATIONS OF WALL PRESSURE FLUCTUATIONS IN A TURBULENT BOUNDARY LAYER AFTER 1/3 – OCTAVE FILTERING.

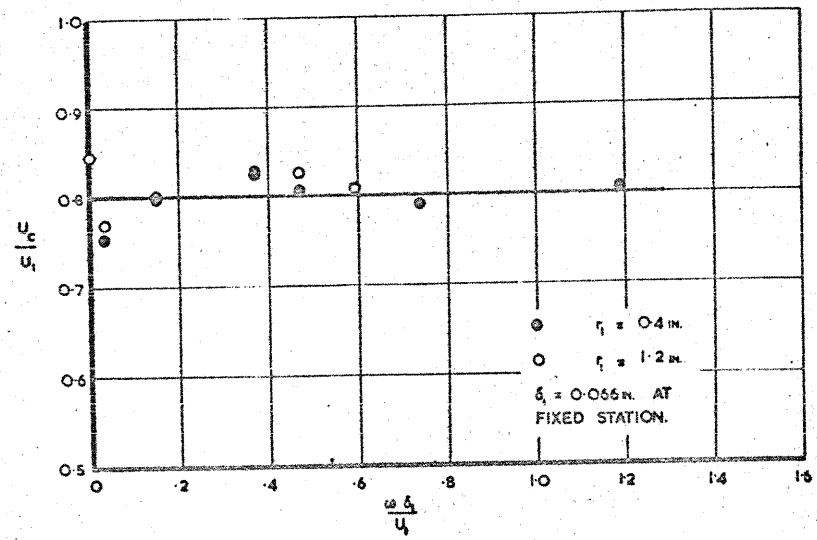

FIG. 25. 2½ IN. X 2½ IN. TUNNEL. VARIATION OF AVERAGE CONVECTION VELOCITY OF PRESSURE FIELD WITH STROUHAL NUMBER. U_1 = 464 ft/sec.

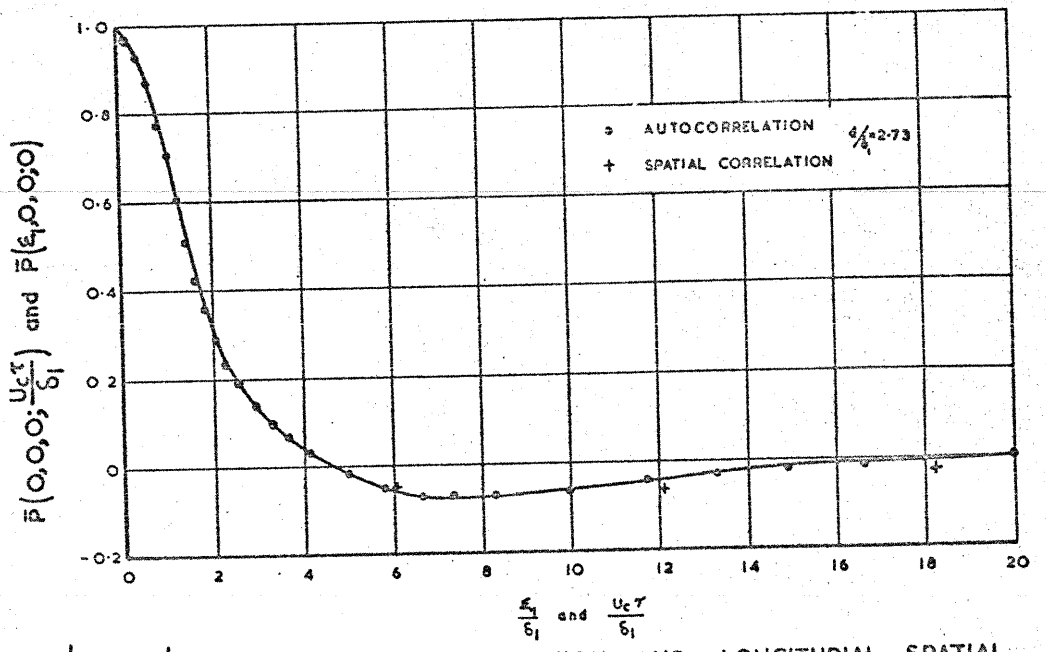

FIG. 26. 2½ IN. x 2½ IN. TUNNEL, AUTOCORRELATION AND LONGITUDIAL SPATIAL CORRELATION OF WALL PRESSURE FLUCTUATIONS IN A TURBULENT BOUNDARY LAYER. M=0·423., U_1 = 464 ft/sec., δ_1 = 0·066 IN.

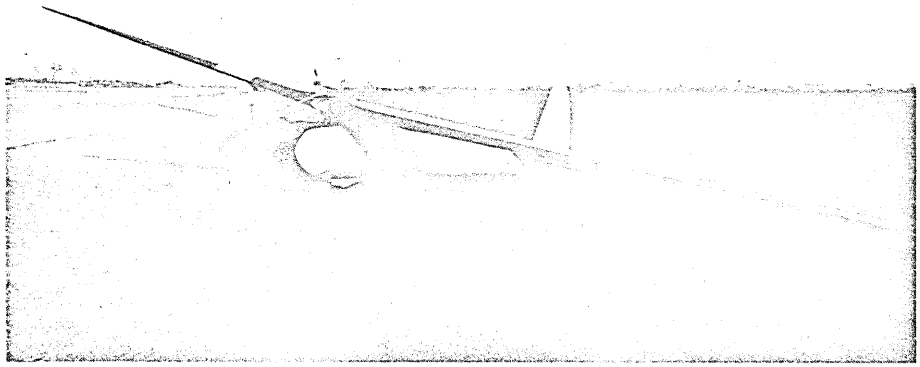

FIG. 27a. VIEW OF OLYMPIA EON GLIDER.

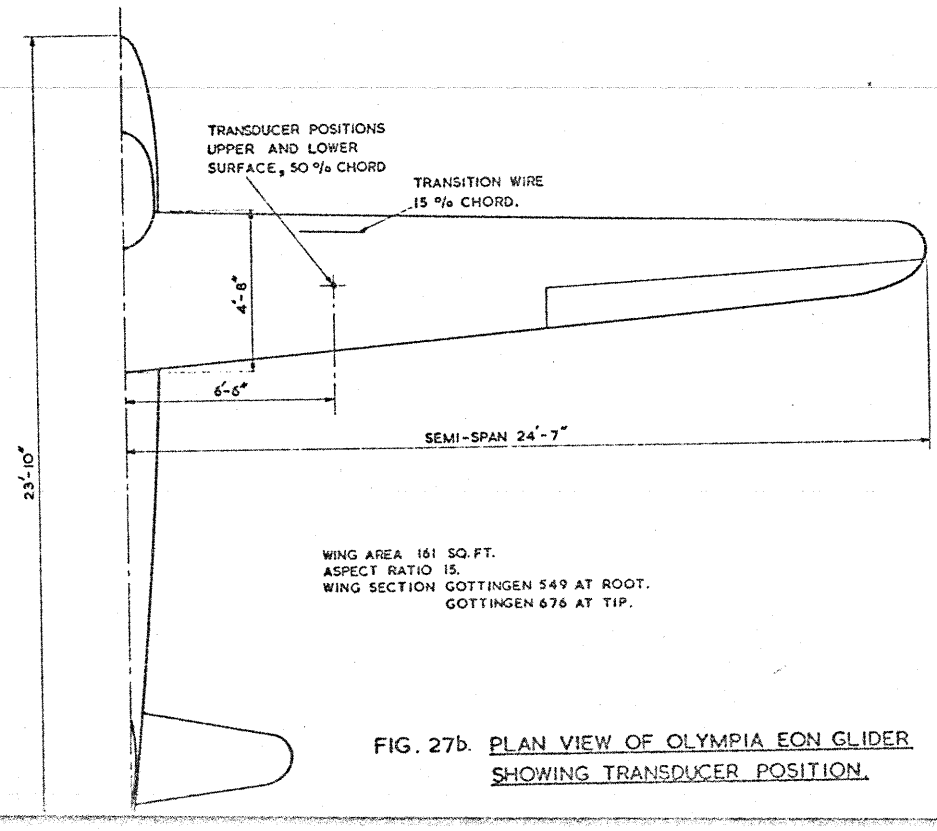

FIG. 27b. PLAN VIEW OF OLYMPIA EON GLIDER SHOWING TRANSDUCER POSITION.

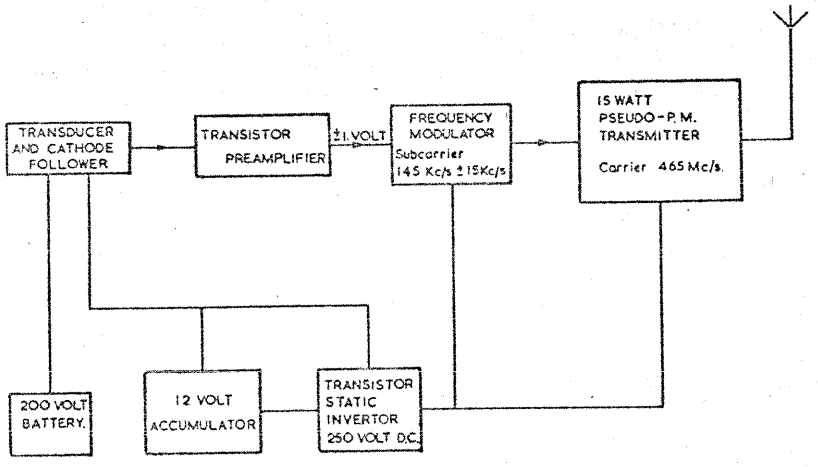

FIG. 28a. TELEMETRY IN OLYMPIA GLIDER.

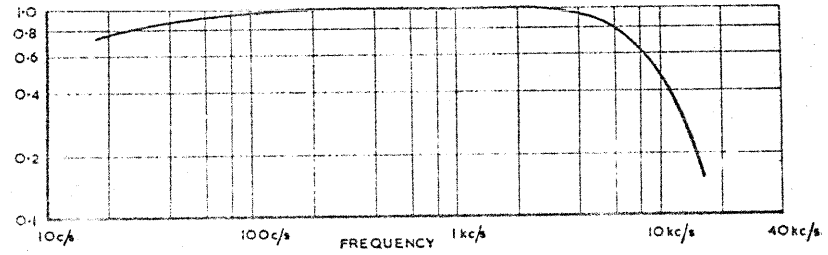

FIG. 28b. OVERALL FREQUENCY RESPONSE OF TELEMETRY SYSTEM.

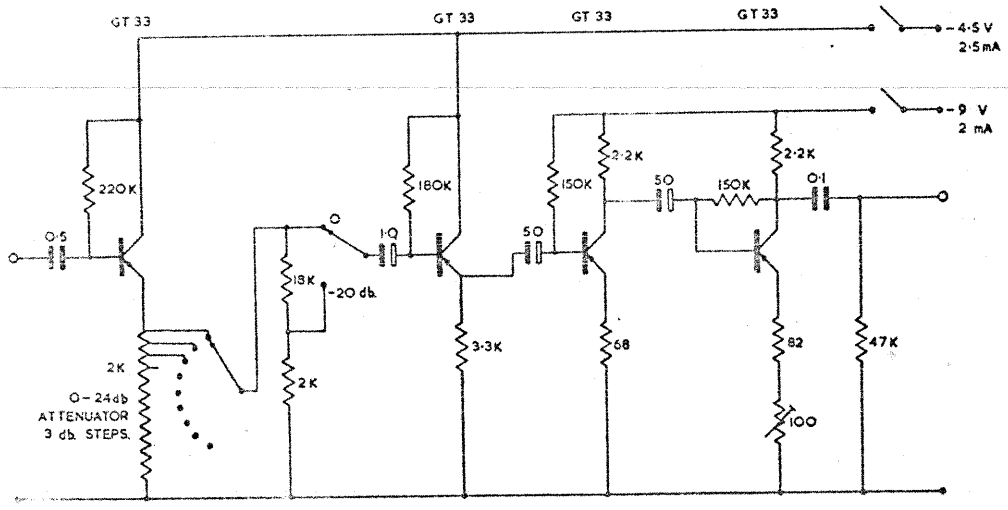

GAIN 300 MAX.
BANDWIDTH 6 c/s - 30 Kc/s (-3 db).
INPUT NOISE LEVEL 50 μV. R.M.S.
OVERLOAD LEVEL 2 V. R.M.S. OUTPUT.

ALL RESISTORS IN OHMS,
CAPACITORS IN mfds.

FIG. 29. TRANSISTORISED PREAMPLIFIER IN OLYMPIA GLIDER.

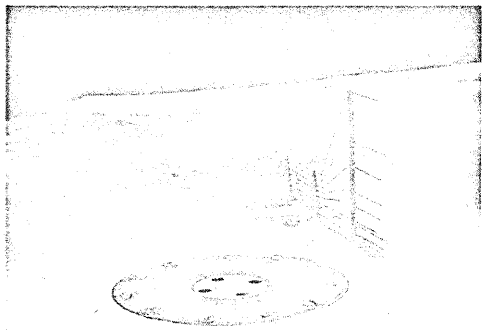

FIG.30. FLUSH MOUNTING OF BK4133 TRANSDUCER IN WING UPPER SURFACE.

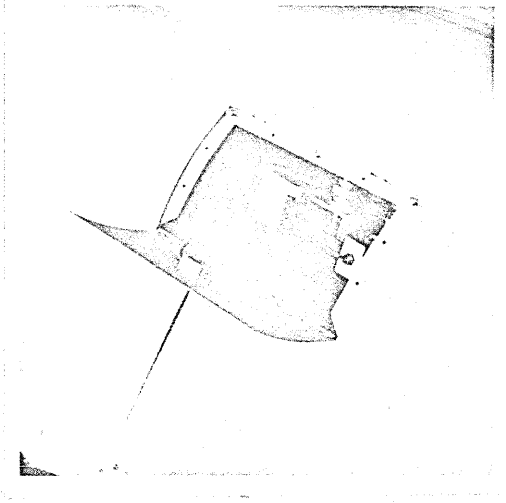

FIG.31. TELEMETRY AND AERIAL INSTALLATION IN FUSELAGE.

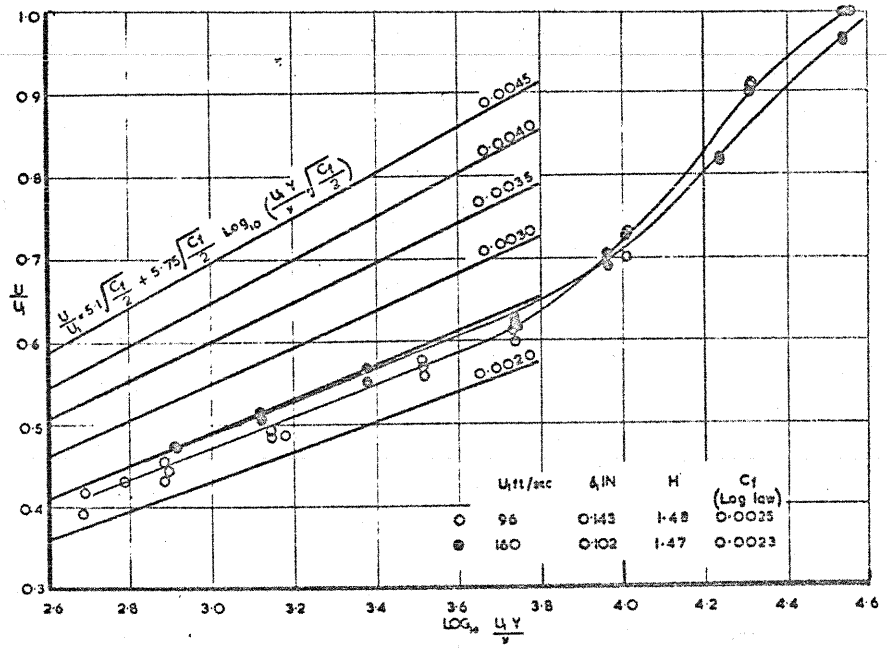

FIG. 32. OLYMPIA GLIDER. TURBULENT BOUNDARY LAYER VELOCITY PROFILES ON WING UPPER SURFACE AT 50% CHORD. TRANSITION WIRE AT 15% CHORD.

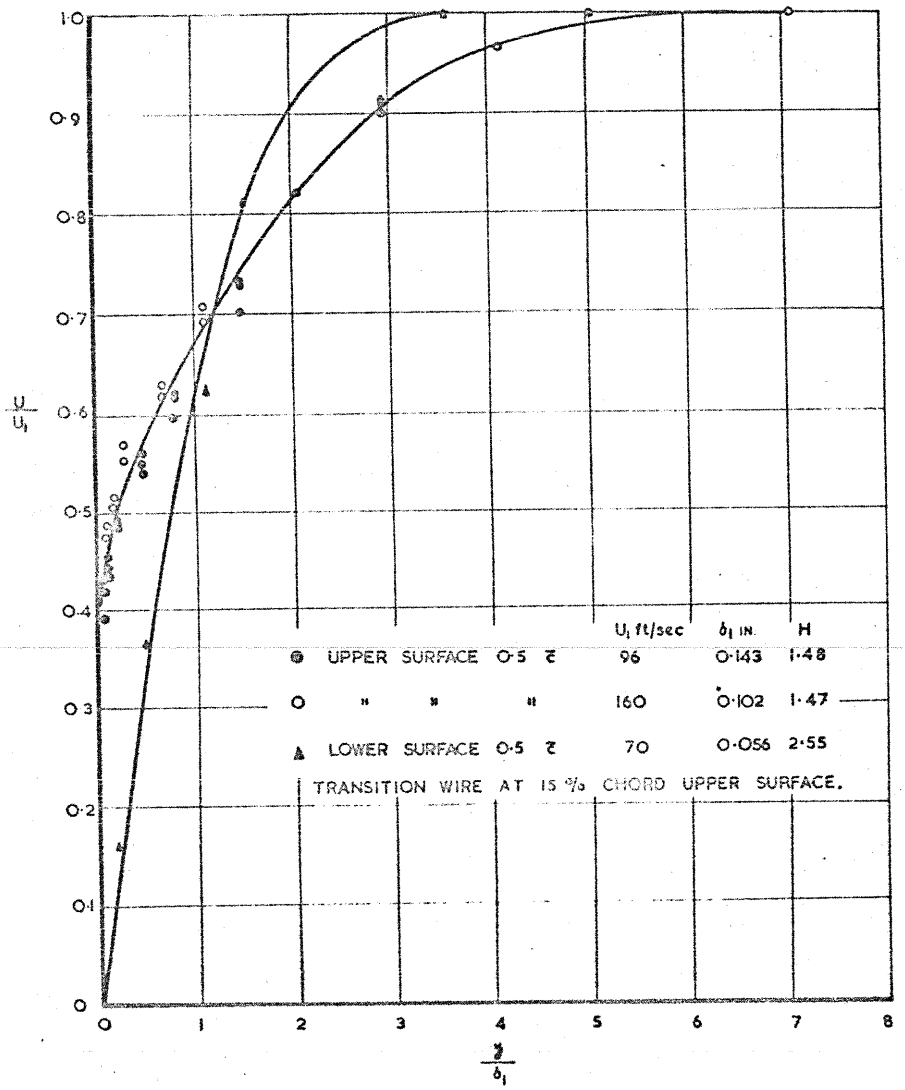

FIG. 33. OLYMPIA GLIDER. TURBULENT BOUNDARY LAYER VELOCITY PROFILES ON WING UPPER SURFACE AND LAMINAR PROFILE ON LOWER SURFACE.

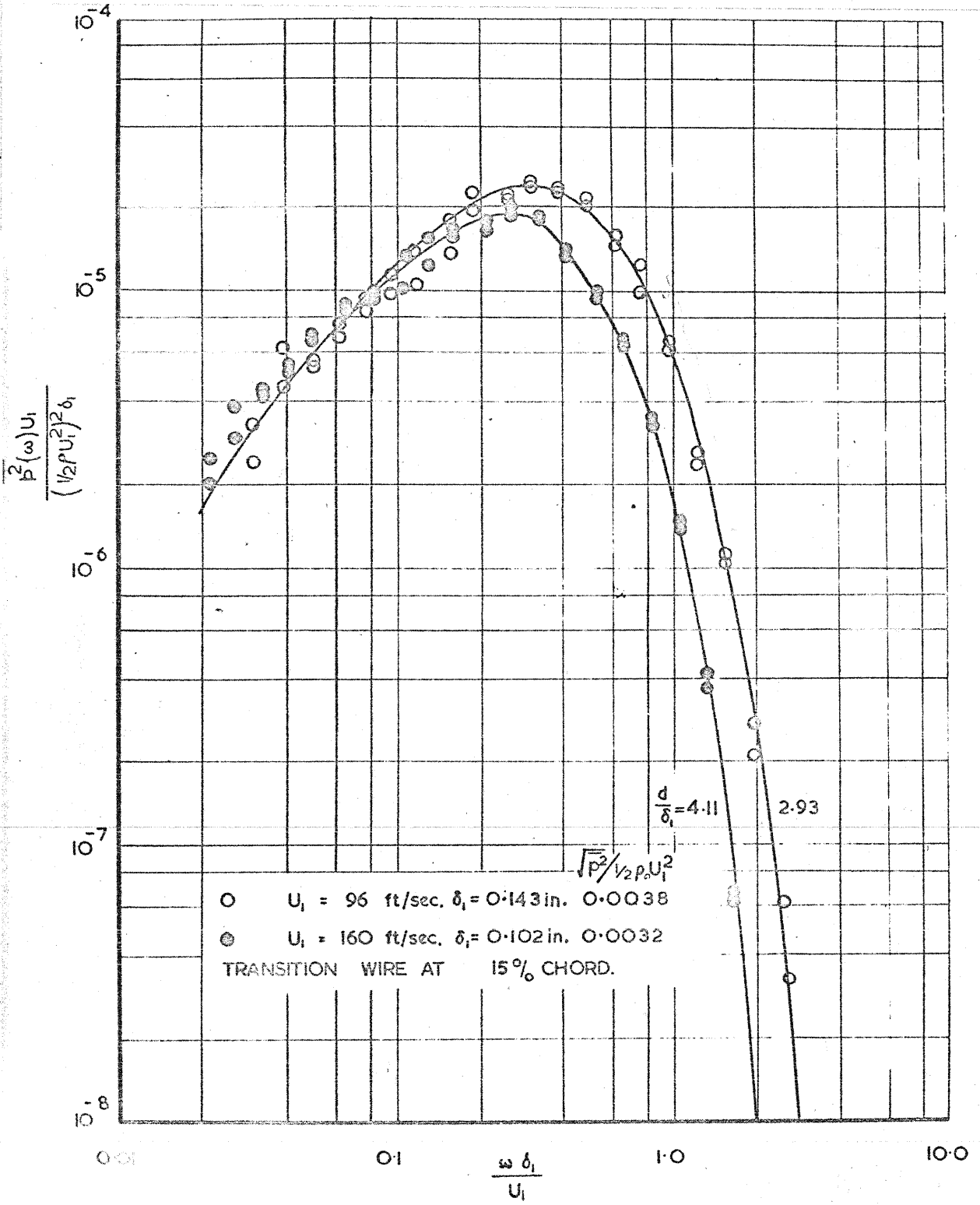

G. 34. OLYMPIA GLIDER. POWER SPECTRAL DENSITY OF SURFACE PRESSURE FLUCTUATIONS IN A TURBULENT BOUNDARY LAYER ON WING UPPER SURFACE. 50% CHORD.

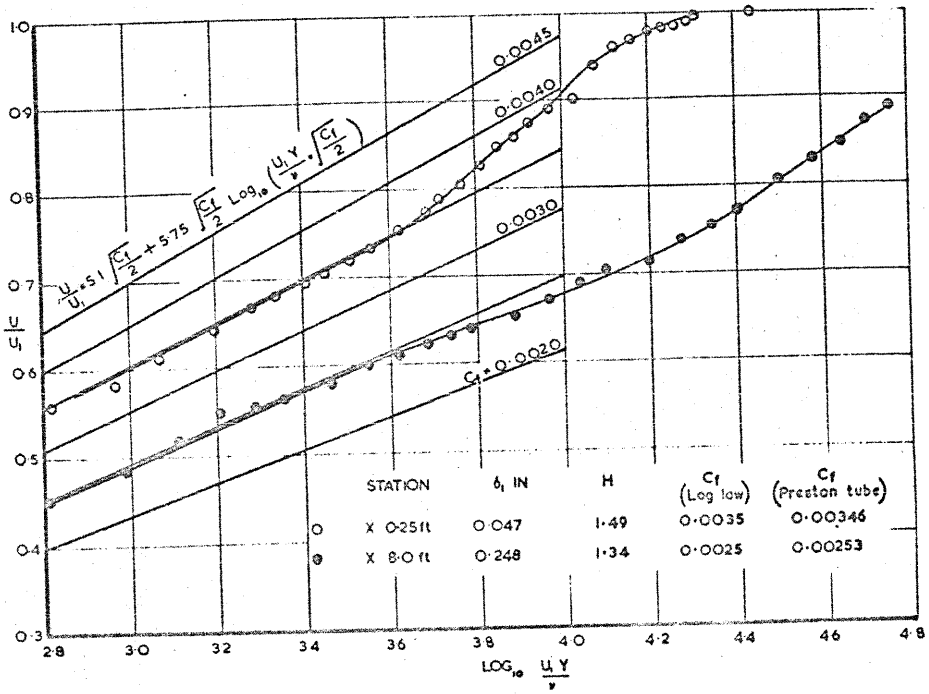

FIG. 35a. 20 IN. X 10 IN. TUNNEL. TURBULENT BOUNDARY LAYER VELOCITY PROFILES ON WORKING-SECTION WALL. U_1=126 ft/sec.

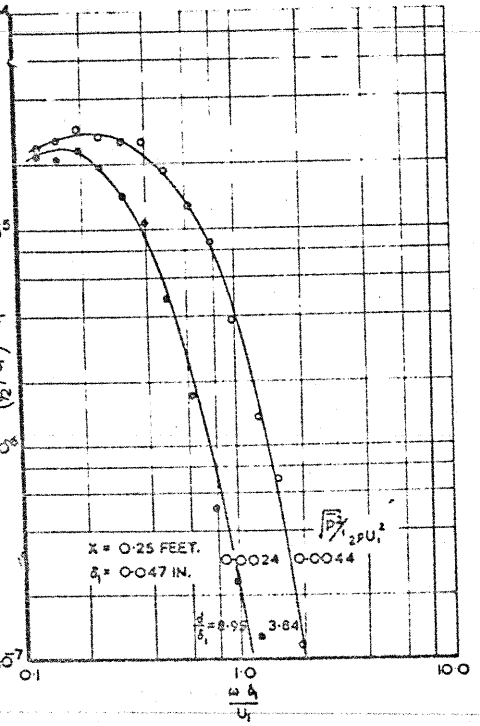

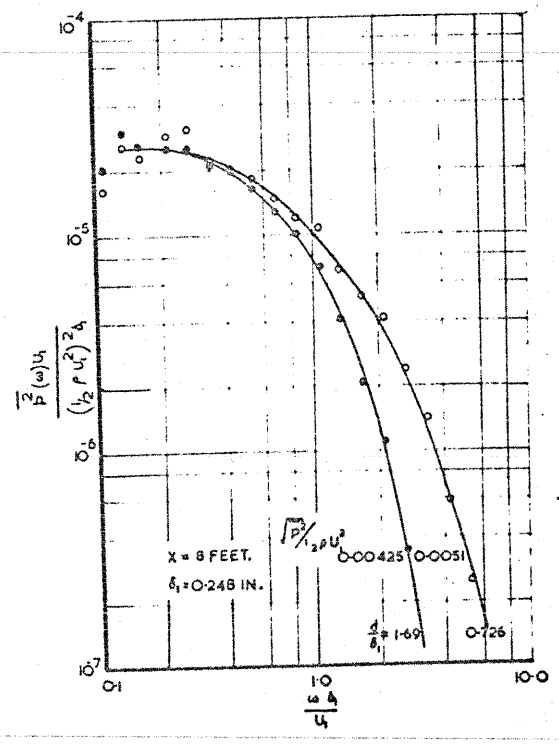

20 IN. X 10 IN. TUNNEL. POWER SPECTRAL DENSITY OF SURFACE PRESSURE FLUCTUATIONS

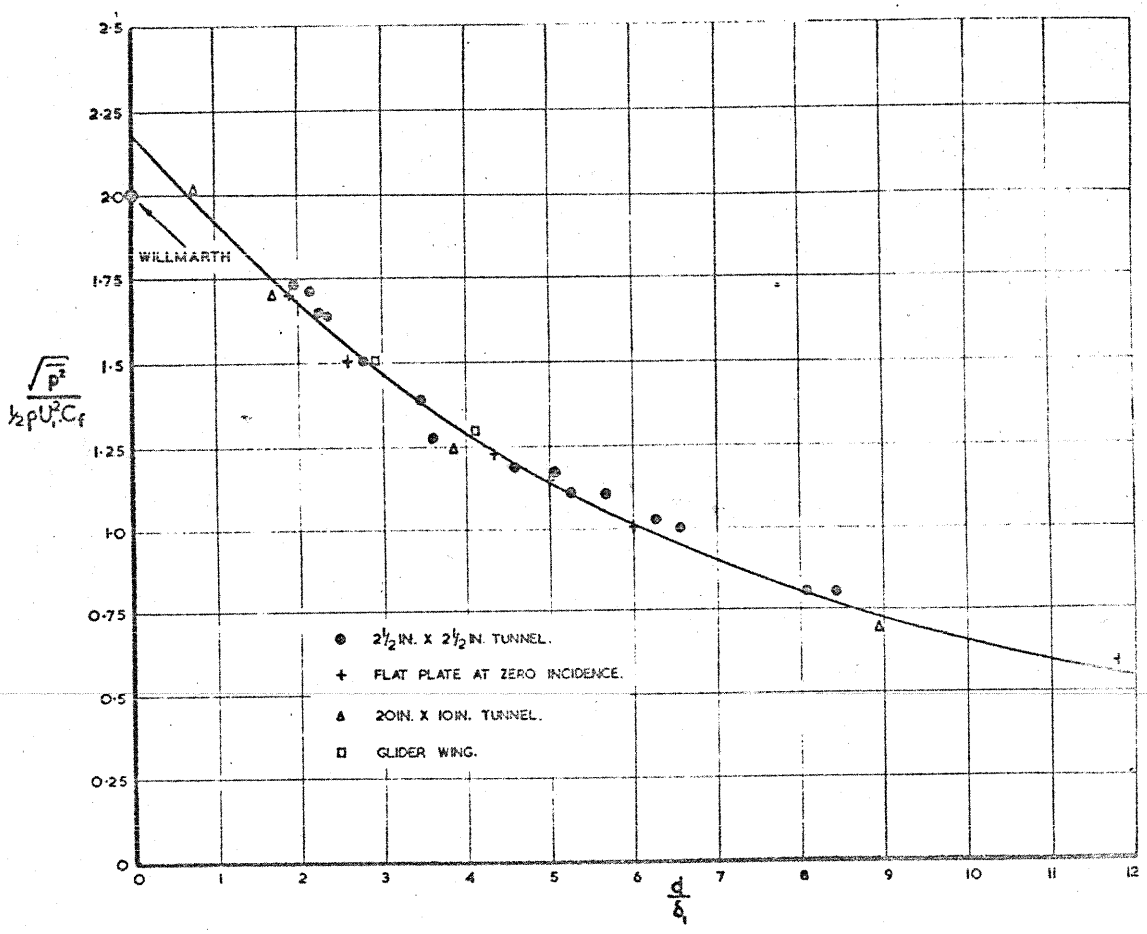

FIG. 36. VARIATION OF NON-DIMENSIONAL WALL PRESSURE FLUCTUATIONS IN A TURBULENT BOUNDARY LAYER WITH MICROPHONE DIAMETER AND SKIN-FRICTION COEFFICIENT.

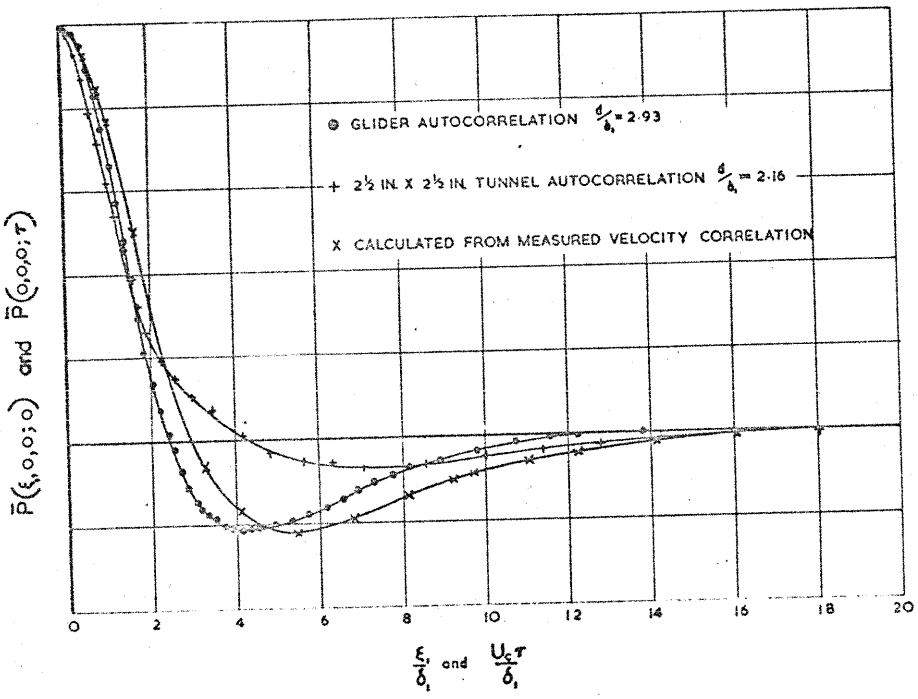

FIG. 37 COMPARISON OF SPATIAL CORRELATION AND AUTOCORRELATION OF WALL PRESSURE FLUCTUATIONS IN A TURBULENT BOUNDARY LAYER.

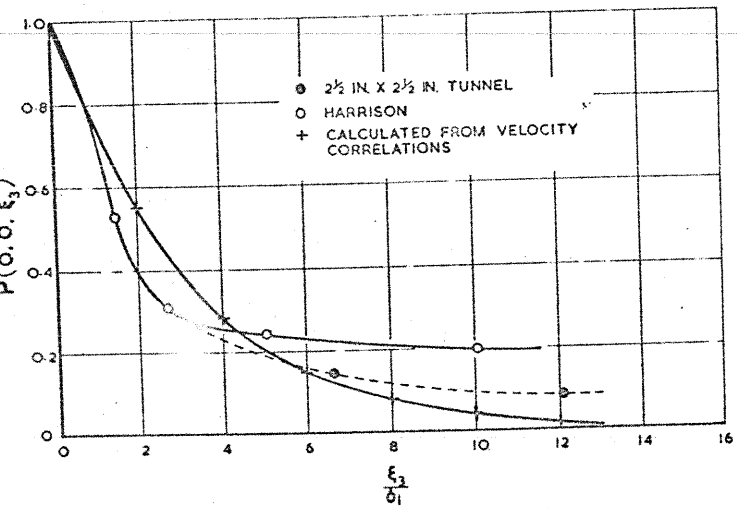

$2\frac{1}{2}$ IN. X $2\frac{1}{2}$ IN. TUNNEL. TRANSVERSE SPATIAL CORRELATION OF WALL PRESSURE FLUCTUATIONS IN A TURBULENT BOUNDARY LAYER.

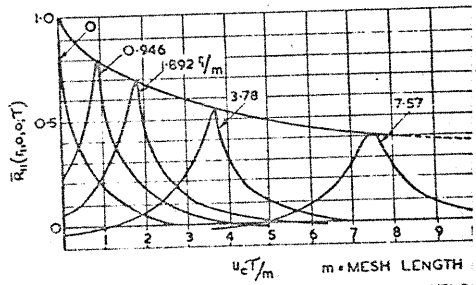

SPACE-TIME CORRELATION OF LONGITUDINAL VELOCITY COMPONENT FOR GRID TUBULENCE (FAVRE 1958).

FIG. 39.

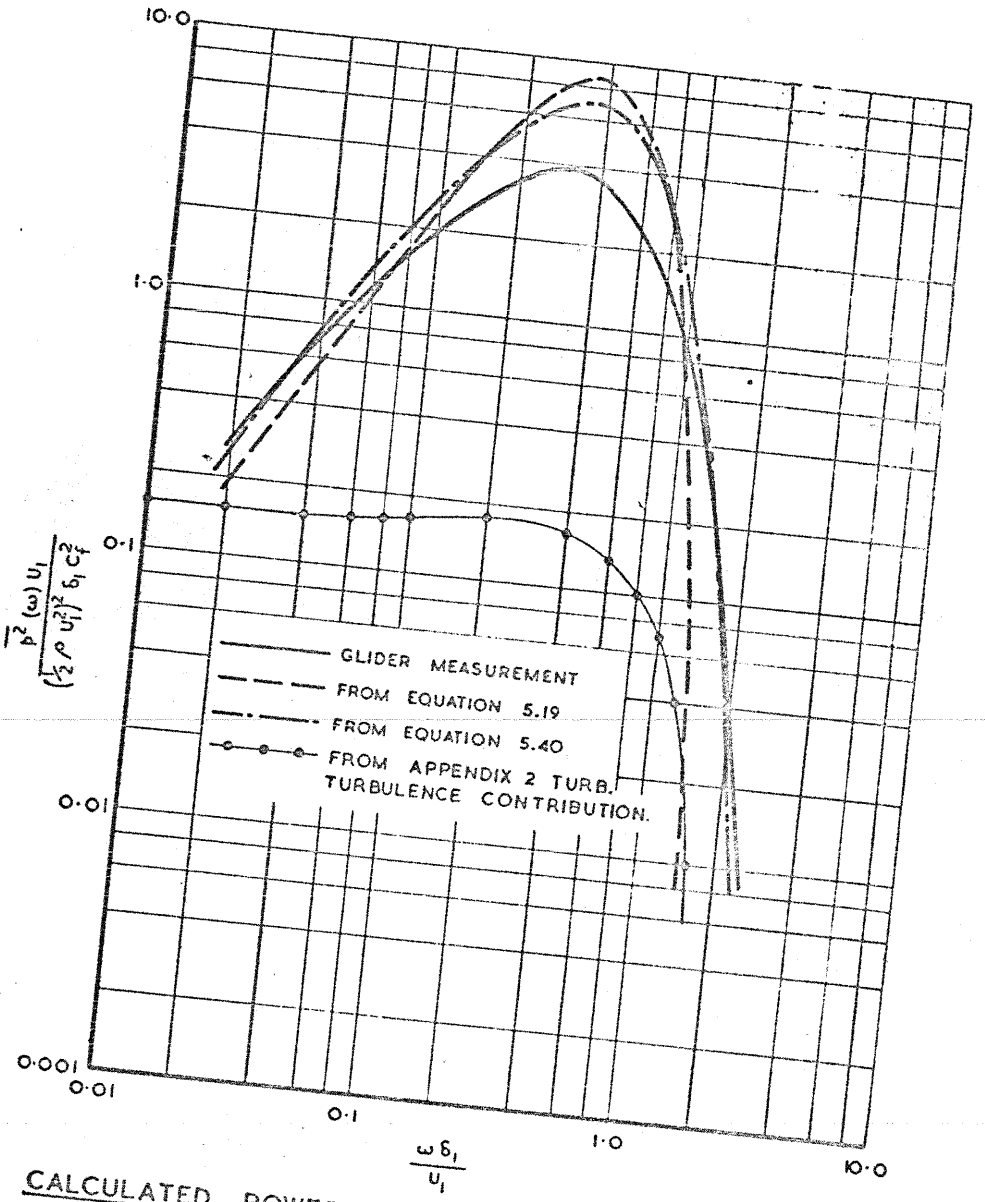

FIG. 40. CALCULATED POWER SPECTRAL DENSITY OF SURFACE PRESSURE FLUCTUATIONS IN A TURBULENT BOUNDARY LAYER

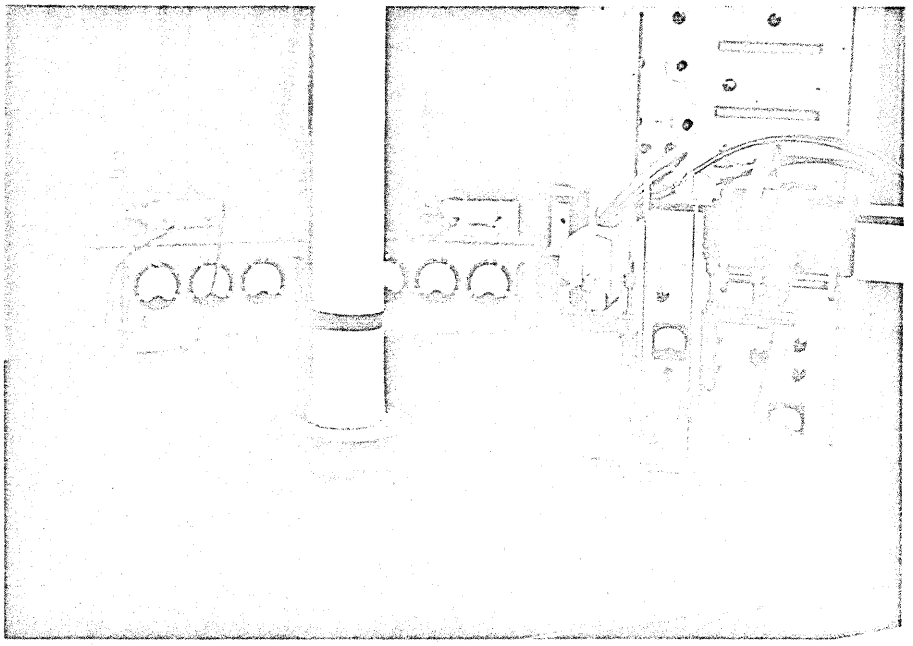

FIG. 41a. VIEW OF RADIAL WALL-JET FACILITY AND HOT-WIRE TRAVERSING GEAR.

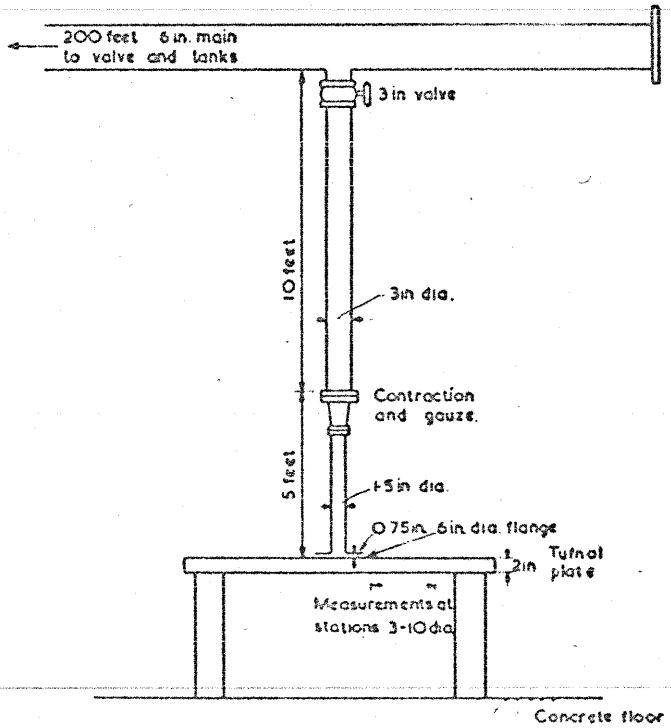

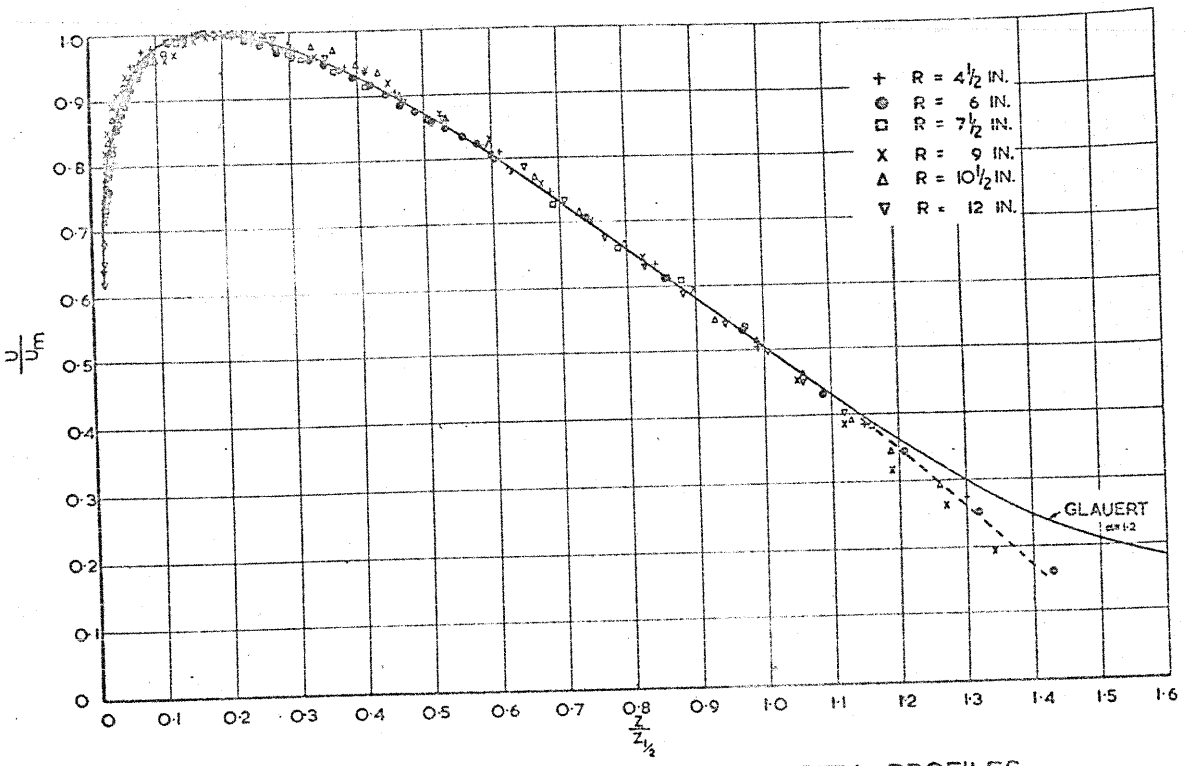

FIG. 42a. RADIAL WALL-JET. MEAN VELOCITY PROFILES.

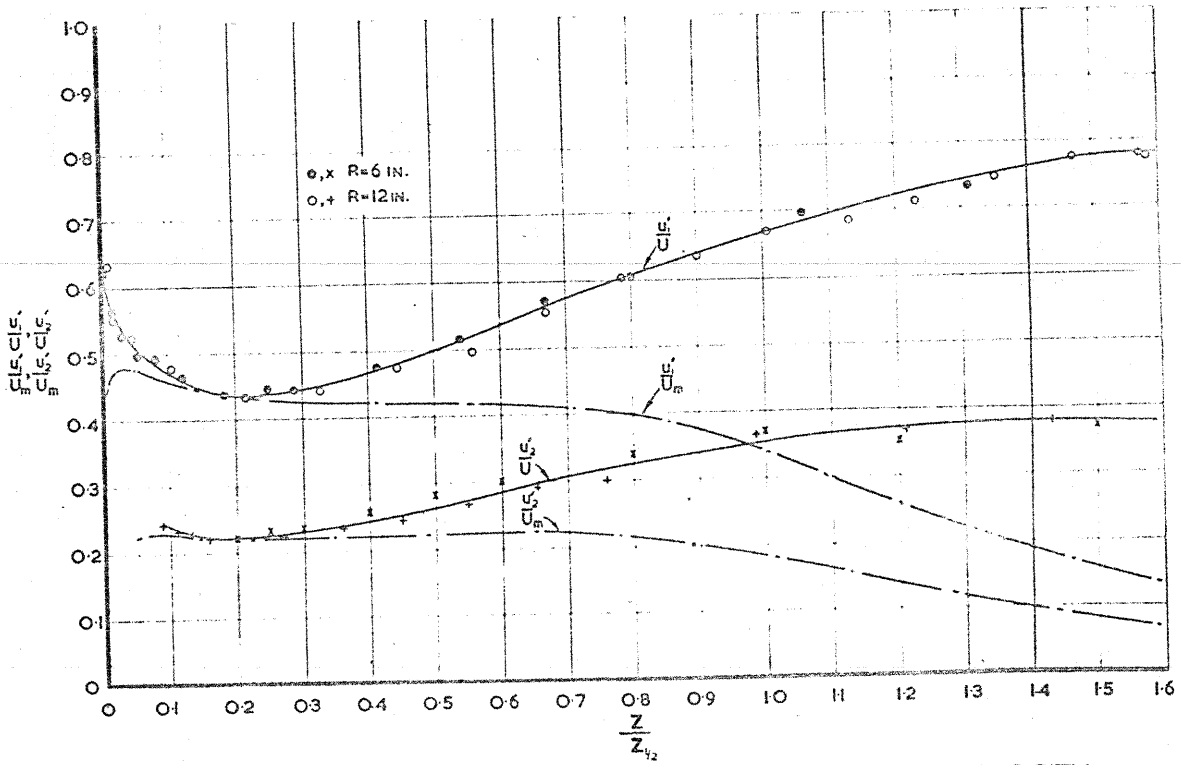

FIG. 42b. RADIAL WALL-JET. LATERAL VARIATION OF TURBULENT VELOCITY INTENSITIES.

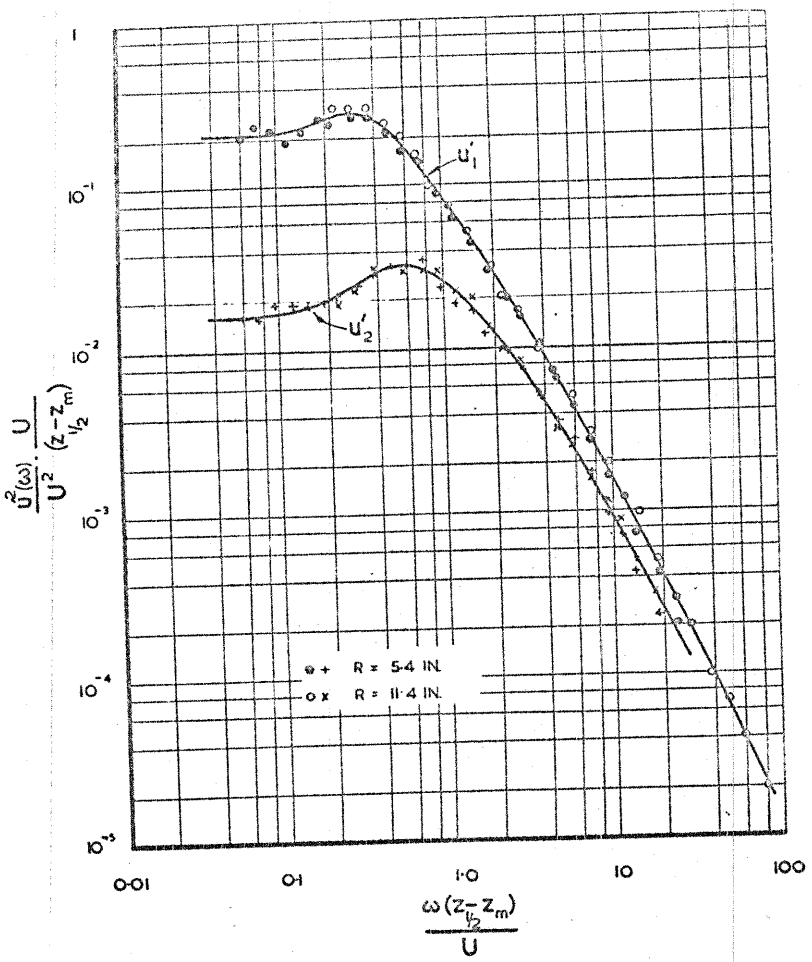

FIG. 43a. RADIAL WALL-JET. POWER SPECTRAL DENSITY OF u_1' AND u_2' TURBULENT VELOCITY FLUCTUATIONS AT $z/z_{1/2}=0·6$, $U/U_m\simeq 0·8$.

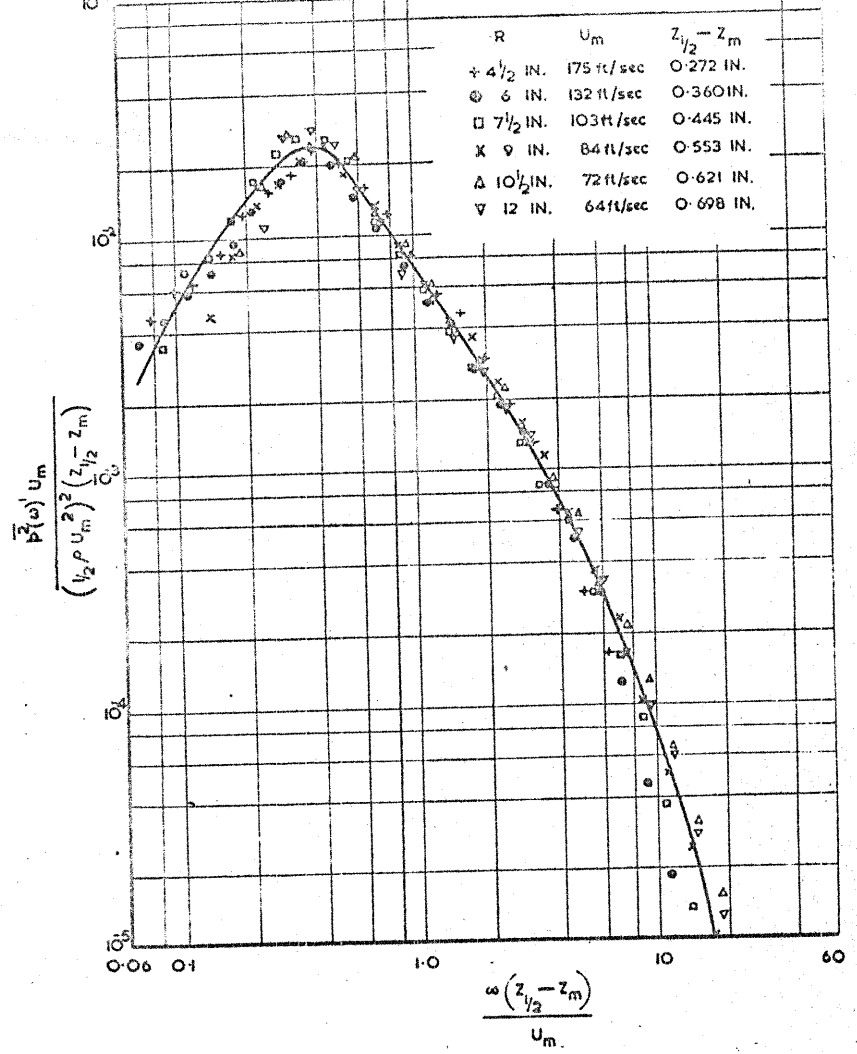

FIG. 43b. RADIAL WALL-JET. POWER SPECTRAL DENSITY OF SURFACE PRESSURE FLUCTUATIONS.

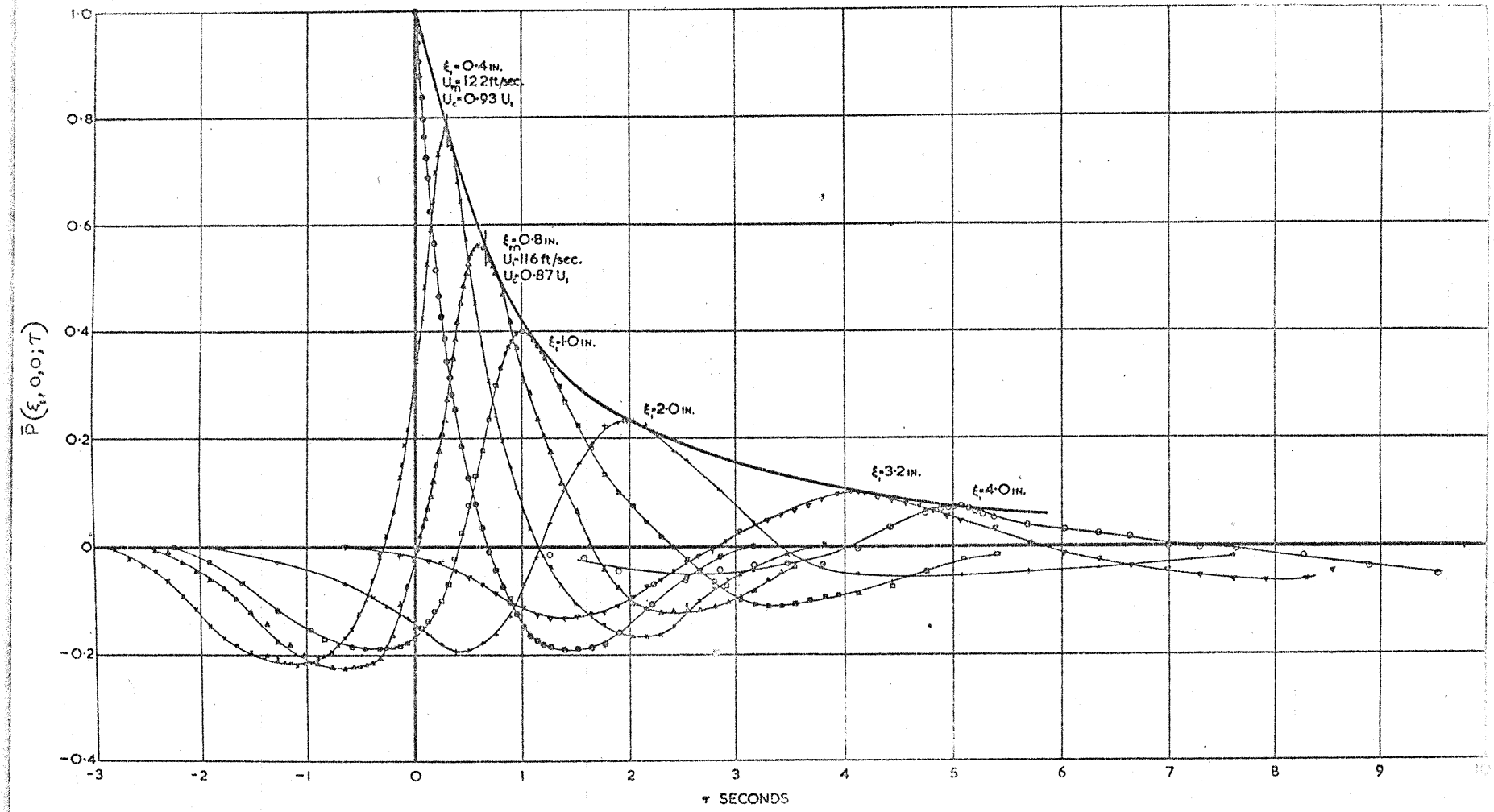

G.44. RADIAL WALL-JET. LONGITUDINAL SPACE-TIME CORRELATION OF SURFACE PRESSURE FLUCTUATIONS

R = 6·3 IN. U_m = 129 ft/sec, $z_{1/2}$ = 0·45 IN. AT FIXED STATION.

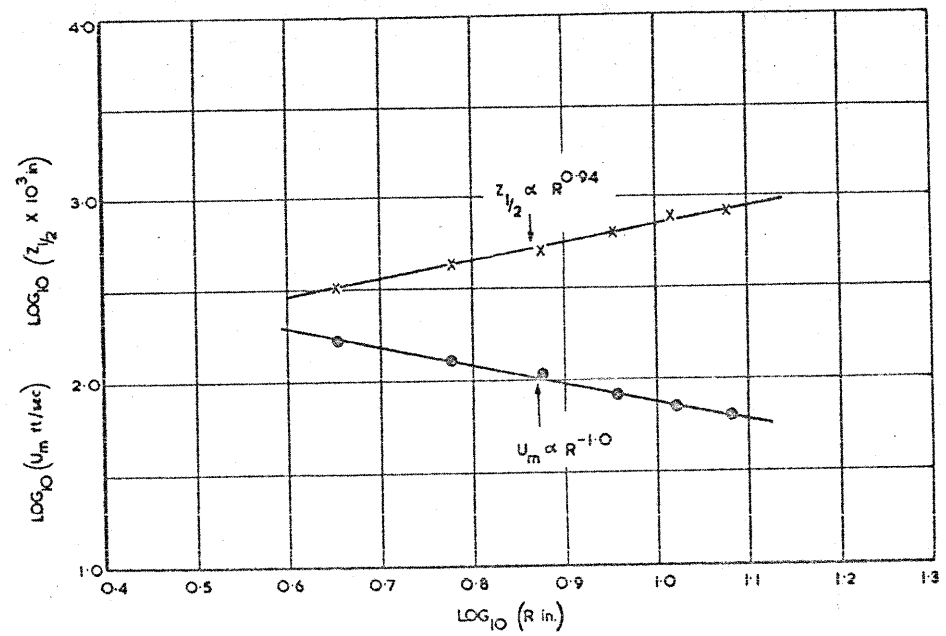

FIG. 45. RADIAL WALL-JET. VARIATION OF JET THICKNESS $z_{1/2}$ AND MAXIMUM VELOCITY U_m WITH RADIUS R.

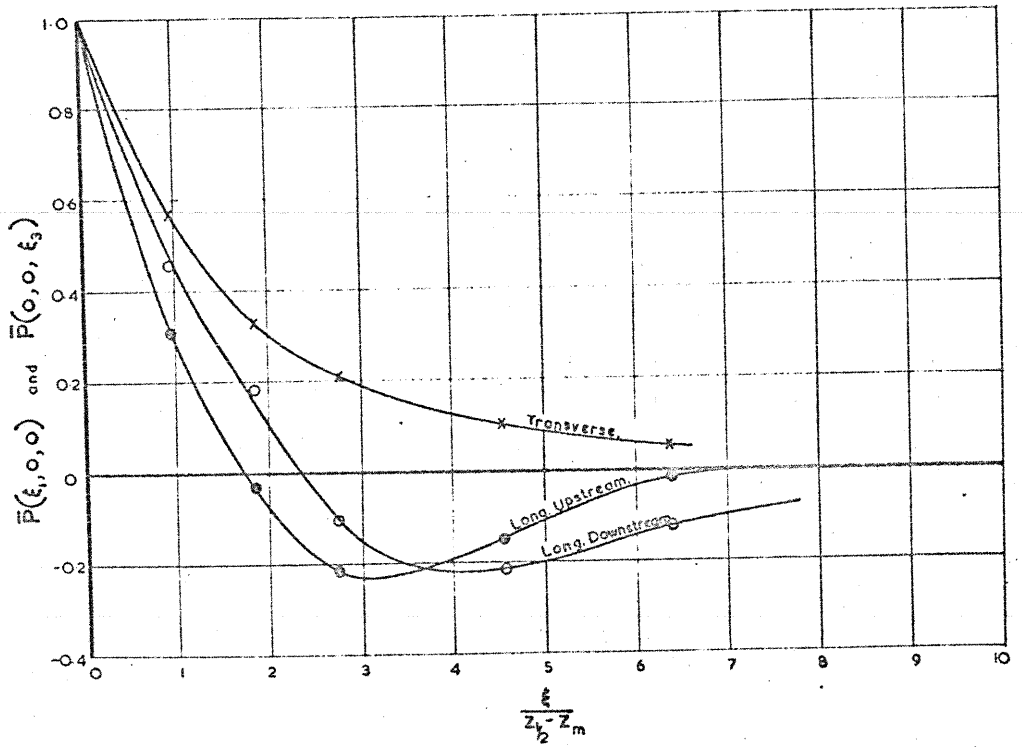

FIG. 46. RADIAL WALL-JET. LONGITUDINAL AND TRANSVERSE SPATIAL CORRELATIONS OF SURFACE PRESSURE FLUCTUATIONS. R=7·5IN., U=103 ft/sec, $z_{1/2}$=0·53 IN AT FIXED STATION.

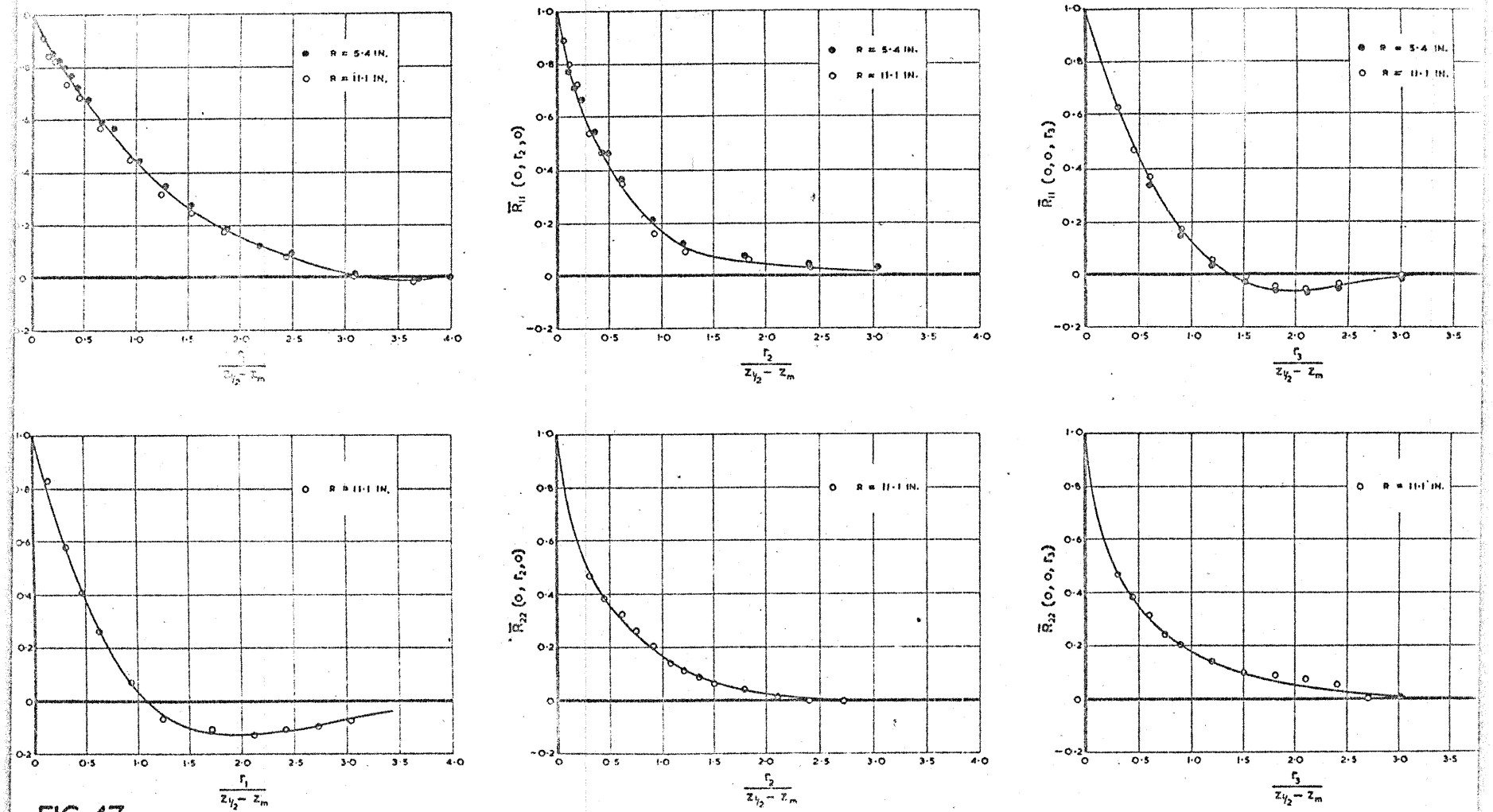

FIG. 47.

RADIAL WALL-JET. SPATIAL CORRELATIONS OF u' AND u', VELOCITY FLUCTUATIONS. FIXED PROBE AT $\frac{z}{z_{1/2}} = c$

$\frac{U}{U_m} = 0{\cdot}8$.

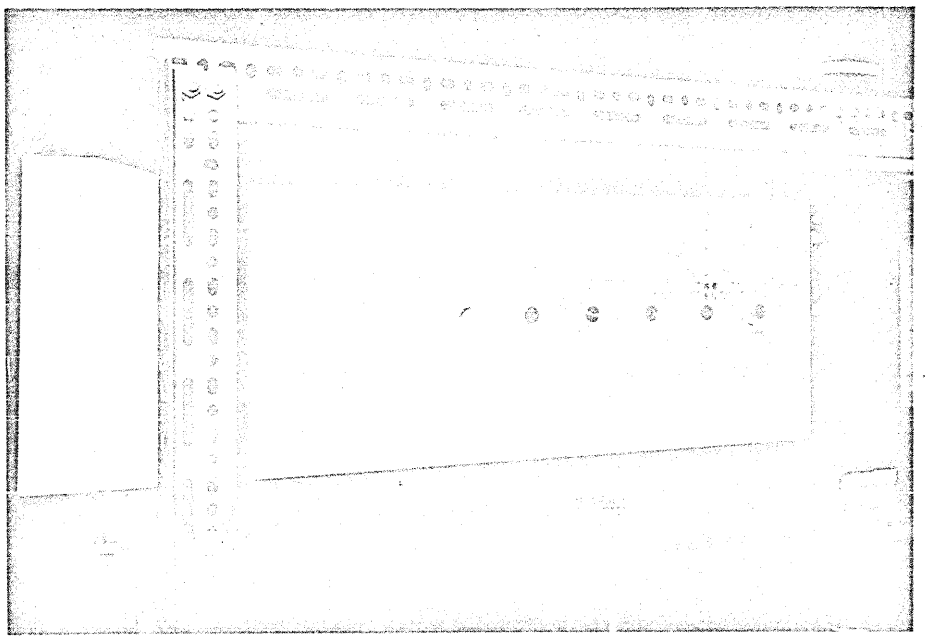

FIG. 48a. VIEW OF TWO-DIMENSIONAL WALL-JET FACILITY.

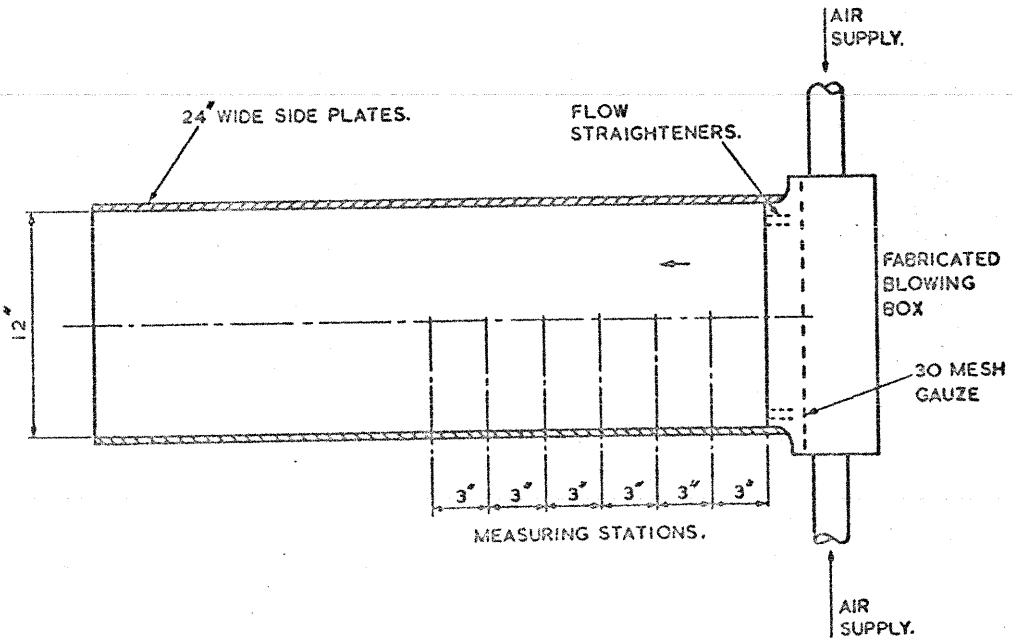

FIG. 48b. TWO-DIMENSIONAL WALL JET CONFIGURATION.

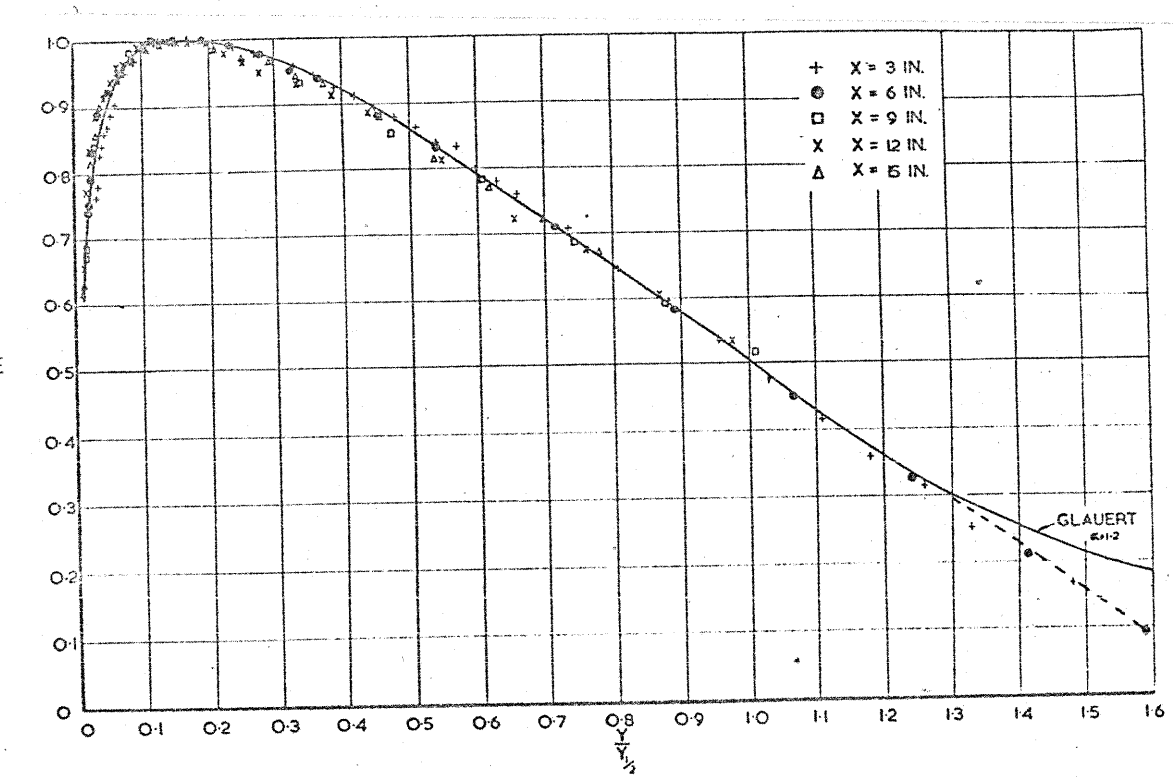

FIG. 49a. TWO-DIMENSIONAL WALL-JET MEAN VELOCITY PROFILES

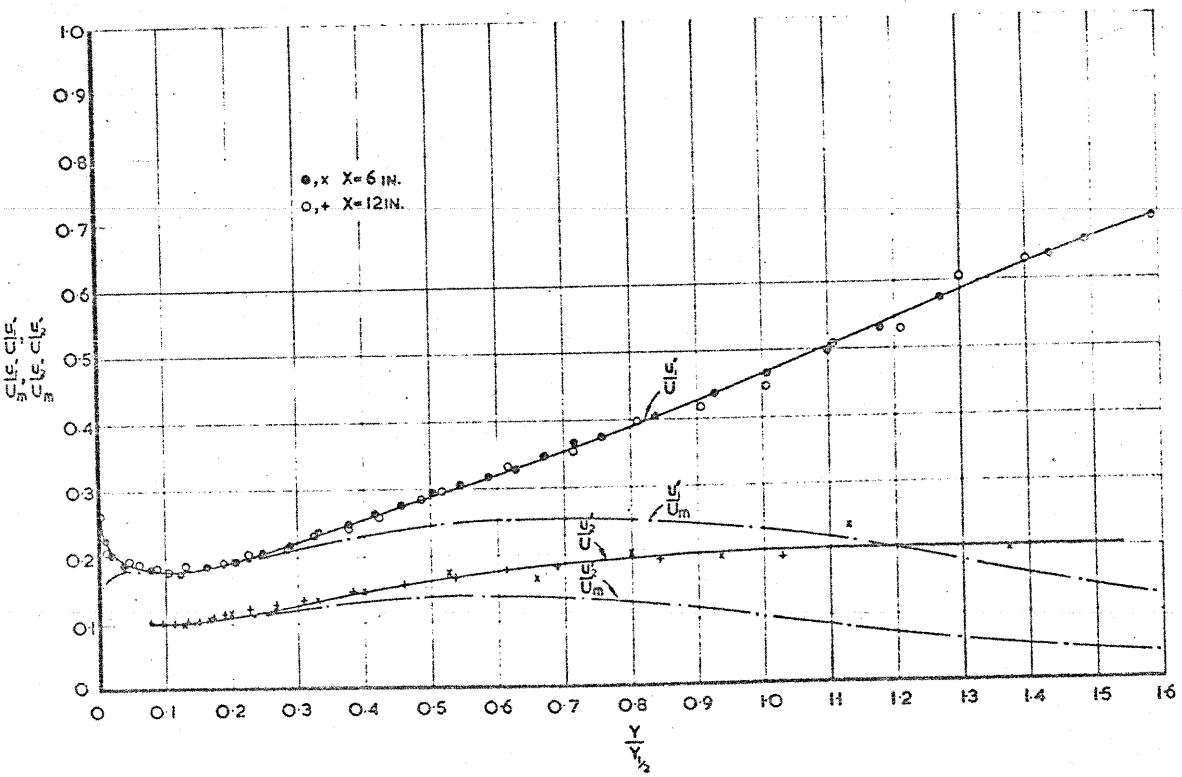

FIG. 49b. TWO-DIMENSIONAL WALL-JET. LATERAL VARIATION OF TURBULENT VELOCITY INTENSITIES.

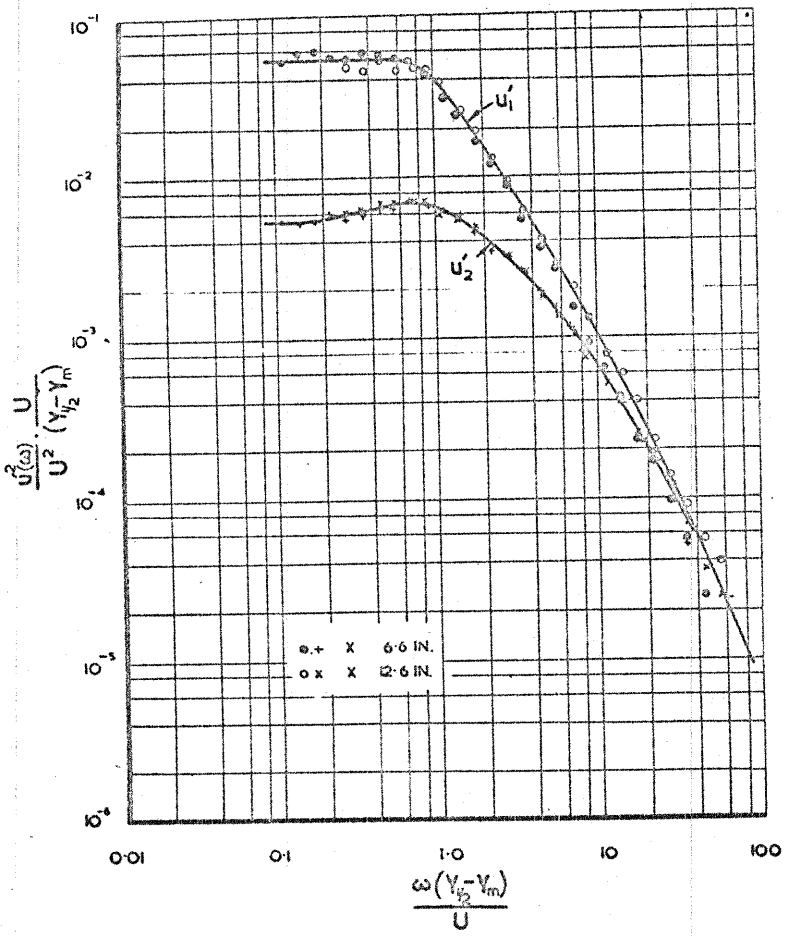

FIG. 50a TWO-DIMENSIONAL WALL-JET. POWER SPECTRAL DENSITY OF u_1' AND u_2' TURBULENT VELOCITY FLUCTUATIONS AT $Y/Y_{1/2}$ 0·6. U/U_m 0·8.

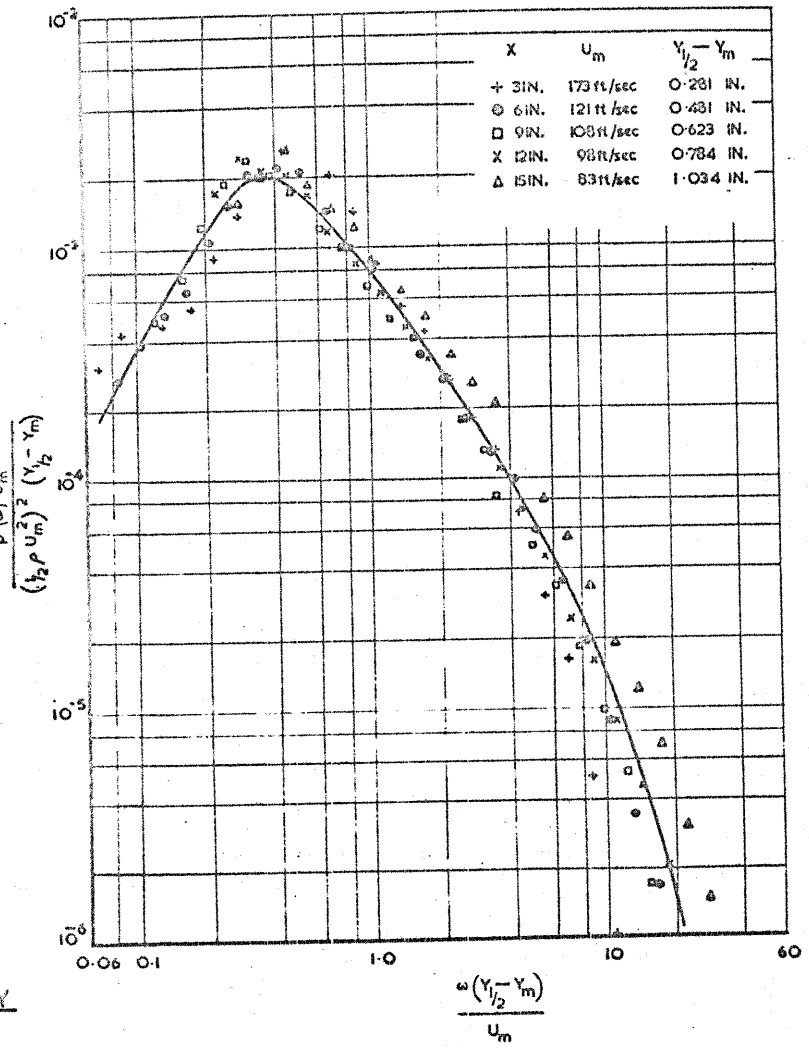

FIG. 50b. TWO-DIMENSIONAL WALL-JET. POWER SPECTRAL DENSITY OF SURFACE PRESSURE FLUCTUATIONS.

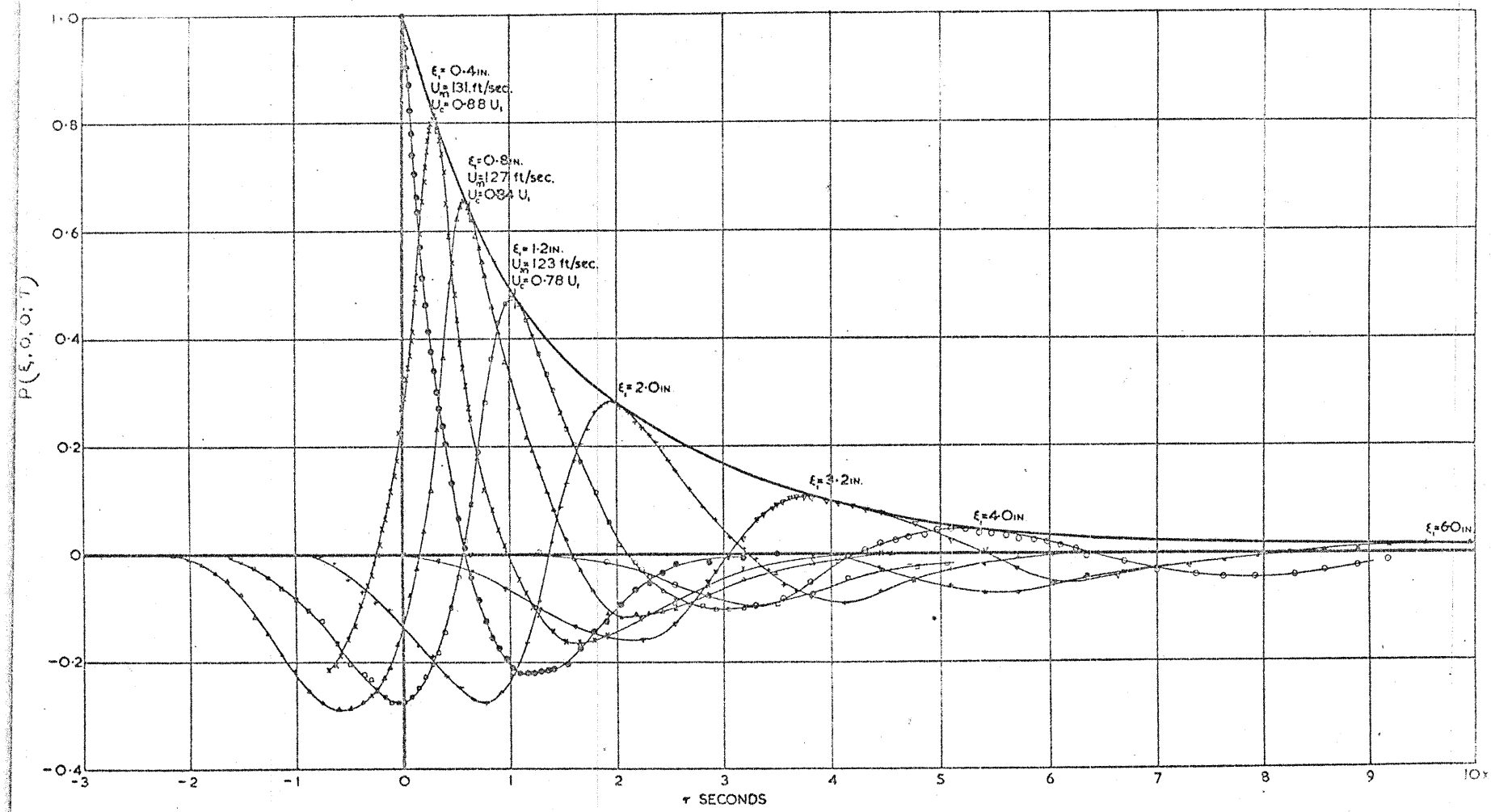

G. 51. TWO-DIMENSIONAL WALL JET. LONGITUDINAL SPACE-TIME CORRELATION OF SURFACE PRESSURE FLUCTUATIONS $X = 4{\cdot}8$ IN. $U_m = 136$ ft/sec, $Y_{1/2} = 0{\cdot}47$ IN. AT FIXED STATION.

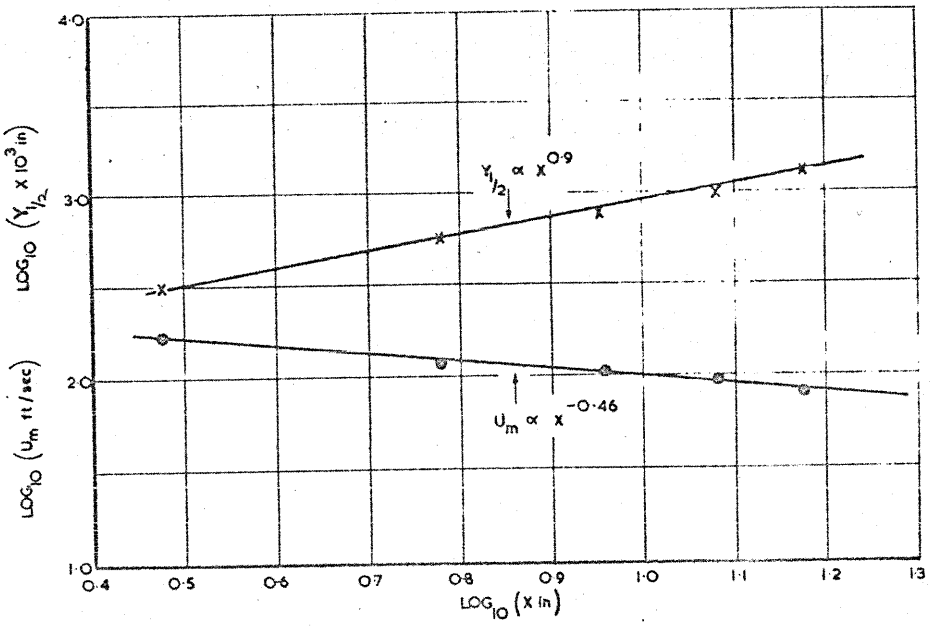

FIG. 52. TWO-DIMENSIONAL WALL-JET. VARIATION OF JET THICKNESS $Y_{1/2}$ AND MAXIMUM VELOCITY U_m WITH DISTANCE X.

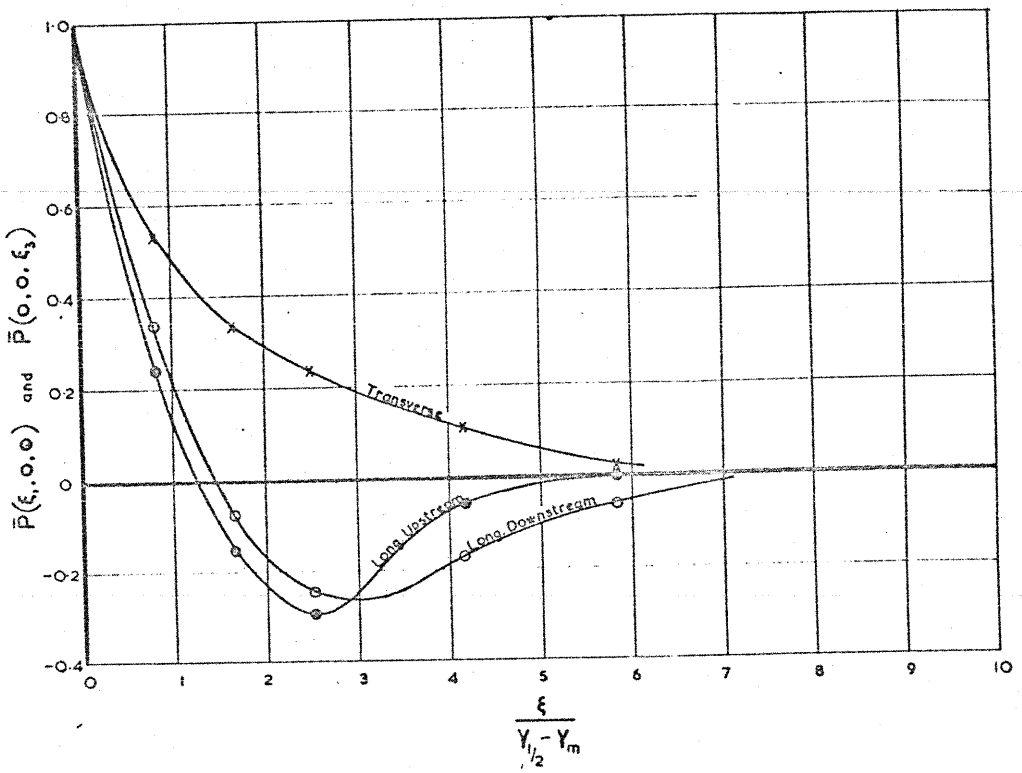

FIG. 53 TWO-DIMENSIONAL WALL-JET. LONGITUDINAL AND TRANSVERSE SPATIAL CORRELATIONS OF SURFACE PRESSURE FLUCTUATIONS. X = 6IN. U_m = 123 ft/sec. $Y_{1/2}$ = 0·55IN AT FIXED STATION.

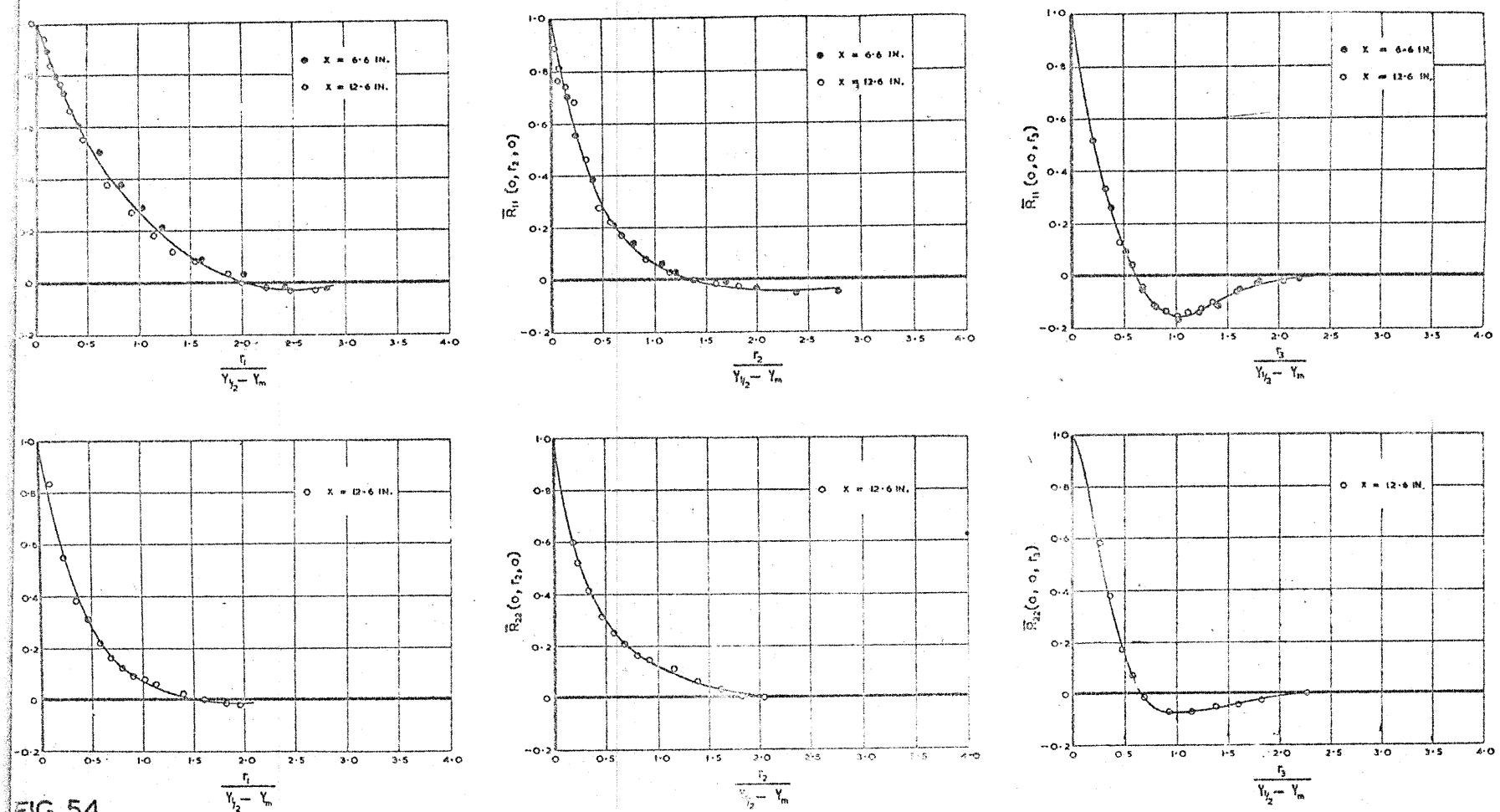

FIG. 54.

TWO-DIMENSIONAL WALL-JET. SPATIAL CORRELATIONS OF u' AND u' VELOCITY FLUCTUATIONS. FIXED PROBE AT $\frac{Y}{Y_{1/2}} = 0{\cdot}6$, $\frac{U}{U_m} = 0{\cdot}8$.

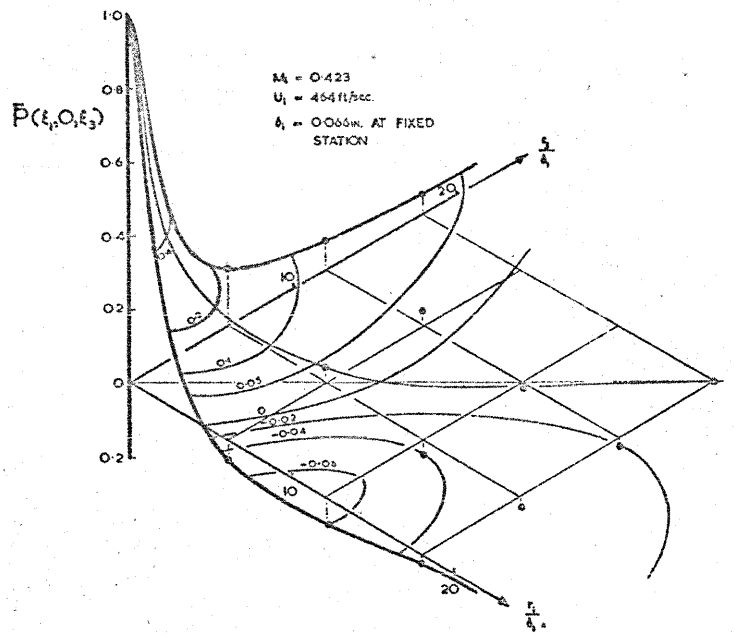

FIG.56a. $2\frac{1}{2}$IN X $2\frac{1}{2}$IN. TUNNEL. SURFACE SPATIAL CORRELATION OF WALL PRESSURE FLUCTUATIONS IN A TURBULENT BOUNDARY LAYER.

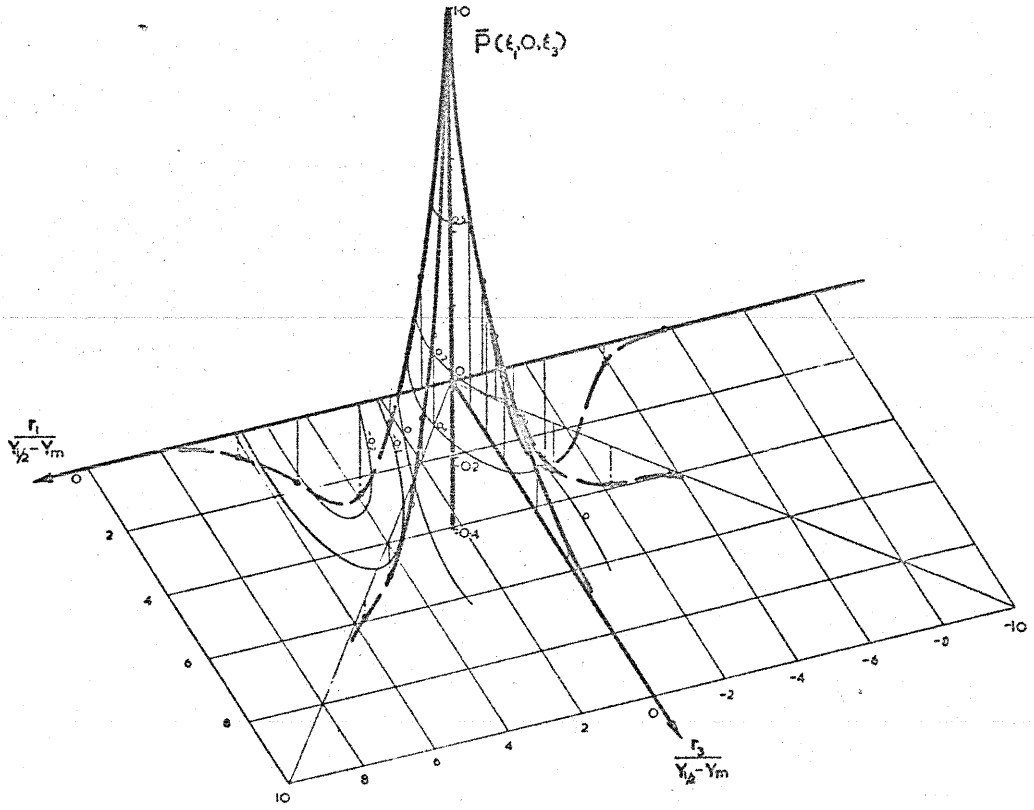

FIG.56b. TWO DIMENSIONAL WALL-JET. SURFACE SPATIAL CORRELATION OF WALL PRESSURE FLUCTUATIONS.

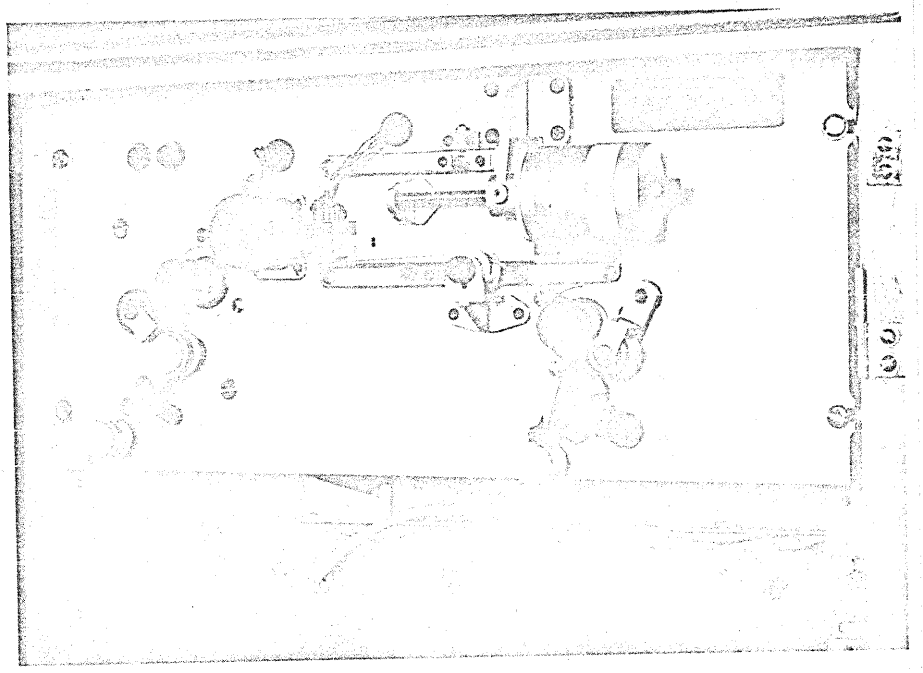

FIG.57a. THE TIME CORRELATOR TAPE-DECK.

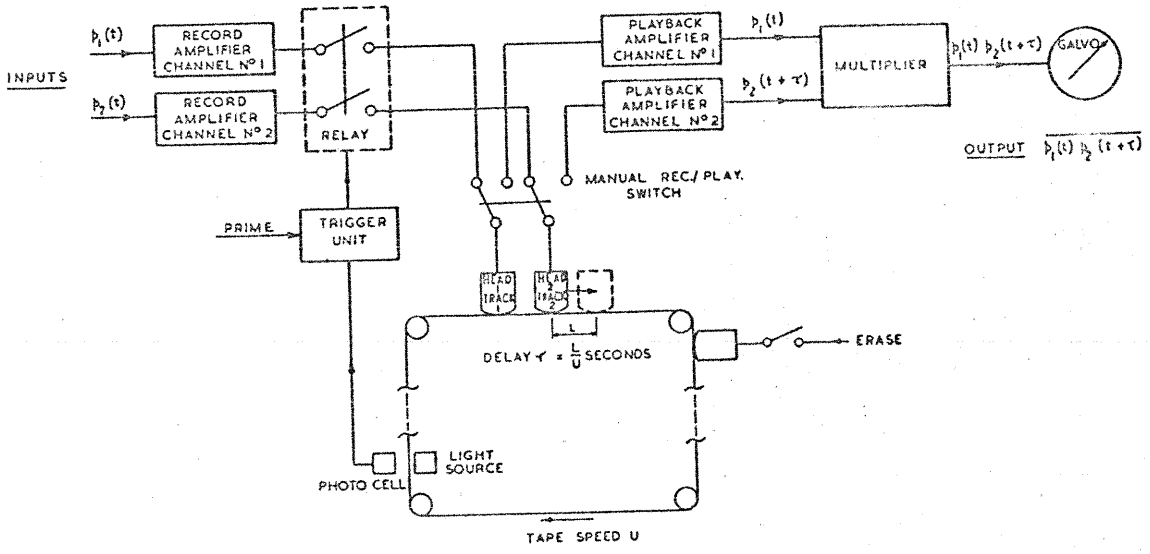

FIG.57b. DIAGRAM OF TIME CORRELATOR OPERATION

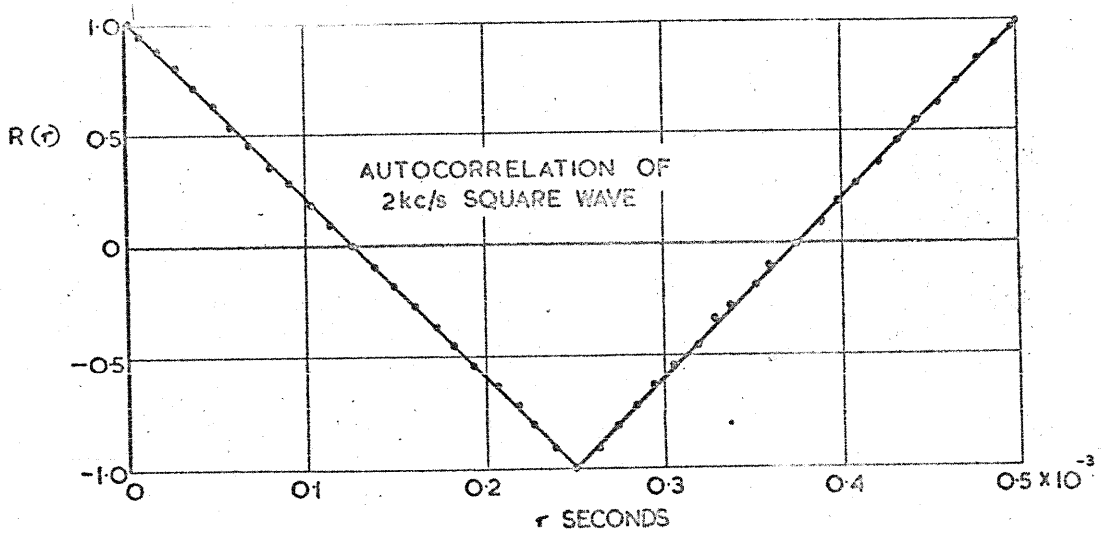

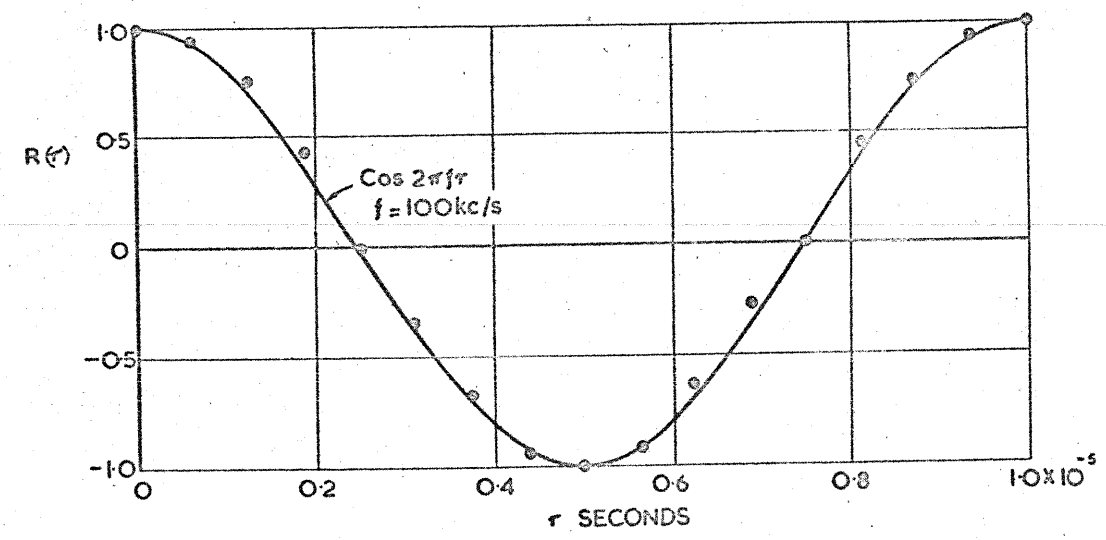

FIG. 58. AUTOCORRELATION OF 2Kc/s SQUARE-WAVE AND 100Kc/s SINE-WAVE SHOWING PERFORMANCE OF CORRELATOR.

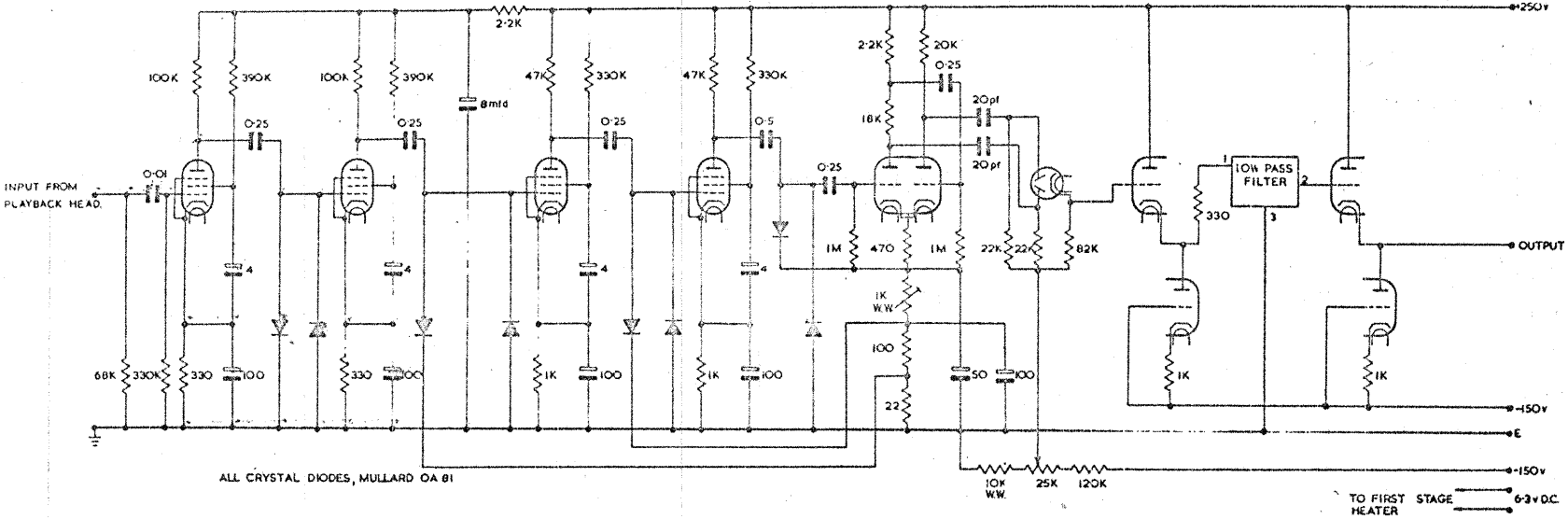

F.M. PLAYBACK AMPLIFIER

ALL RESISTORS IN OHMS.
ALL CAPACITORS IN MFDS.
UNLESS STATED.

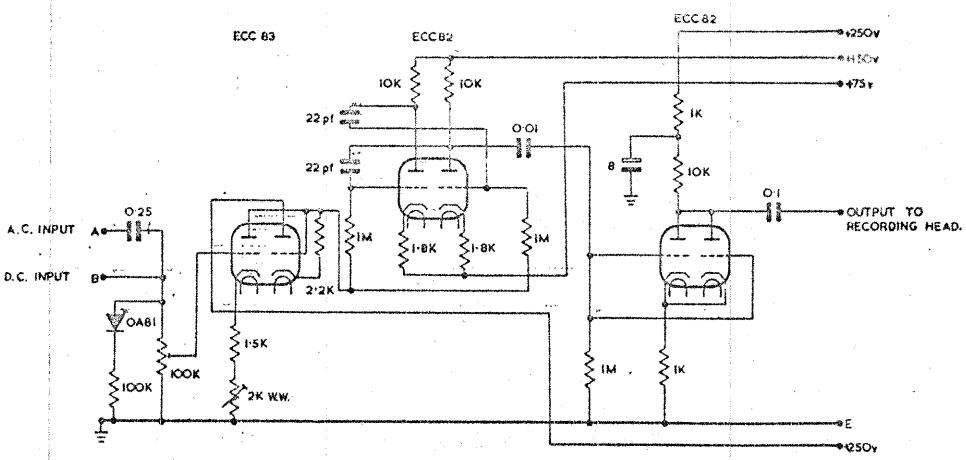

F.M. RECORD AMPLIFIER

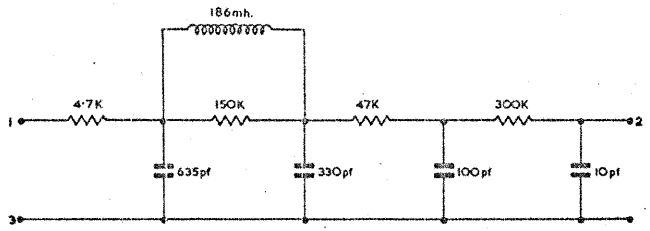

LOW PASS FILTER.

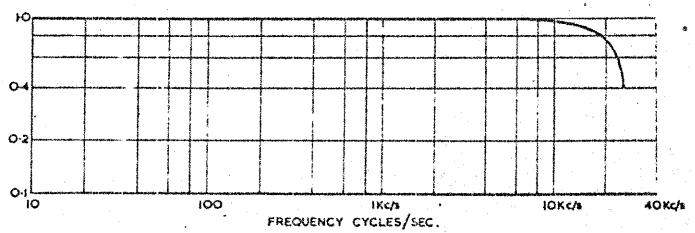

FREQUENCY RESPONSE OF F.M. TAPE CHANNEL.

FIG.59. F.M. TAPE SYSTEM.

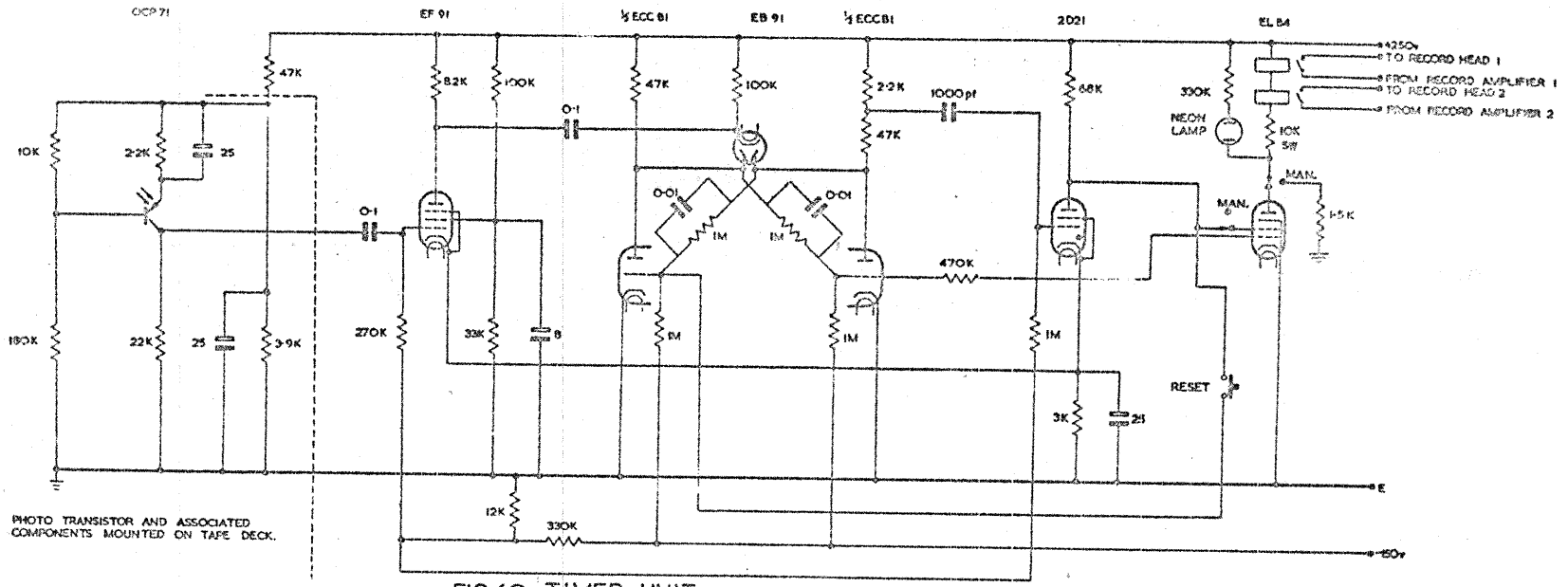

FIG.60. TIMER UNIT.

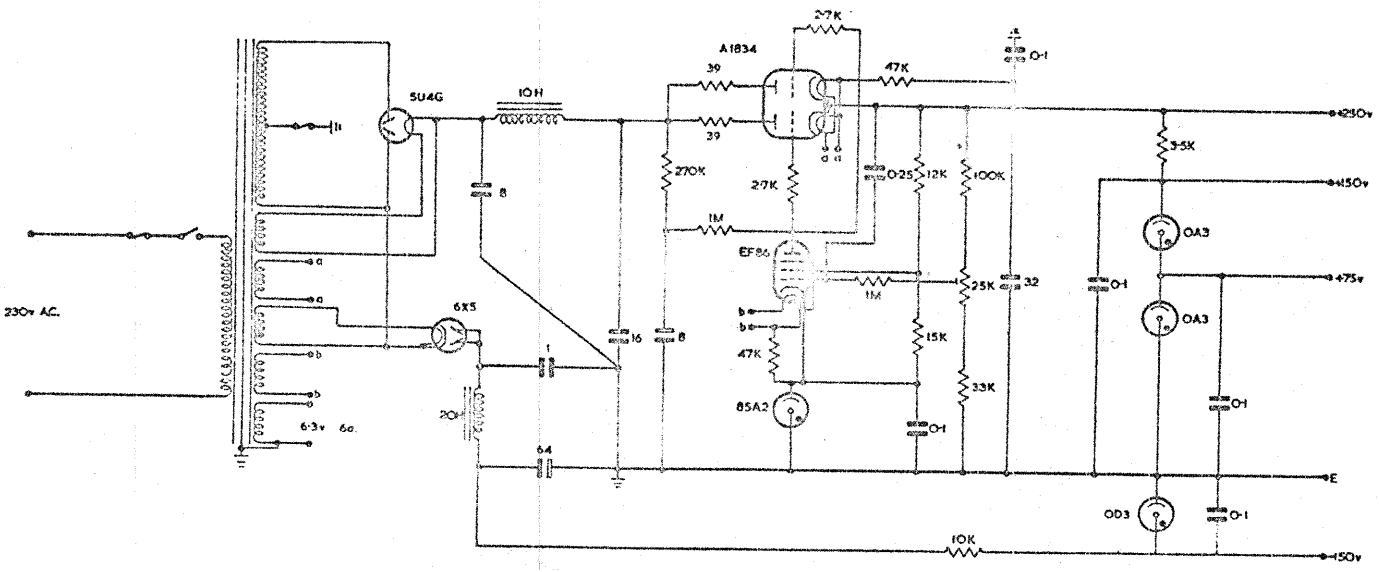

FIG.61. POWER SUPPLY FOR TAPE RECORDER.

ALL RESISTORS IN OHMS, CAPACITORS IN mfds. UNLESS STATED.

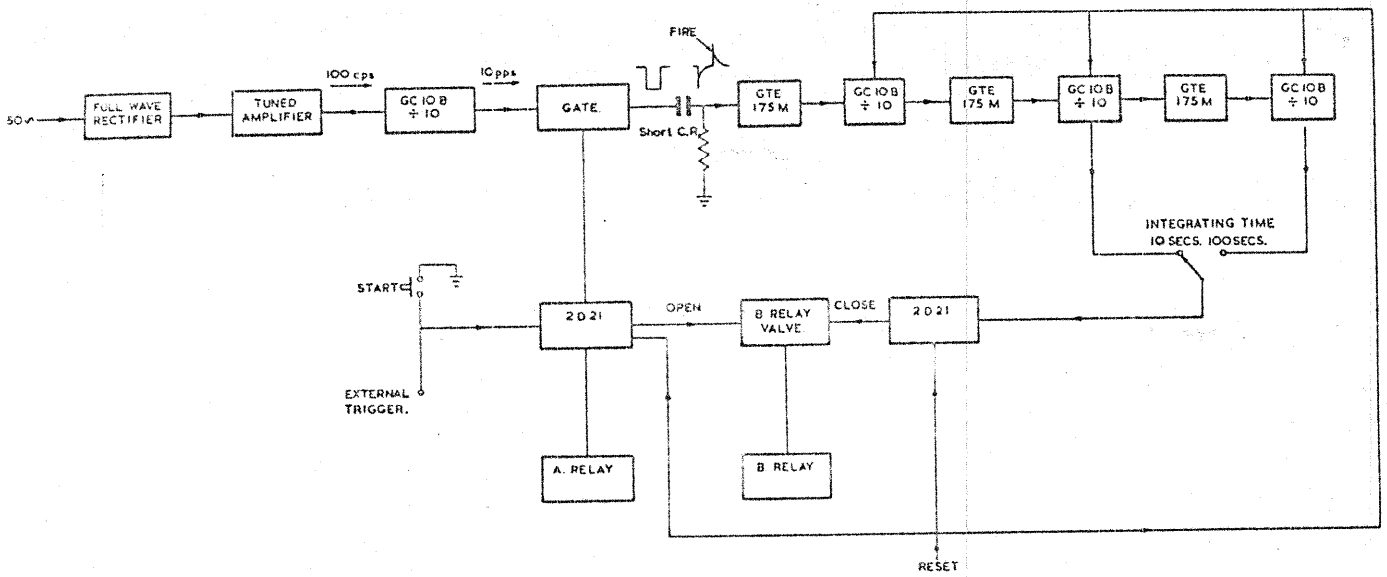

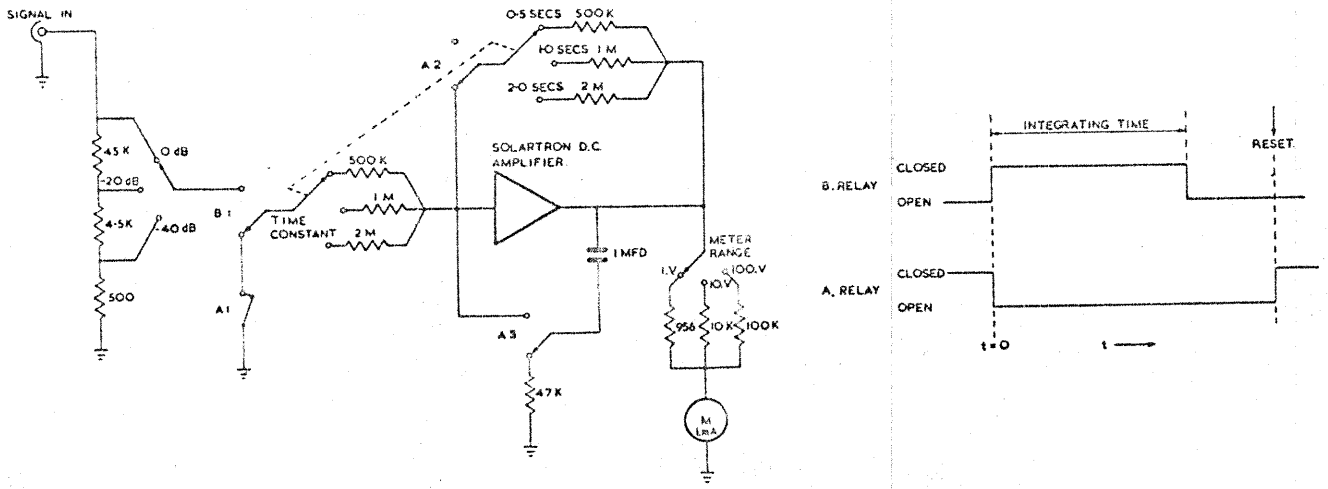

FIG.62 INTEGRATOR.

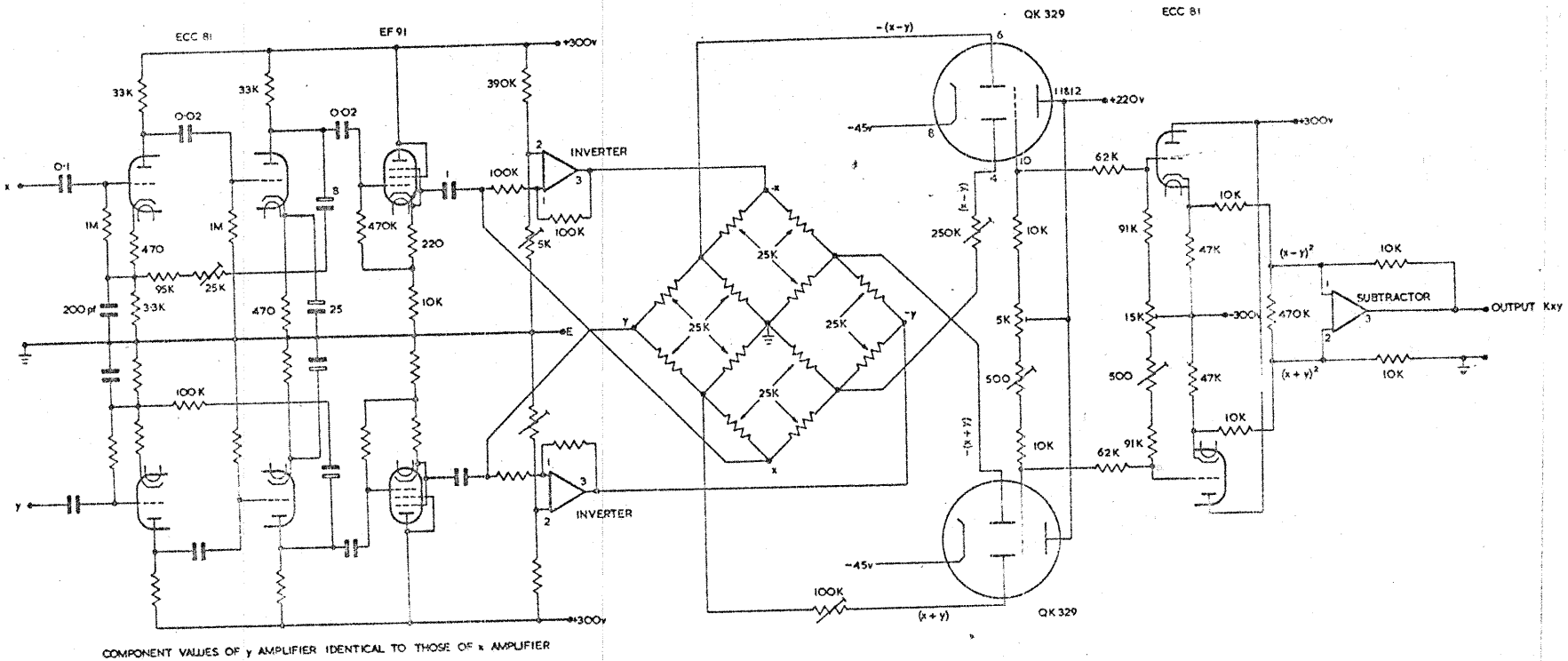

FIG. 63. MULTIPLIER.

ALL RESISTORS IN OHMS.
CAPACITORS IN MFDS.
UNLESS STATED.